



KAPITAŁ LUDZKI
NARODOWA STRATEGIA SPÓJNOŚCI



Politechnika Wrocławska

UNIA EUROPEJSKA
EUROPEJSKI
FUNDUSZ SPOŁECZNY



ROZWÓJ POTENCJAŁU I OFERTY DYDAKTYCZNEJ POLITECHNIKI WROCŁAWSKIEJ

Wrocław University of Technology

Electronics, Photonics, Microsystems

Sergiusz Patela, Marcin Wielichowski,
Szymon Lis, Konrad Ptasieński

OPTICAL FIBERS

Wrocław 2011

Projekt współfinansowany ze środków Unii Europejskiej w ramach
Europejskiego Funduszu Społecznego

Wrocław University of Technology

Electronics, Photonics, Microsystems

**Sergiusz Patela, Marcin Wielichowski,
Szymon Lis, Konrad Ptasieński**

OPTICAL FIBERS

Wrocław 2011

Copyright © by Wrocław University of Technology
Wrocław 2011

Reviewer: Anna Sankowska

ISBN 978-83-62098-27-9

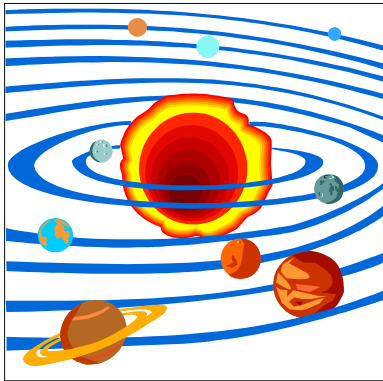
Published by PRINTPAP Łódź, www.printpap.pl

Table of Contents

1	Optical Fibers – Introduction.....	5
2	Fundamental properties of optical waveguides	9
3	Wave theory of optical fibers.....	15
4	Mode equation for a planar waveguide	24
5	Optical and mechanical properties of optical fibers	31
6	Technology of optical fibers	37
7	Passive devices (fundamentals and examples).....	46
8	Active devices – telecom sources and detectors.....	64
9	Connecting of passive and active photonic elements	79
10	Dispersion of optical fibers.....	87
11	Telecommunication fiber optic system	95
12	Measurements of optical fiber	99
13	Optical Time Domain Reflectometer (OTDR).....	109

1 Optical Fibers – Introduction

Contemporary long distance telecommunications are based almost exclusively on optical fiber cables. The optical fibers are extensively used also for other applications, such as access networks, sensors or lightening.



Fiber to the Sun, and in 24 hours through the Earth

Till now ~150 millions km of optical fiber has been installed

Fig. 1.1 Total length of fiber installed in the world.

Optical fibers are considered to be very advanced and hard to get transmission media. However, adding up all the fiber installed in the world, we get total of 150 million km. That’s the distance equal to that from the Earth to the Sun.

Every day ~15 000 km is installed.

- Long distance communications,
- Metropolitan networks
- Fiber to the (every home)



Fig. 1.2 Length of fiber installed every day.

Even if the astronomical amount of fiber has been installed to, large amount of fiber is still installed every day. That daily amount is approximately equal to the diameter of the Earth. Initially optical fibers were used for long distance telecommunications. Today new fiber is installed mainly in metropolitan and access networks.

At this point, one may ask a question: “Well, a lot of fiber has been installed, but what are the consequences? Does it really matter?”. The answer is, that with all the power supply lines installed, electronic devices and electrical appliances are available everywhere, so there is possibility that soon photonics devices will be as popular as electrical or electronic. Fiber optics is the main factor enabling photonics development.

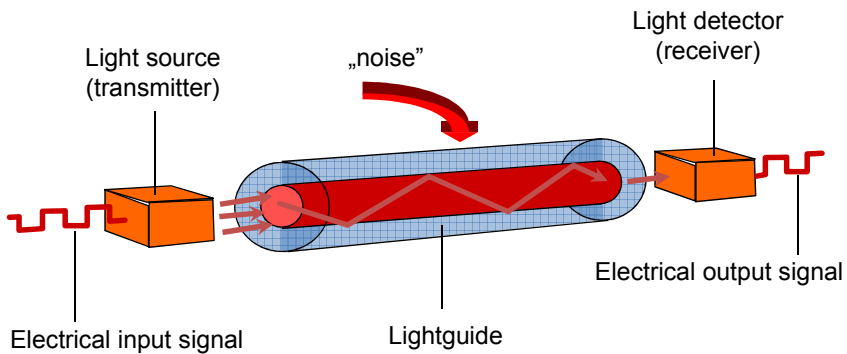


Fig. 1.3 Schematic diagram of fiber optic system.

Communication systems consist of three main components: a transmitter of the signal, a communication line and a receiver. Additionally, one has to consider limiting factors of the transmission capabilities of the systems – these are sometime called “noise”. In the case of optical communication system a light source takes the role of the transmitter, an optical fiber serves as the transmission line, and a photodiode is used as the receiver. The main limiting factor of optical transmission line are attenuation and dispersion.

1.1 Fundamental features of fiber-optic transmission

To understand advantages and limitation of optical fiber transmission, one has to take into account the following three factors:

- **Transmission speed** - In fiber optic transmission a signal is conducted by light - electromagnetic wave of frequency 3×10^{14} Hz, (300 THz). Capacity of any transmission channel can be multiplied by sending simultaneously many colors of light through one fiber.
- **Link span**- Very low attenuation of silica glass and total internal reflection at the boundaries of the core make long-range repeater-less transmission possible.
- **Optical-fiber modes. Wave nature of light and fiber modes** - Many waveguide parameters and construction details can be explained only if one takes into account the fact that light is a wave, guided by a structure of very low transversal dimensions.

In optical fibers, light is guided in the form of “modes”. In a waveguide or cavity, the mode is one of the possible patterns of electromagnetic field. Available patterns are derived from Maxwell's equations and the applicable boundary conditions. Two examples of modes:

- waveguide mode - fiber optic mode
- cavity mode - laser mode

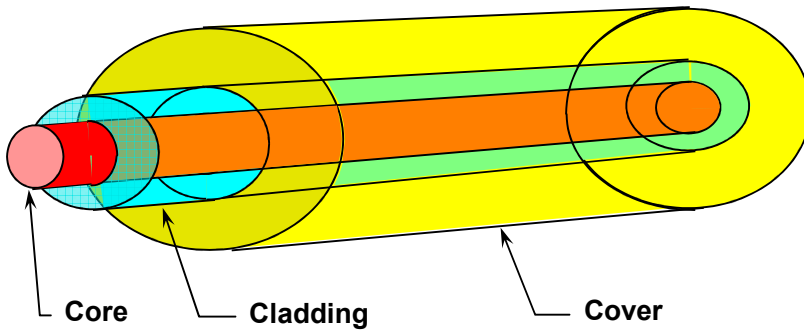
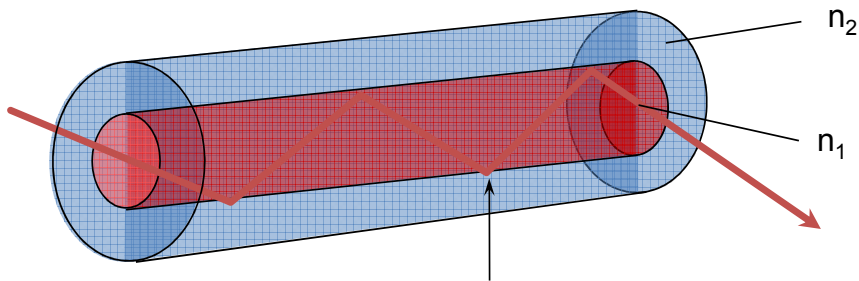


Fig. 1.4 Structure of optical fiber.

An optical waveguide, and in particular the optical fiber-waveguide, is typically composed of three parts: core, cladding and cover. In the case of the optical fiber, core and cladding are typically fabricated of glass, and the cover is prepared from polymer.

To describe and analyze optical waveguiding structures, one has to introduce the notion of refractive index of the material. For dielectric materials, the refractive index may be defined as the ratio of the speed of light in a vacuum to the speed of light in the material.

$$n = \frac{c}{v} \tag{1.1}$$



Total internal reflection at the boundary core-cladding

Fig. 1.5 Total internal reflection. Fiber diameter: 10 to 50 μm at 1 m distance creates 10 000 reflections. For the reflection coefficient of 99% after 1 m the signal will be attenuated by $0.99^{10\,000} = 10^{-44}$.

The crucial optical phenomenon utilized in optical fibers, is total internal reflection (TIR). As the name puts it, it is the phenomenon where light is reflected from some boundary in such a way, that 100% of optical power is reflected back towards the first medium. It is essential that the total internal reflection is used, as any other reflection from typical, e.g. metallic, mirror creates unacceptable losses (see comment on Fig. 1.5). Total internal reflection is possible under condition that the refractive index of the first medium is higher than refractive index of the second medium.

For the fiber diameter of $10\ \mu\text{m}$ at the distance of $1\ \text{m}$ the light beam will be reflected approximately $10\ 000$ times. For the reflection coefficient of 99% after $1\ \text{m}$ the signal will be attenuated by $0,99^{10\ 000} = 10^{-44}$.

1.2 Classification of optical waveguides

In principle, surrounding high refractive index material with low refractive index cladding enables building of a light guiding structure. Different structures are possible. Waveguides may be classified according to several factors:

- Geometry: planar, strip or fiber waveguides
- Mode structure: single-mode, multi-mode
- Refractive index distribution: step or gradient index
- Material: glass, polymer, semiconductor
- Guiding mechanism – standard (TIR) and photonic crystal waveguides

Different possible structures of optical waveguides are explained in the pictures below.

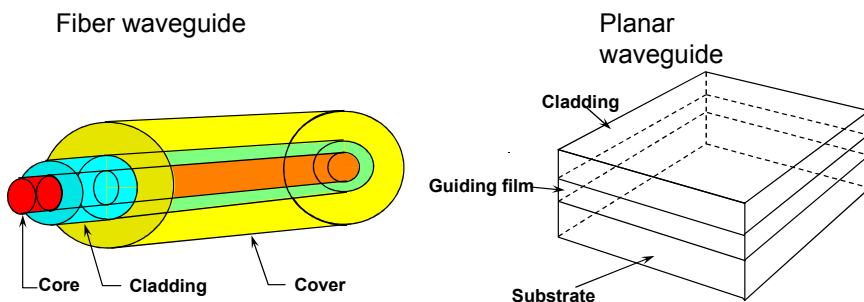


Fig. 1.6 Basic classification of waveguides: fiber versus planar waveguides.

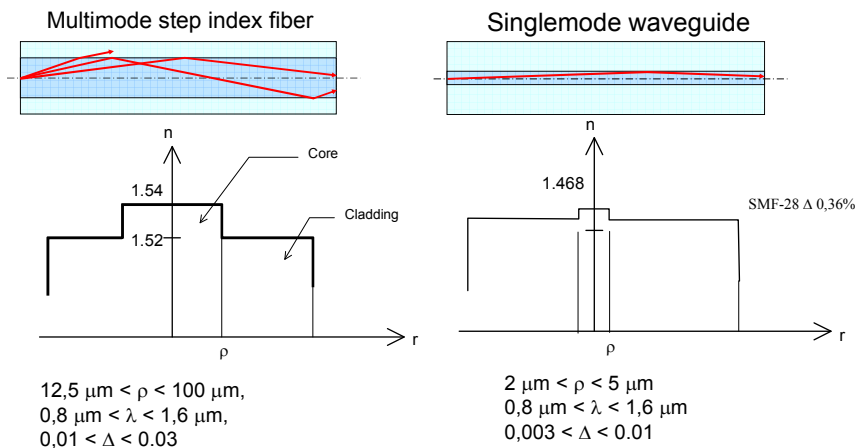


Fig. 1.7 Single and multimode waveguides.

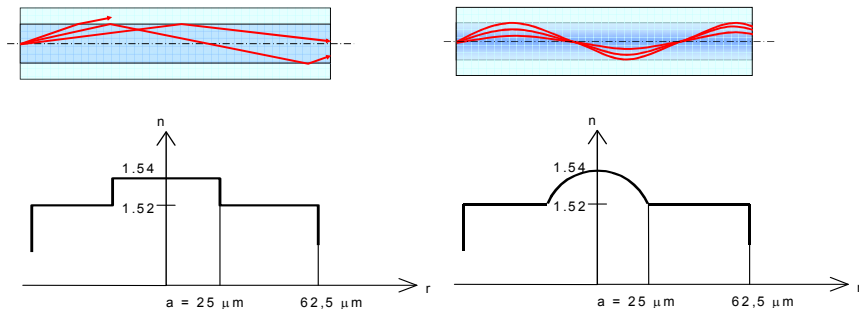


Fig. 1.8 Step-index and gradient waveguides.

- | | |
|--------|---|
| fibers | <ul style="list-style-type: none"> • SiO₂ (doped) • ZBLAN (Zr, Ba, La, Al, Na) • Plastic Optical Fibers (PMMA) • Epitaxial multilayers (eg. GaAs/AlGaAs) |
| layers | <hr/> <ul style="list-style-type: none"> • Dielectric layers (Ta₂O₅, ZnO, Si₃N₄/SiO₂) • Polymer (PMMA, PS) |

Fig. 1.9 Waveguide classification: materials.

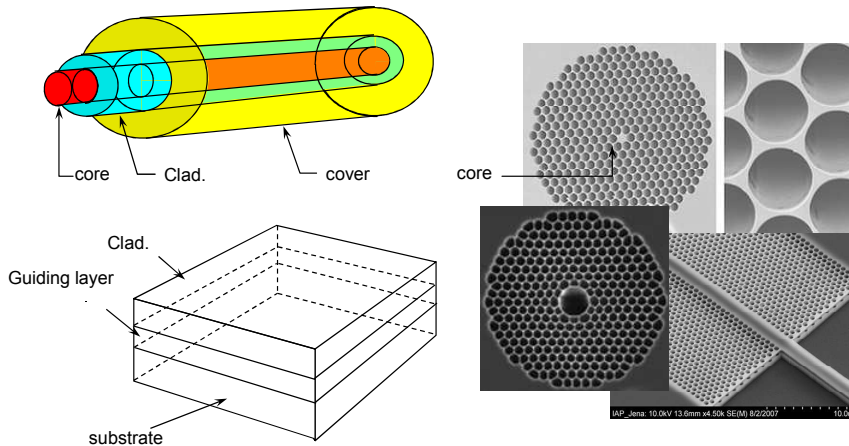


Fig. 1.10 Standard and photonic waveguides.

1.3 Non-telecommunication waveguide applications

Optical waveguides are mainly used in telecommunications, however there are other popular and interesting applications. Optical waveguides may be used in industry for sensing, illumination and displays. There are important applications of optical fiber in medicine, such as

endoscopy or surgery. Another interesting group of applications include art works and clothes with optical fibers embedded for decorative purposes.

1.4 10 advantages of optical fibers

Optical fiber waveguides are important for future communication systems. Below is a list of ten advantages of optical fibers that make them superior to copper cables.

1. High information capacity of a single fiber.
2. Low loss, repeater-less transmission over long distances is possible.
3. Absolute immunity from EMI (electro-magnetic interference).
4. Low weight.
5. Small dimensions (diameter).
6. High work safety (low risk of fire, explosion, ignition).
7. Transmission safety (almost impossible data tapping).
8. Relatively low cost (getting lower).
9. High reliability.
- 10 Simplicity of installation.

2 Fundamental properties of optical waveguides

2.1 Parameters of optical waveguides - classification

Optical waveguides are characterized by a number of parameters. Four parameter categories are listed below together with names of the most commonly used parameters.

- optical
 - attenuation
 - dispersion
 - cut-off wavelengths
 - refractive indices
 - numerical aperture
 - modal properties
 - temperature stability of parameters
- geometrical
 - transversal dimensions
 - tolerances
- mechanical
 - tensile strength
 - allowable bending radius
- additional parameters (defined for specialty fibers)
 - active dopant,
 - beating length.

In lectures that follow we will study the above parameters in detail.

2.2 Telecommunication windows and generations of fiber optic systems

Attenuation of a standard, silica-glass telecommunication fiber in the function of light wavelength, is depicted in figure Fig. 2.1. Three attenuation minima, known as the telecommunication windows, can be seen. Telecommunication windows are separated by

spectral ranges in which absorption peaks caused by the -OH ions, are located. The peak at 1.4 μm , the one separating the second window and the third window, can be removed or minimized by means of special fiber manufacturing techniques that enable ultra-low -OH concentrations. From a historical perspective, the earliest optical transmission systems utilized the first telecommunication window. Then, the next-generation systems were based on the second window, while in today's systems, the third telecommunication window is widely utilized.

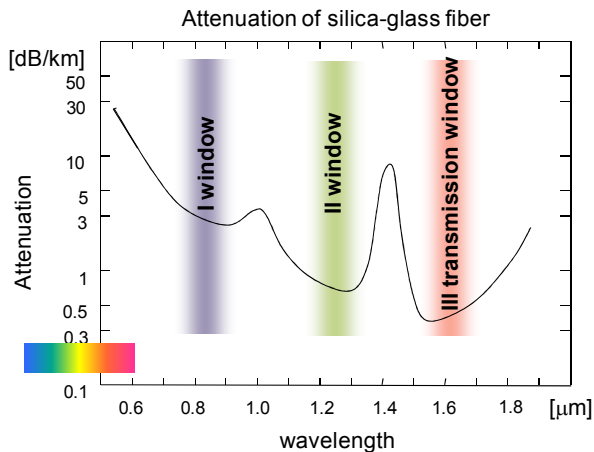


Fig. 2.1 Attenuation of silica-glass fiber.

Names and wavelength ranges of fiber optics telecommunication bands within the third transmission window:

- S : 1460 – 1530 nm
- C : 1530 – 1565 nm
- L : 1565 – 1625 nm
- U : 1625 – 1675 nm

2.3 Fundamental parameters of optical waveguides – attenuation

Optical waveguide attenuation is a gradual decrease in energy (optical power) carried by the lightwave as it propagates along the waveguide. Numerical value of attenuation – the attenuation coefficient – is expressed in the units of [dB / km], which translates into: what part (in decibels, dB) of the initial optical power is lost due to attenuation assuming the light has travelled a path of the length of 1 kilometer (km) inside the waveguide. Optical waveguides we are mostly dealing with throughout this lecture, are optical fibers. Below, there are some typical values of attenuation usually found in silica-glass optical fibers.

Single mode fibers

- 1310 nm 0.33-0.42 dB/km
- 1550 nm 0.18-0.25 dB/km

Multimode fibers (gradient)

- 850 nm 2.4-2.7 (50/125) 2.7-3.2 (62.5/125) dB/km
- 1300 nm 0.5-0.8 0.6-0.9 dB/km

Values in brackets denote fiber's core and cladding diameters, respectively. The diameters are expressed in micrometers (μm). Numbers expressed in nanometers (nm) are wavelengths of light for which given attenuation values were measured.

2.4 Characterization of optical waveguide – measurement units

Optical wavelength, i.e. length of one period of lightwave, is expressed in

- $\mu\text{m} = 10^{-6} \text{ m}$
- $\text{nm} = 10^{-9} \text{ m}$

The above units were chosen for convenience as optical wavelengths used in telecommunications are of the order of 10^{-6} m , i.e. about one micrometer (cf. paragraph 2.2). Usually, when optical wavelength is given, it is assumed that light propagates in vacuum. The actual wavelength in e.g. a bulk of silica glass is smaller by a factor equal to the silica glass refractive index.

Waveguide attenuation is calculated according to the formula:

$$A [\text{dB/km}] = \frac{10 \log \frac{P_{\text{WY}}}{P_{\text{WE}}}}{L} \quad (2.1)$$

where L is the waveguide length. Note that for the output power (P_{OUT}) being lower than the input power (P_{IN}), which is always the case, when no optical amplifiers are present, attenuation value is less than zero. The minus sign is, however, customarily omitted in optical fiber specifications.

If one kilometer of an optical waveguide (e.g. optical fiber) has an attenuation of 3 dB, this means that only half (50%) of the input power exits the waveguide as the output power ($P_{\text{OUT}} = 0.5 * P_{\text{IN}}$). This example and several more are listed below.

- 3 dB \approx 50%
- 20 dB = 1%
- 30 dB = 0.1%
- 40 dB = 0.01%

In general, $x \text{ dB} = 100 * 10^{-(x/10)} \%$.

2.5 Effective waveguide thickness

In the following paragraphs we will use laws of geometrical optics to describe some physical phenomena related to lightwave propagation in optical fibers. The application of geometrical optics provides an intuitive picture of the fundamental properties of optical fibers. In a more complete description of the problem, i.e. of lightwave propagation in structures having the cross-sectional dimensions comparable to wavelength, it is necessary to employ the wave optics methods. When using the wave optics methods, it is, however, more difficult to get an intuitive physical insight into fundamental properties of optical waveguides.

Let us define a parameter using the following relation (Bass, 2001a), (Agrawal, 2002)

$$V = \frac{2 \cdot \pi \cdot \rho}{\lambda_0} (n_1^2 - n_2^2)^{1/2} \quad (2.2)$$

where: n_1 , n_2 - refractive index of core and cladding, ρ - core radius, and λ_0 - light wavelength. The parameter V is called the effective (or characteristic) waveguide thickness and it can be used for estimating the applicability of the geometrical-optics tools to study any optical waveguide under consideration. The greater the effective thickness V , the higher the number of modes that are supported (guided) by the waveguide. We can use geometrical-optics tools (methods of analysis) if $V \gg 1$.

It is clear from (2.2) that V will take lower values with decreasing the core-cladding refractive index difference ($n_1 - n_2$). However, with decreasing the light wavelength (λ_0), the value of V will become higher. This means, in general, that for low core-cladding refractive index differences, a sufficiently short light wavelength can be selected to make the waveguide support more guided modes (e.g. make it multimode).

2.6 Laws of reflection and refraction

We will now consider a ray of light hitting (impinging on) a boundary between two dielectric materials as it is illustrated in figure Fig. 2.2. Indexes of refraction (refractive indexes) of the materials equal n_{co} and n_{cl} . The subscripts used stand for the core and cladding, respectively, because all the formulas derived here will later be used to describe optical fibers.

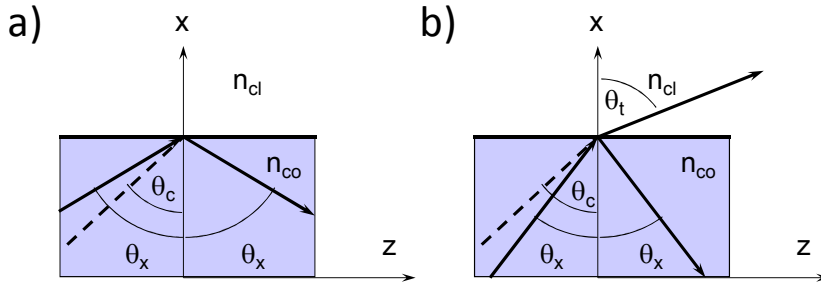


Fig. 2.2 Illustration of the a) law of reflection and b) law of refraction.

Depending on the value of the incidence angle (i.e. value of angle at which light hits the boundary), two different phenomena may occur:

- total internal reflection – when optical power is completely reflected off the boundary, and
- refraction – when optical power is only partly reflected, and the remaining part is refracted, i.e. it crosses the boundary and its propagation direction changes.

Laws of reflection and refraction give further description of the above phenomena.

2.6.1 Law of reflection

In figure Fig. 2.2 a), a light beam (light ray) hitting the dielectric boundary surface is completely reflected – it undergoes the total internal reflection. Note that all angles are measures to the so called surface normal, which is perpendicular to the surface.

The law of reflection states that:

- 1) The angle of incidence θ_x , angle of reflection θ_r , and the (surface) normal are all in the same plane.
- 2) The angle of incidence equals the angle of reflection.

2.6.2 Law of refraction

In figure Fig. 2.2 b) a light beam (light ray) hitting the dielectric boundary surface is both reflected and refracted. Refraction is a process of bending of light as it goes from one media to another. Law of refractions states that:

- 1) The incidence angle and the refraction angle are strictly related. The relation is expressed with the Snell's law (which will be discussed in the next paragraph).

Similarly to the law of reflection, all angles and the normal are in the same plane.

2.7 Snell's law and critical angle

Values of all the angles indicated in figure Fig. 2.2, are connected with strict relationships. These relationships are mathematically expressed as Snell's law and as a formula for the critical angle.

Snell's law, also called law of refraction or refractive law, states that the refraction angle θ_t relates to the incidence angle θ_x in the following way

$$n_{co} \sin(\theta_c) = n_{cl} \sin(\theta_t) \quad (2.3)$$

Now, looking at diagram b) in figure Fig. 2.2 we can see that once refraction angle θ_t reaches the value of 90° transmission of optical power across the boundary does not occur any more. So, the condition of total internal reflection is fulfilled. The (value of) incidence angle at which the above takes place, is called the critical angle and is denoted as θ_c in the diagram. Using Snell's law, i.e. substituting $\theta_t = 90^\circ$ into (2.3), we arrive at the following equation

$$n_{co} \sin(\theta_c) = n_{cl} \sin(90^\circ) \quad (2.4)$$

This equation can easily be solved to get the formula for the critical angle θ_c

$$\theta_c = \arcsin\left\{\frac{n_{cl}}{n_{co}}\right\} \quad (2.5)$$

The notion of the critical angle is fundamental for the classification of waveguide rays and for the derivation of the numerical aperture formula. Both subjects are discussed in subsequent paragraphs.

2.8 Classification of waveguide rays

Depending on light ray's propagation direction within optical waveguide and on the type of the waveguide itself, there can occur three types of waveguide rays, i.e. three possibilities of how light propagates when it is completely or partly bound within the waveguide. The case when light is not bound within the waveguide at all, will not be discussed here. The three types of waveguide rays are depicted in figure Fig. 2.3.

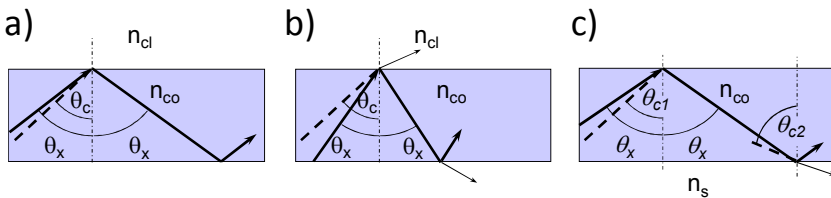


Fig. 2.3 Illustration of a) guided rays, b) leaky rays, and c) substrate rays.

Considering the values of the angle θ_x , waveguide rays can be classified as:

- guided rays: $90^\circ \geq \theta_x > \theta_c$
- leaky rays: $\theta_c \geq \theta_x \geq 0$
- substrate rays (substrate modes): $\theta_{c2} \geq \theta_x \geq \theta_{c1}$ (only occurring in asymmetrical waveguides)

The θ_x is the angle at which light rays impinge on the core-cladding and the core-substrate boundaries.

In other words, when light undergoes the total internal reflection at both the dielectric boundaries defining the waveguide, we get the guided rays. In an ideal (theoretical) optical waveguide, guided rays propagate without any loss – entire optical power remains trapped within the waveguide independently of how long the propagation distance is. In real-life optical waveguides (both planar waveguides and fibers) propagation losses are greater than zero due to other physical mechanisms (like e.g. dielectric boundary roughness) not considered in the simplified model discussed here.

Unlike the guided rays, the leaky rays are an inherently lossy type of light propagation within waveguide – optical power gradually “leaks” out of the waveguide along the propagation distance. This is because leaky rays do not undergo the total internal reflection neither at the core-cladding, nor at the core-substrate boundary.

In an asymmetrical waveguide, i.e. a one, in which values of the cladding refractive index (n_{cl}) and the substrate refractive index (n_s) are different, the substrate rays can propagate. Again,

this type of light propagation within waveguide shows inherent losses – optical power “leaks” out of the waveguide. This leakage, however, is now only present at the core-substrate boundary. At the core-cladding boundary, light undergoes the total internal reflection. Note that we have implicitly assumed $n_c < n_s$ here. In case of planar waveguides, this relation is often fulfilled because air ($n_c \approx 1$) plays the role of the cladding in some of the popular waveguide types (e.g. the silicon-on-insulator (SOI) planar waveguides). Optical fibers are in principle of the symmetric type, and thus substrate modes (substrate rays) are not the case when optical fibers are considered.

2.9 Numerical aperture

By means of the critical angle discussed in 2.7 it is possible to explain, why there is only a limited interval of input angle values that allow an external ray of light to become a guided ray within the waveguide. There is a limiting input angle (value) that still ensures the occurrence of the guided rays. This limiting angle is called the acceptance angle of the waveguide. A dimensionless quantity that equals the sine function computed for the acceptance angle is called the numerical aperture (NA) of the waveguide. A waveguide under consideration (it needs to be of the symmetric type) together with an input ray and a propagating (guided) ray are shown in figure Fig. 2.4.

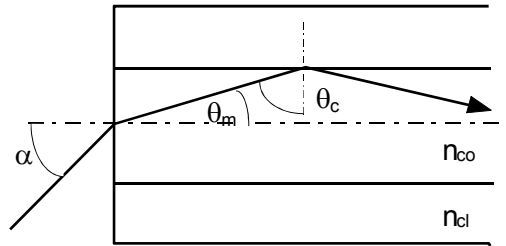


Fig. 2.4 Idea of the acceptance angle (see text).

One can also say that angle 2α (see figure) is the full angle of the cone of light rays that can pass through the system.

For a given optical waveguide (planar or fiber), numerical aperture value is calculated with the formula (Bass, 2001a), (Agrawal, 2002)

$$NA = \sin \alpha = \sqrt{n_{co}^2 - n_{cl}^2} \quad (2.6)$$

As we can see, NA only depends on waveguide's core and cladding refractive indexes. In particular, NA does not depend on e.g. waveguide's core width or, in the case of fibers, core diameter. A detailed derivation of (2.6) is presented below.

2.9.1 Derivation of the formula for NA

For clarity of the derivation, some of the formulas already discussed, will be repeated here.

From Snell's law (the law of refraction) we have

$$n_{co} \sin(\theta_c) = n_{cl} \sin(90^\circ) = n_{cl} \quad (2.7)$$

From the relation of the sum of angles in a triangle

$$\theta_m + \theta_c + 90^\circ = 180^\circ \quad (2.8)$$

$$n_{co} \sin(\theta_c) = n_{co} \sin(90^\circ - \theta_m) = n_{cl} \quad (2.9)$$

$$n_{co} \sin(90^\circ - \theta_m) = n_{cl} \quad (2.10)$$

From trigonometric identities

$$n_{co} \cos(\theta_m) = n_{cl} \quad (2.11)$$

$$n_{co} \sqrt{1 - \sin^2 \theta_m} = n_{cl} \quad (2.12)$$

Now, let us square both sides of the equation(2.12)

$$n_{co}^2 (1 - \sin^2 \theta_m) = n_{cl}^2 \quad (2.13)$$

$$n_{co}^2 - n_{co}^2 \sin^2 \theta_m = n_{cl}^2 \quad (2.14)$$

Applying the reflection law to the glass-air boundary

$$n_{co}^2 \sin^2 \theta_m = 1 \sin^2(\alpha) \quad (2.15)$$

$$n_{co}^2 - \sin^2 \alpha = n_{cl}^2 \quad (2.16)$$

Finally we arrive at

$$NA = \sin \alpha = \sqrt{n_{co}^2 - n_{cl}^2} \quad (2.17)$$

Applying an approximate relation

$$\Delta = \frac{n_{co} - n_{cl}}{n_{co}} = \frac{n_{co} - n_{cl}}{n_{co}} \frac{n_{co} + n_{cl}}{n_{co} + n_{cl}} \approx \frac{n_{co}^2 - n_{cl}^2}{2n_{co}^2} \quad (2.18)$$

$$n_{co}^2 - n_{cl}^2 = 2 n_{co}^2 \Delta \quad (2.19)$$

$$NA = n_{co} \sqrt{2\Delta} \quad (2.20)$$

The formula (2.18) is correct as long as $n_{co} \approx n_{cl}$, i.e. the difference between the core and the cladding refractive index values is small compared to the values of the indexes themselves. This assumption is called the weakly guiding approximation. The weakly guiding approximation always holds for the typical silica-glass telecommunication fibers.

2.10 Problems

Problem 1

Derive the formula for Numerical Aperture of a waveguide immersed in water.

Calculate Numerical Aperture and acceptance angle assuming that:

refractive index of water = 1.33

refractive index of the waveguide core = 1.5

relative difference of core-cladding indices = 1%

3 Wave theory of optical fibers

In this chapter we will discuss the Maxwell's equations applied to the electromagnetic wave propagation within a uniform, lossless medium. We will also go into some details of the derivation of the wave equation for the dielectric planar waveguide together with appropriate boundary conditions. The following lecture is based on three books (Garmire & Tamir, 1975; Midwinter, 1983; Tadeusiak A., Crosignani B., 1987).

3.1 Maxwell's field Equation (SI unit)

In order to describe the electromagnetic wave propagation in optical waveguide, one needs to use the Maxwell's equations. Generally speaking, they connect the electric field with the magnetic field. Maxwell's equations for a lossless, uniform medium take the form

$$\nabla \times \vec{E} = -\frac{\partial \vec{B}}{\partial t} \quad (3.1)$$

$$\nabla \times \vec{H} = \frac{\partial \vec{D}}{\partial t} + J \quad (3.2)$$

$$\nabla \cdot \vec{B} = 0 \quad (3.3)$$

$$\nabla \cdot \vec{D} = \rho \quad (3.4)$$

where E and H – vectors of electric and magnetic fields, respectively, B and D – vectors of magnetic and electric flux densities, respectively, J – (electric) current density, and t – time.

Medium in which electromagnetic wave propagates, may be described with the electric permittivity ϵ and the magnetic permeability μ , the quantities that connect field vectors with flux density vectors according to the equations

$$\vec{D} = \epsilon \vec{E} = \epsilon_0 \vec{E} + \vec{P} \quad (3.5)$$

$$\vec{B} = \mu \vec{H} = \mu_0 \vec{H} + \vec{M} \quad (3.6)$$

where P – vector of electric polarization of the medium, M – vector of magnetization of the medium, and ϵ_0 and μ_0 are electric permittivity of vacuum and magnetic permeability of vacuum, respectively.

In table Tab 3.1 there is a list of all the parameters (quantities) present in Maxwell's equations together with symbols that are customarily used in literature and with SI units. Table 3.2 lists values of physical constants present in Maxwell's equations.

Tab. 3.1 Physical quantities in Maxwell's equations.

Symbol	Physical quantity	SI unit	Abbreviation
E	Electric field strength	volts per meter	V / m
D	Electric displacement	coulombs per square meter	C / m ²
P	Polarization		
H	Magnetic field strength	amperes per meter	A / m
M	Magnetization		
j	Electric current density	amperes per square meter	A / m ²
B	Magnetic flux density or magnetic induction	tesla	T
ρ	Electric charge density	coulombs per cubic meter	C / m ³

σ	Electric conductivity	siemens per meter	S / m
μ	Permeability	henries per meter	H / m
ε	Permittivity	farads per meter	F / m

Tab. 3.2. Physical constants in Maxwell's equations.

Symbol	Physical quantity	Value
c	Speed of light in vacuum	2.998×10^8 m/s
μ_0	Permeability of a vacuum	$4\pi \times 10^{-7}$ H/m
ε_0	Permittivity of a vacuum	8.854×10^{-12} F/m

3.2 Differential operators and vectorial operator identities

Because electromagnetic field is a vector field, we will need a basic knowledge concerning some special mathematical operations, the so called vector operators, to fully understand and mathematically describe light propagation within optical waveguides. In definitions below, letters F and Φ will consequently be used to denote vector fields and scalar fields, respectively.

Let us first discuss the gradient operator. It is applied to vector fields and its result (for a given point of the vector field) is a vector. This vector expresses the speed and direction of the vector field variation. Gradient operator is usually denoted with the symbol ∇ , which is called „nabla“. This is the definition of the gradient operator (in Cartesian coordinates)

$$\nabla\Phi(x, y, z) = \frac{\partial\Phi}{\partial x}\hat{i} + \frac{\partial\Phi}{\partial y}\hat{j} + \frac{\partial\Phi}{\partial z}\hat{k} \quad (3.7)$$

Divergence operator acts on scalar fields. Its result (for a given point of the scalar field) is a scalar value (number). Generally speaking, the resulting number describes the flow of the scalar field from or to the given point. Divergence operator is denoted with nabla (∇) followed by the scalar product symbol (\cdot). The definition of the divergence operator (in Cartesian coordinates) is

$$\nabla \cdot \vec{F}(x, y, z) = \frac{\partial F_x}{\partial x} + \frac{\partial F_y}{\partial y} + \frac{\partial F_z}{\partial z} \quad (3.8)$$

Rotation operator, also called the curl operator, acts on vector fields and (for a given point of the vector field) it results in a vector. Speaking in general terms again, the resulting vector carries information about how much the vector field is “curled”. Rotation operator is denoted with nabla (∇) followed by the vector product symbol (\times). The definition of the rotation operator (in Cartesian coordinates) is.

$$\begin{aligned} \nabla \times \vec{F}(x, y, z) &= \begin{vmatrix} \hat{i} & \hat{j} & \hat{k} \\ \frac{\partial}{\partial x} & \frac{\partial}{\partial y} & \frac{\partial}{\partial z} \\ \vec{F}_x & \vec{F}_y & \vec{F}_z \end{vmatrix} \\ &= \left(\frac{\partial \vec{F}_z}{\partial y} - \frac{\partial \vec{F}_y}{\partial z} \right) \hat{i} + \left(\frac{\partial \vec{F}_x}{\partial z} - \frac{\partial \vec{F}_z}{\partial x} \right) \hat{j} + \left(\frac{\partial \vec{F}_y}{\partial x} - \frac{\partial \vec{F}_x}{\partial y} \right) \hat{k} \end{aligned} \quad (3.9)$$

Finally, the last operator used in dealing with Maxwell's equations, is the Laplace operator, which is defined (in Cartesian coordinates) with the following formula

$$\nabla^2\Phi = \frac{\partial^2\Phi}{\partial x^2} + \frac{\partial^2\Phi}{\partial y^2} + \frac{\partial^2\Phi}{\partial z^2} \quad (3.10)$$

There are many formulas, the so called vector calculus identities, that describe mutual relations between operators we have discussed above. Out of a larger set of vector calculus identities, four are of special significance (usefulness) in Maxwell's equations-related calculations. The identities are:

- o rotation of vector's F rotation equals the gradient of divergence minus the vector laplacian

$$\text{rot rot}\vec{F} = \nabla \times (\nabla \times \vec{F}) = \nabla(\nabla \cdot \vec{F}) - \nabla^2\vec{F} \quad (3.11)$$

- o **divergence** of vector product of vectors F and G equals the scalar product of vector G and rotation of **vector F minus scalar product of vector F and rotation of vector G**

$$\nabla \cdot (\vec{F} \times \vec{G}) = \vec{G} \cdot (\nabla \times \vec{F}) - \vec{F} \cdot (\nabla \times \vec{G}) \quad (3.12)$$

- o rotation of scalar product of scalar Φ and vector F equals the rotation of vector F multiplied by scalar Φ plus the rotation of vector product of scalar Φ and vector F

$$\nabla \times (\Phi\vec{F}) = \Phi\nabla \times \vec{F} + \nabla\Phi \times \vec{F} \quad (3.13)$$

- o divergence of scalar product of scalar Φ and vector F equals the divergence of vector F multiplied by scalar Φ plus divergence of scalar Φ multiplied by vector F

$$\nabla \cdot (\Phi\vec{F}) = \Phi\nabla \cdot \vec{F} + \vec{F} \cdot \nabla\Phi \quad (3.14)$$

3.3 Boundary conditions

Maxwell's equations discussed in 3.1 describe the electromagnetic wave propagation in an infinite medium. In real-life problems, however, propagation media are finite (of finite dimensions) and thus a problem of a boundary between two different media arises. A model situation is depicted in figure Fig. 3.1. A fundamental tool in dealing with the media boundary problem is the Ostrogradsky-Gauss theorem (also known as the divergence theorem). It relates the outward flow of a vector field on a surface to the behavior of the vector field inside the surface. The theorem states this relation in the following way

$$\iiint_V \nabla \cdot \vec{F} dV = \iint_S \vec{F} \cdot d\vec{S} \quad (3.15)$$

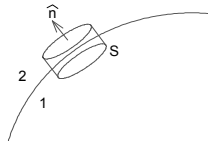


Fig. 3.1 Refractive index change at the boundary between two different materials – boundary conditions, where S is the boundary of V oriented by outward-pointing normal.

3.3.1 Bound. conditions for field B

Using the third Maxwell's equation (3.3), which states that there are no point sources of magnetic field (otherwise divergence of B could be different than zero) and using the Ostrogradsky-Gauss theorem (3.15), we determine the magnetic flux density for each of the media

$$0 = \int_V \nabla \cdot \vec{B} dV = \int_S \vec{B} d\vec{S} = \hat{n} \cdot \vec{B}_2 - \hat{n} \cdot \vec{B}_1 = \hat{n} \cdot (\vec{B}_2 - \vec{B}_1) \quad (3.16)$$

In calculations, we assume the integrals over volume boundaries (i.e. over surfaces bounding the volume) to be zero.

3.3.2 Boundary condition for field D

We now apply a similar procedure to the electric field but this time the fourth Maxwell's equation (3.4) is used and, in analogy to the magnetic field, we find the boundary conditions for the electric flux density

$$\sigma = \int \rho dV = \hat{n} \cdot (D_2 - D_1) \quad (3.17)$$

3.4 Boundary conditions for field strength vectors

Boundary conditions for the electric field vector E and the magnetic field vector H we will find by utilizing the Stokes' theorem. Stokes' theorem relates the surface integral of the curl (rotation) of a vector field over a surface S to the line integral of the vector field over its boundary

$$\iint_S \nabla \times \vec{F} \cdot d\vec{S} = \oint_L \vec{F} \cdot d\vec{l} \quad (3.18)$$

This idea is illustrated in figure Fig. 3.2.

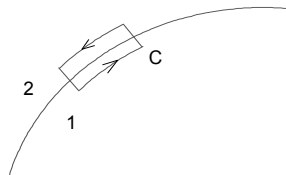


Fig. 3.2 The Stokes' theorem idea - the surface integral of the curl of a vector field over a surface S to the line integral of the vector field over its boundary.

Starting off with the Maxwell's equation relating the rotations of magnetic and electric fields (3.2), we can use the Stokes' theorem for deriving the boundary conditions for the magnetic field vector. Integrating both sides of the equation over the surface, we make the left-hand side of the equation to take shape of Stokes' theorem. Due to a small area of integration, the surface integral of the electric density flux differential equals zero. Let us designate by K the surface density of current. Then, the boundary conditions so derived are given by (3.20).

Taking an integral over a surface

$$\int_S \nabla \times \vec{H} dS = \int_S \left(\frac{\partial \vec{D}}{\partial t} + \vec{j} \right) dS \quad (3.19)$$

and applying the Stokes' theorem to (3.19), we get

$$n \times (\vec{H}_1 - \vec{H}_2) = \vec{K} \quad (3.20)$$

Boundary condition for E field

$$n \times (\vec{E}_1 - \vec{E}_2) = 0 \quad (3.21)$$

The boundary conditions derived above, fall into two groups according to the vector's direction. The magnetic flux density and the electric flux density vectors are normal components (3.16) (3.17). The electric field and the magnetic field vectors are tangential components (3.20) (3.21).

3.5 Derivation of electromagnetic wave equation (homogeneous medium)

We will use the first Maxwell's equation (3.1) in order to derive the wave equation for a uniform medium. Acting with the curl operator upon the first Maxwell's equation

$$\nabla \times (\nabla \times \vec{E}) = \nabla \times \left(-\frac{\partial \vec{B}}{\partial t} \right) \quad (3.22)$$

Then, transforming the left-hand side of (3.22) with the vector identity (3.11) and assuming that there are no space charges ($\nabla \cdot \vec{E} = 0$) and that the medium is homogeneous and isotropic ($n = \text{const}$) we obtain

$$\nabla \times \left(-\frac{\partial \vec{B}}{\partial t} \right) = \nabla \times \left(-\mu \frac{\partial \vec{H}}{\partial t} \right) = -\mu \frac{\partial}{\partial t} (\nabla \times \vec{H}) = -\mu \varepsilon \frac{\partial^2 \vec{E}}{\partial t^2} \quad (3.23)$$

Now, for curl H , we substitute the second Maxwell's equation (3.2) and this way we have derived the electric field wave equation

$$\nabla^2 \vec{E} - \mu \varepsilon \frac{\partial^2 \vec{E}}{\partial t^2} = 0 \quad (3.24)$$

Starting off with the second Maxwell's equation (3.2) and then following a procedure analogous to the one described above, the magnetic field wave equation can be derived

$$\nabla^2 \vec{H} - \mu \varepsilon \frac{\partial^2 \vec{H}}{\partial t^2} = 0 \quad (3.25)$$

One of the possible (allowable) solutions to both the wave equations is the plane wave. The plane wave is mathematically described as

$$\Psi = e^{i(\omega t - \vec{k} \cdot \vec{r})} \quad (3.26)$$

where k is the wave-vector's projection on the propagation direction Z . Length of the vector k is

$$|k| = \omega\sqrt{\mu\epsilon} \quad (3.27)$$

3.6 Simplifying wave equation for the planewave solution

In planar waveguides, the electromagnetic wave propagates within the so called guiding layer, i.e. a medium having the refractive index value higher than that of the surrounding media. Schematic view of planar waveguide is shown in figure Fig. 3.3.

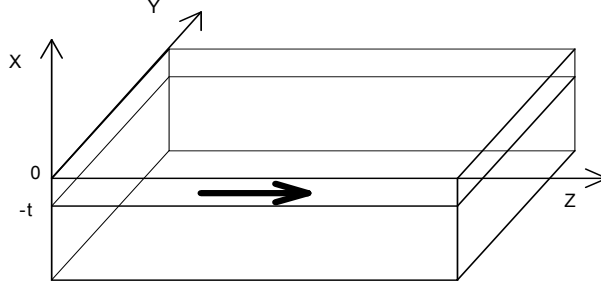


Fig. 3.3 Planar waveguide structure. The layer of the thickness t is the guiding layer. Light propagation direction along the direction Z is indicated with arrow.

One of the solutions to the wave equation within structures of the above type, is the plane wave given as (similarly to (3.26))

$$E = E_0 e^{i(\omega t - \beta z)} \quad (3.28)$$

β – propagation constant (wave-vector's projection on the propagation direction Z).

Light can propagate within planar waveguide in two types of (spatial) modes both of which have the Z -component of the electric or magnetic field, respectively, equaling zero. These are the so called transverse electric (TE) and transverse magnetic modes (TM). In TE modes, $E_z = 0$ and $H_z \neq 0$, and in TM modes, $H_z = 0$ and $E_z \neq 0$.

Let us assume a TE-type solution to the wave equation in planar structure

$$E_y = E_{0y}(x) \exp[i(\omega t - \beta z)] \quad (3.29)$$

On substituting the assumed solution into the wave equation we obtain

$$\frac{\partial^2 E_y}{\partial x^2} + \frac{\partial^2 E_y}{\partial y^2} + \frac{\partial^2 E_y}{\partial z^2} - \mu\epsilon \frac{\partial^2 E_y}{\partial t^2} = 0 \quad (3.30)$$

For the E_y component, we calculate the second-order partial derivatives in space

$$\begin{aligned} \frac{\partial^2 E_y}{\partial x^2} &= \frac{\partial}{\partial x} \left\{ \frac{\partial}{\partial x} E_{0y}(x) \exp[i(\omega t - \beta z)] \right\} = \frac{\partial}{\partial x} \left\{ \exp[i(\omega t - \beta z)] \frac{\partial E_{0y}(x)}{\partial x} \right\} \\ &= \frac{\partial^2 E_{0y}(x)}{\partial x^2} \exp[i(\omega t - \beta z)] \end{aligned} \quad (3.31)$$

$$\frac{\partial^2 E_y}{\partial y^2} = \frac{\partial}{\partial y} \left\{ \frac{\partial}{\partial y} E_{0y}(x) \exp[i(\omega t - \beta z)] \right\} = 0 \quad (3.32)$$

$$\begin{aligned}\frac{\partial^2 E_y}{\partial z^2} &= \frac{\partial}{\partial z} \left\{ \frac{\partial}{\partial z} E_{0y}(x) \exp[i(\omega t - \beta z)] \right\} = \frac{\partial}{\partial z} \left\{ -i\beta E_{0y}(x) \exp[i(\omega t - \beta z)] \right\} \\ &= -\beta^2 E_{0y}(x) \exp[i(\omega t - \beta z)]\end{aligned}\quad (3.33)$$

and in time

$$\begin{aligned}\frac{\partial^2 E_y}{\partial t^2} &= \frac{\partial}{\partial t} \left\{ \frac{\partial}{\partial t} E_{0y}(x) \exp[i(\omega t - \beta z)] \right\} = \frac{\partial}{\partial t} \left\{ i\omega E_{0y}(x) \exp[i(\omega t - \beta z)] \right\} \\ &= -\omega^2 E_{0y}(x) \exp[i(\omega t - \beta z)]\end{aligned}\quad (3.34)$$

After substituting the partial derivatives (3.31), (3.32), (3.33), and (3.34) into (3.30), we get

$$\begin{aligned}\frac{\partial^2 E_{0y}(x)}{\partial x^2} \exp[i(\omega t - \beta z)] + 0 - \beta^2 E_{0y}(x) \exp[i(\omega t - \beta z)] \\ - \mu\epsilon \{-\omega^2 E_{0y}(x) \exp[i(\omega t - \beta z)]\} = 0\end{aligned}\quad (3.35)$$

Using the TE-type plane wave (3.29), we reduce (3.35) to the following form

$$\frac{\partial^2 E(x)}{\partial x^2} - [\beta^2 - \mu\epsilon\omega^2]E(x) = 0\quad (3.36)$$

With the following dependencies in mind

$$n = \frac{c}{v}, c = \frac{1}{\sqrt{\mu_0\epsilon_0}}, v = \frac{1}{\sqrt{\mu\epsilon}}, \lambda_0 = cT\quad (3.37)$$

we have

$$k = \frac{2\pi}{\lambda} = \frac{2\pi}{\lambda_0} n = \frac{\omega}{c} n = \frac{\omega}{v}\quad (3.38)$$

Using (3.38) we can express the product of magnetic permeability, electric permittivity, and wave frequency squared, as the wave-vector squared

$$\mu\epsilon\omega^2 = \left(\frac{\omega}{\frac{1}{\sqrt{\mu\epsilon}}} \right)^2 = \left(\frac{\omega}{v} \right)^2 = k^2\quad (3.39)$$

Finally, we arrive at the final form of the wave equation for TE modes of planar waveguide

$$\frac{\partial^2 E_{0y}}{\partial x^2} + [k^2 - \beta^2]E_{0y} = 0\quad (3.40)$$

In the next step, boundary conditions will be found for a guided TE mode of planar structure. Each TE mode has only one non-zero component of the electric field vector (E_y) and two non-zero components of the magnetic field vector (H_z and H_x). From equation (3.21), the boundary conditions for E_y are

$$E_{0y1} = E_{0y2} \quad (3.41)$$

Boundary conditions for the two magnetic field components H_z and H_x can be found from (3.20), with the surface current density $K = 0$ assumed (zero current density is correct, as we deal with dielectrics, and not with conducting materials). We are interested in the component H_z

$$E_y(x, z, t) = E_{0y}(x)e^{i(\omega t - \beta z)} \quad (3.42)$$

From the first of Maxwell's equations (3.1) and the definition of the curl (rotation) operator (3.9)

$$\frac{\partial E_y}{\partial x} - \frac{\partial E_x}{\partial y} = -\frac{\partial B_z}{\partial t} \quad (3.43)$$

Substituting the formula (3.6) for the magnetic flux density

$$\frac{\partial E_{0y}}{\partial x} - \frac{\partial E_{0x}}{\partial y} = -i\omega\mu H_{0z} \quad (3.44)$$

Calculating H_{0z} , from (3.44), we get

$$H_{0z} = -\frac{1}{i\omega\mu} \frac{\partial E_{0y}}{\partial x} = \frac{i}{\omega\mu} \frac{\partial E_{0y}}{\partial x} \quad (3.45)$$

Due to magnetic field vector continuity (3.46) at the boundary between two media

$$H_{0z1} = H_{0z2} \quad (3.46)$$

Finally, the searched boundary conditions are (3.41) and

$$\frac{\partial E_{0y1}}{\partial x} = \frac{\partial E_{0y2}}{\partial x} \quad (3.47)$$

4 Mode equation for a planar waveguide

4.1 Wave equation for a planar waveguide.

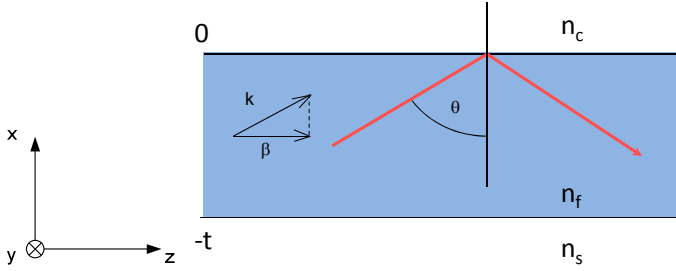


Fig. 4.1 Light propagation in a planar waveguide structure – the total internal reflection.

Let us consider a planar waveguide structure consisting of three layers as presented in figure Fig. 4.1. Let us assume that layers of the refractive indexes n_1 and n_3 are semi-infinite, i.e. they extend to infinity in the directions $+x$ and $-x$, respectively. An advantage of such an assumption is the lack of reflections along the x -direction anywhere except for the $n_c - n_f$ and the $n_f - n_s$ boundaries. Now, substituting, into the wave equation

$$\nabla^2 \vec{E} - \mu \varepsilon \frac{\partial^2 \vec{E}}{\partial t^2} = 0 \quad (4.1)$$

a solution of the form (plane wave)

$$\vec{E} = E_0(x, y, z) \exp[i(\omega t - \vec{k} \cdot \vec{r})] \quad (4.2)$$

we get

$$\frac{\partial^2 \vec{E}}{\partial x^2} - [k^2 - \beta^2] E = 0 \quad (4.3)$$

where

$$k = \frac{2\pi}{\lambda} = \frac{2\pi}{\lambda_0} n = \frac{\omega}{c} n \quad (4.4)$$

$$\beta = k_0 n_f \sin(\theta) \quad (4.5)$$

which is exactly the result already discussed in Chapter 3. In a TE-polarized plane wave propagating along the z -direction, there are three nonzero field vector components: E_y , H_x i H_z . Considering only the electric field, we omit the magnetic field components along the z - and x -directions. Moreover, the electric field component E_y does not depend on y and z because waveguide layers extend to infinity along these directions, thus no reflections or standing waves can occur. Spatial distribution of E_y along the x -direction in the planar waveguide under consideration (figure Fig. 4.1) takes the form of a system of three equations involving four unknowns (variables) (Hunsperger, 2009)

$$E_y(x) = \begin{cases} C e^{-qx} & 0 \leq x \leq \infty \\ C \left[\cos(hx) - \frac{q}{h} \sin(hx) \right] & -t \leq x \leq 0 \\ C \left[\cos(hx) + \frac{q}{h} \sin(hx) \right] e^{p(x+t)} & -\infty \leq x \leq -t \end{cases} \quad (4.6)$$

On substituting the equation (4.2) into (4.1) and using the expression (4.6), the coefficients p , q , and h can be determined (Hunsperger, 2009)

$$\begin{aligned} p^2 &= \beta^2 - n_s^2 k_0^2 \\ q^2 &= \beta^2 - n_c^2 k_0^2 \\ h^2 &= n_f^2 k_0^2 - \beta^2 \end{aligned} \quad (4.7)$$

4.2 TE and TM modes

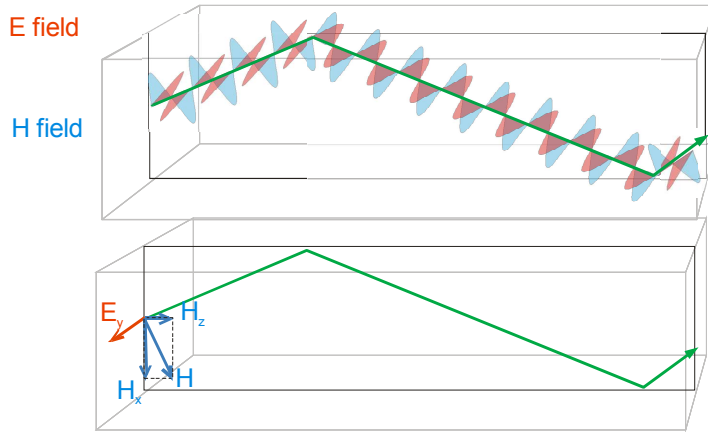


Fig. 4.2 Electromagnetic wave propagation in a planar waveguide. There is shown the TE-polarization case (1) and the nonzero components of the electric and magnetic field vectors (2).

A schematic depiction of TE-polarized mode propagation in a planar waveguide is shown in figure Fig. 4.2. The red and the blue colors represent the electric and the magnetic field vector components, respectively.

As a reminder, electromagnetic waves propagating in planar waveguides fall into two categories:

- the TE modes (TE-polarized modes) with the nonzero components: E_y, H_x, H_z
- the TM modes (TM-polarized modes) with the nonzero components: H_y, E_x, E_z

4.3 Electrical field distribution for the first three modes of a planar waveguide

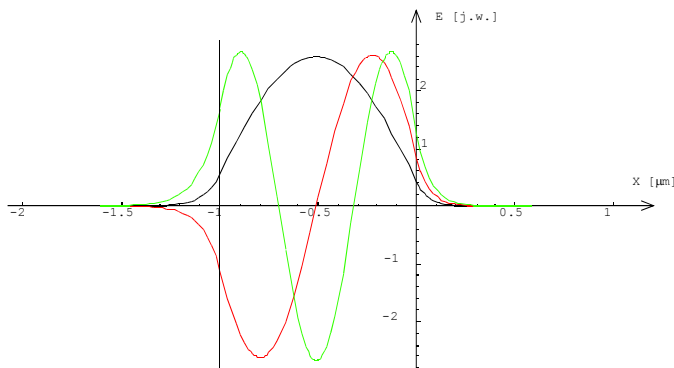


Fig. 4.3 Electric field distribution for the first three lowest-order modes of a planar waveguide.

The figure Fig. 4.3 presents the E_y spatial distributions for the three lowest-order modes of a planar waveguide. The planar waveguide parameters used in calculations are: $n_s = 1.5$, $n_f = 2$, $n_c = 1$ and the light wavelength is $\lambda = 633$ nm.

4.4 Boundary conditions

Boundary conditions were discussed in Chapter 3.

4.5 Boundary conditions for a planar waveguide

$$\begin{cases} E_{0y}^c = E_{0y}^f \Big|_{x=0} \\ E_{0y}^f = E_{0y}^s \Big|_{x=-t} \end{cases} \quad (4.8)$$

$$\begin{cases} \frac{\partial E_{0y}^c}{\partial x} = \frac{\partial E_{0y}^f}{\partial x} \Big|_{x=0} \\ \frac{\partial E_{0y}^f}{\partial x} = \frac{\partial E_{0y}^s}{\partial x} \Big|_{x=-t} \end{cases} \quad (4.9)$$

Planar waveguide boundary conditions (derived in Chapter 3) – field continuity at boundaries between the waveguide layers (dielectric boundaries) $n_c - n_f$ and $n_f - n_s$.

4.6 Boundary conditions for a planar waveguide – verification

By substituting the equation (4.6) into the boundary conditions from the system of equations (4.8), we can check whether the solutions assumed are correct. At the dielectric boundary $n_c - n_f$, i.e. at the point $x = 0$, the value of the electric field vector y -component equals C . At the opposite side of the n_f layer (guiding layer), i.e. at the $n_f - n_s$ boundary ($x = -t$), the electric field takes the value of $C \left[\cos(ht) - \frac{q}{h} \sin(ht) \right]$. A condition from the system of equations (4.8) is met, thus the correctness of the solutions assumed has been confirmed.

The second boundary condition enforces the field continuity at the dielectric boundaries $x = 0$ i $x = -t$. First derivative of the electric field distribution at the point $x = 0$ equals $-qC$ and it meets the condition from (4.9). Thus, constants present in the equations are correct.

4.7 Derivation of the mode equation

Making the electric field continuity condition (4.9) be true at the dielectric boundary $n_f - n_s$, we derive the mode equation

$$h \sin(ht) - q \cos(ht) = p \left[\cos(ht) + \frac{q}{h} \sin(ht) \right] \quad (4.10)$$

4.8 Transformation of mode equation into a tangent based form

Dividing both sides of the equation (4.10) by $\cos(ht)$, we get

$$\tan(ht) - \frac{q}{h} = \frac{p}{h} + \frac{pq}{h^2} \tan(ht) \quad (4.11)$$

Then, by grouping like terms

$$\tan(ht) - \frac{pq}{h^2} \tan(ht) = \frac{p}{h} + \frac{q}{h} \quad (4.12)$$

and applying some straightforward algebraic manipulations, we arrive at a mode equation form that involves the tangent (tan) function (Hunsperger, 2009)

$$\tan(ht) = \frac{p+q}{h(1-pq/h^2)} \quad (4.13)$$

The mode equation form shown above will be later used in the derivation of the additive form of the mode equation.

4.9 Additive form of mode equation

In order to find all the mode equation solutions that represent all the possible waveguide modes, one needs to transform the tangent-function form (4.13) into the additive form (Hunsperger, 2009)

$$2k_0 n_f t \cos(\theta) - 2\Phi_s - 2\Phi_c = 2\pi m, \quad m = 0, 1, 2, \dots \quad (4.14)$$

where m is the waveguide mode number, Φ_s and Φ_c are the Fresnel coefficients. Both the coefficients describe the electromagnetic wave phase shift due to reflection at the dielectric boundaries $n_c - n_f$ and $n_f - n_s$.

We transform the tangent-function form of the mode equation into a form that will allow the application of the following trigonometric identity

$$\arctan\left(\frac{u+v}{1-uv}\right) = \arctan u + \arctan v \quad (4.15)$$

$$\tan(ht) = \frac{p+q}{h(1-pq/h^2)} = \frac{\frac{1}{h}(p+q)}{\left(1 - \frac{pq}{h^2}\right)} = \frac{\frac{p}{h} + \frac{q}{h}}{\left(1 - \frac{p}{h} \frac{q}{h}\right)} \quad (4.16)$$

4.10 Derivation of additive form of mode equation

Let us derive the additive form of the mode equation. Utilizing the arctangent (arctan) function properties, the left-hand side of (4.16) takes the form

$$L \arctan[\tan(ht)] = ht \pm m\pi, \quad (4.17)$$

Then, by handling the right-hand side of the equation in a similar way and applying the trigonometric identity (4.15), we get

$$R \arctan \left[\frac{\frac{p}{h} + \frac{q}{h}}{\left(1 - \frac{p}{h} \frac{q}{h}\right)} \right] = \arctan \left(\frac{p}{h} \right) + \arctan \left(\frac{q}{h} \right) \quad (4.18)$$

Finally, after grouping like terms, we arrive at the additive form of the planar waveguide mode equation

$$ht \pm m\pi = \arctan \left(\frac{p}{h} \right) + \arctan \left(\frac{q}{h} \right) \quad (4.19)$$

$$ht - \arctan \left(\frac{p}{h} \right) - \arctan \left(\frac{q}{h} \right) = \pi n \quad (4.20)$$

4.11 Total internal reflection is accompanied by a phase shift – TE mode (Fresnel coefficients)

Using the formulas (4.7), we will determine the Fresnel coefficients for the additive form of the planar waveguide mode equation (4.14). From (4.20) we can see, that the Fresnel coefficient Φ_s equals the arctangent of the quotient of p and h

$$\frac{p}{h} = \frac{\sqrt{\beta^2 - n_s^2 k_0^2}}{\sqrt{n_f^2 k_0^2 - \beta^2}} \quad (4.21)$$

Substituting the propagation constant given by (4.5) and applying some straightforward trigonometric manipulations, we get a formula for the Fresnel coefficient Φ_s

$$\frac{p}{h} = \frac{\sqrt{n_f^2 \sin^2 \theta k_0^2 - n_s^2 k_0^2}}{\sqrt{n_f^2 k_0^2 - n_f^2 \sin^2 \theta k_0^2}} = \frac{\sqrt{n_f^2 \sin^2 \theta - n_s^2}}{\sqrt{n_f^2 (1 - \sin^2 \theta)}} = \frac{\sqrt{n_f^2 \sin^2 \theta - n_s^2}}{n_f \cos \theta} \quad (4.22)$$

$$\Phi_s = \arctan \left(\frac{p}{h} \right) = \arctan \left(\frac{\sqrt{n_f^2 \sin^2 \theta - n_s^2}}{n_f \cos \theta} \right) \quad (4.23)$$

In an analogous way, the coefficient Φ_c can be determined

$$\frac{q}{h} = \frac{\sqrt{\beta^2 - n_c^2 k_0^2}}{\sqrt{n_f^2 k_0^2 - \beta^2}} \quad (4.24)$$

$$\frac{q}{h} = \frac{\sqrt{n_f^2 \sin^2 \theta k_0^2 - n_c^2 k_0^2}}{\sqrt{n_f^2 k_0^2 - n_f^2 \sin^2 \theta k_0^2}} = \frac{\sqrt{n_f^2 \sin^2 \theta - n_c^2}}{\sqrt{n_f^2 (1 - \sin^2 \theta)}} = \frac{\sqrt{n_f^2 \sin^2 \theta - n_c^2}}{n_f \cos \theta} \quad (4.25)$$

$$\Phi_c = \arctan \left(\frac{q}{h} \right) = \arctan \left(\frac{\sqrt{n_f^2 \sin^2 \theta - n_c^2}}{n_f \cos \theta} \right) \quad (4.26)$$

4.12 ht component

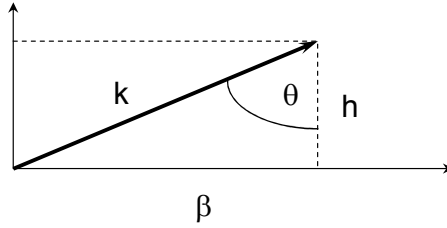


Fig. 4.4 Geometrical (vectorial) dependence between propagation constants in a planar waveguide.

In order to derive a complete additive form of the planar waveguide mode equation, one needs to calculate the ht expression present in the equation (4.20). It can be done by utilizing the right triangle (right-angled triangle) properties. Let us identify the h and β as triangle sides and the k as triangle hypotenuse, as depicted in figure Fig. 4.4. Then, the coefficient h is given by

$$h^2 = n_j^2 k_0^2 - \beta^2 = k^2 - \beta^2 \quad (4.27)$$

On the other hand, the length of the triangle side identified as h can also be related to angle θ (see figure Fig. 4.4). This is done with the following formula

$$h = k \cos(\theta) = k_0 n \cos(\theta) \quad (4.28)$$

Multiplying both sides of (4.28) by t , we get the expression for ht

$$ht = tk_0 n \cos(\theta) \quad (4.29)$$

Now, it is enough to substitute the expression for ht into (4.20)

$$2k_0 n_j t \cos(\theta) - 2 \arctan \frac{q}{h} - 2 \arctan \frac{p}{h} = 2\pi m, \quad m = 0, 1, 2, \dots \quad (4.30)$$

Finally, substituting the Fresnel coefficients given by (4.23) and (4.26), we arrive at a complete additive form of the planar waveguide mode equation

$$2k_0 n_j t \cos(\theta) - 2\Phi_s - 2\Phi_c = 2\pi m, \quad m = 0, 1, 2, \dots \quad (4.31)$$

4.13 Mode diagram: Neff or angle

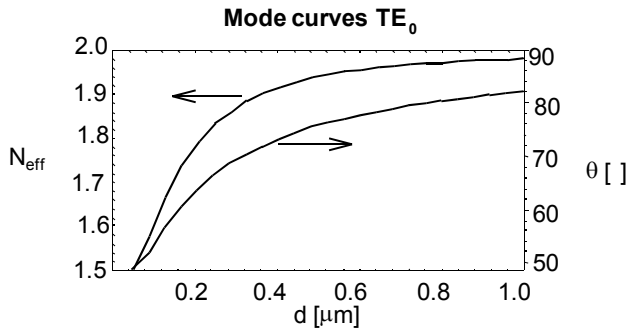


Fig. 4.5 Mode curves $N_{eff}(d)$ and $\theta(d)$.

Let us compare the mode curves defined as $N_{eff}(d)$ and $\theta(d)$. Such a comparison visible in figure Fig. 4.5 was plotted for a planar waveguide of the following parameters: $n_f = 2$, $n_s = 1.5$, $n_c = 1$. For the increasing values of the waveguide thickness d , the waveguide mode effective refractive index N_{eff} increases. In a similar way behaves the angle θ that is the angle at which a given mode propagates. The higher the waveguide thickness, the higher the propagation angle (θ).

4.14 Mode diagram: TE and TM

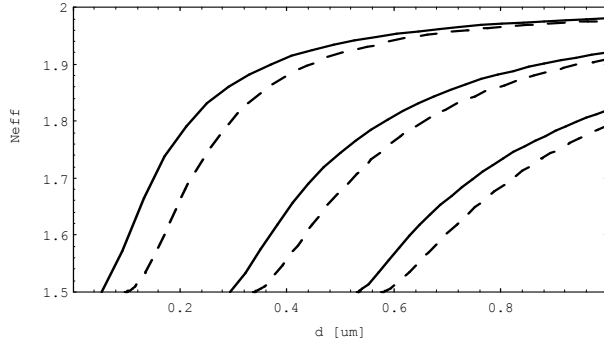


Fig. 4.6 Mode curves $N_{eff}(d)$ calculated for the TE-polarized (solid lines) and the TM-polarized (dashed lines) planar waveguide modes.

Figure Fig. 4.6 presents a comparison of the behavior of $N_{eff}(d)$ for the TE-polarized and the TM-polarized three lowest-order planar waveguide modes. The calculations were performed for a waveguide of the parameters: $n_f = 2$, $n_s = 1.5$, $n_c = 1$. On a closer inspection of the diagram, it becomes clear that up to the thickness of about $0.3 \mu\text{m}$, the planar waveguide under consideration remains single-mode (supports only one mode). In other words, for the thickness values higher than the mentioned $0.3 \mu\text{m}$, the effective refractive index of the second-order mode becomes higher than the substrate refractive index and the second-order mode can propagate in the waveguide. Waveguide modes of higher orders become guided (i.e. able to propagate in the waveguide) in a similar fashion as we have just discussed for the second-order mode. To summarize, the thicker the waveguide, the higher the number of guided modes.

4.15 Mode measurements - prism coupler method

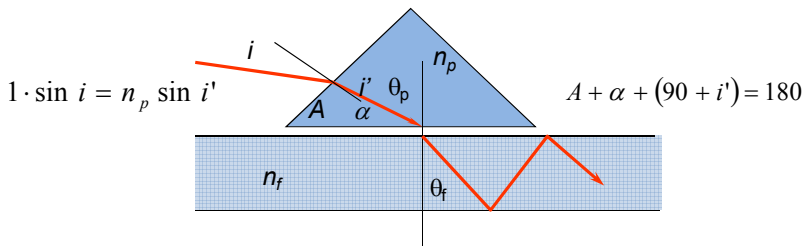


Fig. 4.7 Idea of the prism coupling (prism coupler method).

Coupling light into a thin structure of a planar waveguide is an important problem in the measurements of the planar waveguide guided modes. Among a number of possible methods of light coupling into sub-micrometer waveguide structures, one of the most popular is the so called prism coupling. In prism coupling, light enters the planar waveguide through waveguide's top surface. As shown in figure Fig. 4.7, the prism is positioned above the planar waveguide. A thin air-gap exists between prism base and waveguide top surface. The air-gap thickness is of the order of half the light wavelength or less. Laser light enters the prism and undergoes the total internal reflection at prism base. An evanescent wave that is created in the total internal

reflection phenomenon penetrates the air gap and thus light can be coupled into the waveguide. (Chang, 2009)

By using a triangle property (triangle angles sum up to 180°) and some other basic geometrical relationships, we can determine angle θ_p at which light impinges on (hits) the prism base surface

$$\theta_p = 90 - \alpha = 90 - [180 - A - (90 + i')] = A + i' \quad (4.32)$$

Utilizing the Snell's law (law of refraction) and some trigonometric identities, we first calculate angle i'

$$\sin i' = \frac{\sin i}{n_p} \quad (4.33)$$

$$i' = \arcsin\left(\frac{\sin i}{n_p}\right) \quad (4.34)$$

Then, after substituting (4.34) into (4.32), we get a formula for angle θ_p

$$\theta_p = A + \arcsin\left(\frac{\sin i}{n_p}\right) \quad (4.35)$$

4.16 Effective refractive index evaluation

The guided mode effective refractive index obeys the following relation

$$n_p \sin \theta_p = n_f \sin \theta_f = N_{eff} \quad (4.36)$$

Thus, by substituting the θ_p given by (4.35) into (4.36), we can express N_{eff} as

$$N_{eff} = n_p \cdot \sin\left[A + \arcsin\left(\frac{\sin i}{n_p}\right)\right] \quad (4.37)$$

This means that the guided mode effective refractive index can be determined by means of measuring angle i at which light is coupled into the prism.

4.17 Mode separation TE-TM, use of Maxwell's equations

Maxwell's equations were discussed in detail in Chapter 3.

5 Optical and mechanical properties of optical fibers

The following chapter is based on the ITU standard: ITU-T G.650 "Definition and Test Methods for the Relevant Parameters of Single-Mode Fibers" - Series G: Transmission Systems and Media, Digital Systems and Networks Transmission Media Characteristics - Optical Fiber by International Telecommunication Union.

Telecommunication optical cables are highly developed transmission media, optimized for communication application. The fibers are characterized by multiple parameters. The main source of definitions of this parameters is a series of standards published by International Telecommunication Union. The short list of the most important standard is given below.

- G.650 Definition and test methods for the relevant parameters of single-mode fibers
- G.651 Characteristics of a 50/125 μm multimode graded index optical fiber cable
- G.652 Characteristics of a single-mode optical fiber cable
- G.653 Characteristics of a dispersion-shifted single-mode optical fiber cable
- G.654 Characteristics of a 1550 nm wavelength loss-minimized single-mode optical fiber cable
- G.655 Characteristics of a non-zero dispersion single mode optical fiber cable

In this lecture the main properties of optical fibers are described and their definitions are given. In another lecture measurement methods of this parameters will be given.

Parameters of optical fiber waveguides are classified into three main groups:

- Optical parameters
- Geometrical parameters
- Mechanical parameters

According to this classification standardized parameters of the single mode optical fiber can be classified as follows:

- Optical parameters
 - Attenuation
 - Chromatic dispersion
 - Mode field diameter
 - Cut-off wavelength
 - Polarization mode dispersion
- Geometrical parameters
 - Cladding diameter, mode field concentricity error and cladding non-circularity
- Mechanical parameters
 - Proof testing

The most important parameters will be covered in the following chapters.

5.1 Mode field diameter

The mode field is the single-mode field distribution of the LP₀₁ mode giving rise to a spatial intensity distribution in the fiber. The Mode Field Diameter (MFD) $2w$ represents a measure of the transverse extent of the electromagnetic field intensity of the mode in a fiber cross-section. For the reason of simplification of measurement method of this parameter, it is defined from the far field intensity distribution $F^2(\theta)$, θ being the far-field angle, through the following equation:

$$2w = \frac{\lambda}{\pi} \left[\frac{2 \int_0^{\frac{\pi}{2}} F^2(\theta) \sin \theta \cos \theta d\theta}{\int_0^{\frac{\pi}{2}} F^2(\theta) \sin^3 \theta \cos \theta d\theta} \right]^{\frac{1}{2}} \quad (5.1)$$

Theoretical ground for this equation, is a knowledge that far field distribution of optical field is related to the near field distribution (i.e. light intensity distribution at the output face of the fiber) through the Fourier transform. [Iizuka K. Engineering Optics. Springer; 1985].

5.1.1 Other mode-field parameters

The **mode field centre** is the position of the centroid of the spatial intensity distribution in the fiber. The centroid is located at r_c and is the normalized intensity-weighted integral of the position vector r .

$$r_c = \frac{\iint_{Area} rI(r)dA}{\iint_{Area} I(r)dA} \quad (5.2)$$

The **mode field concentricity error** is the distance between the mode field center and the cladding center.

5.2 Cladding diameter, mode field concentricity error and cladding non-circularity

- By definition cladding is the outermost region of constant refractive index in the fiber cross-section.
- Cladding centre: for a cross-section of an optical fiber it is the centre of that circle which best fits the outer limit of the cladding.
- Cladding diameter is the diameter of the circle defining the cladding centre.
- Cladding diameter deviation is the difference between the actual and the nominal values of the cladding diameter.
- Cladding tolerance field: for a cross-section of an optical fiber it is the region between the circle circumscribing the outer limit of the cladding, and the largest circle, concentric with the first one, that fits into the outer limit of the cladding. Both circles shall have the same centre as the cladding.
- Cladding non-circularity: the difference between the diameters of the two circles defined by the cladding tolerance field divided by the nominal cladding diameter.

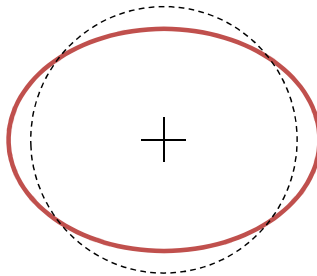


Fig. 5.1 Cladding diameter, cladding center and cladding non circularity

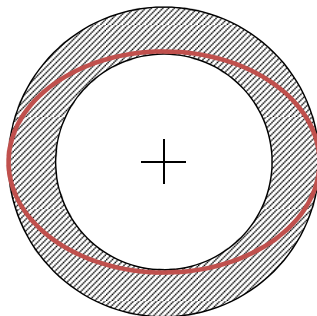


Fig. 5.2 Cladding non-circularity and cladding diameter deviation

5.3 Cut-off wavelength - theoretical definition

Theoretical cut-off wavelength is the shortest wavelength at which a single mode can propagate in a single-mode fiber. At wavelengths below the theoretical cut-off wavelength, several modes propagate and the fiber is no longer single-mode but multimode.

In optical fibers, the change from multimode to single-mode behavior does not occur at an isolated wavelength, but rather smoothly over a range of wavelengths. Cut-off wavelength is defined as the wavelength greater than the wavelength for which the ratio between the total power, including launched higher order modes and the fundamental mode power has decreased to less than 0.1 dB. According to this definition, the second order (LP11) mode undergoes 19.3 dB more attenuation than the fundamental (LP01) mode when the modes are equally excited.

Cut-off wavelength depends on the length and bends of the fiber and its strain condition. Consequently, there are three types of cut-off wavelength defined:

- cable cut-off wavelength (measured prior to installation),
- fiber cut-off wavelength (measured on uncabled primary-coated fiber)
- jumper cable cut-off wavelength.

5.4 Attenuation

The attenuation $A(\lambda)$ at wavelength λ between two cross-sections 1 and 2 separated by distance L of a fiber is defined, as:

$$A(\lambda) = 10 \log \frac{P_1(\lambda)}{P_2(\lambda)} \quad (\text{dB}) \quad (5.3)$$

where $P_1(\lambda)$ is the optical power traversing the cross-section 1, and $P_2(\lambda)$ is the optical power traversing the cross-section 2 at the wavelength λ .

For a uniform fiber, it is possible to define an attenuation per unit length, or an attenuation coefficient which is independent of the length of the fiber:

$$a(\lambda) = \frac{A(\lambda)}{L} \quad (\text{dB/unit length}) \quad (5.4)$$

5.5 Chromatic dispersion

Chromatic-dispersion definition: the spreading of a light pulse in an optical fiber caused by the different group velocities of the different wavelengths composing the source spectrum.

The chromatic dispersion may be due to the following contributions:

- material dispersion,
- waveguide dispersion,
- profile dispersion.

Change of the delay of a light pulse for a unit fiber length caused by a unit wavelength change. It is usually expressed in ps/(nm · km).

The duration of a light pulse per unit source spectrum width after having traversed a unit length of fiber is equal to the chromatic dispersion coefficient, if the following prerequisites are given:

- 1) the source has a wide spectrum;
- 2) the duration of the pulse at the fiber input is short as compared to that at the output, the wavelength is different from the zero-dispersion wavelength



Fig. 5.3 Illustration of the chromatic dispersion. A pulse is widened as it travels along the fiber.

Other dispersion parameters that may be used to characterize single mode telecommunication fibers include:

- Zero-dispersion slope. The slope of the chromatic dispersion coefficient versus wavelength curve at the zero-dispersion wavelength.
- Zero-dispersion wavelength. That wavelength at which the chromatic dispersion vanishes.
- Source wavelength offset. For G.653 fibers only. The absolute difference between the source operating wavelength and 1550 nm.
- Dispersion offset. For G.653 fibers only. The absolute displacement of the zero-dispersion wavelength from 1550 nm.

5.6 Polarization mode dispersion

Polarization mode dispersion is the Differential Group Delay time (DGD) between two orthogonally polarized modes, which causes pulse spreading in digital systems and distortions in analogue systems. Two factors have to be taken into account here:

- Real fibers cannot be perfectly circular and can undergo local stresses; consequently, the propagating light is split into two local polarization modes travelling at different velocities. These asymmetry characteristics vary randomly along the fiber and in time, leading to a statistical behavior of PMD.
- For a given fiber at a given time and optical frequency, there always exist two polarization states, called Principal States of Polarization such that the pulse spreading due to PMD vanishes, if only one PSP is excited. The maximum pulse spread due to PMD occurs when both PSPs are equally excited.

Definition of principal States of Polarization (PSP): when operating an optical fiber at a wavelength longer than the cut-off wavelength in a quasi-monochromatic regime, the output PSPs are the two orthogonal output states of polarization for which the output polarizations do not vary when the optical frequency is varied slightly. The corresponding orthogonal input polarization states are the input PSPs. Two issues have to be taken into account here. The local birefringence changes along the fiber, and the PSP depends on the fiber length (contrary to hi-bi fibers). If a signal has a bandwidth broader than the PSPs bandwidth, second order PMD effects come into play. They may imply a depolarization of the output field, together with an additional chromatic dispersion effect.

Definition of the Differential Group Delay (DGD): the Differential Group Delay (DGD) is the time difference in the group delays of the PSPs. The DGD between two modes is wavelength dependent and can vary in time due to environmental conditions. Variations by one order of magnitude are typical. The statistical distribution of the differential group delays is determined by the mean polarization mode coupling length, h , the average modal birefringence and the degree of coherence of the source. For a standard optical fiber cable of length L , such that $L \gg h$, as is mostly the case in practice, strong mode coupling occurs between the polarization modes. In such a case, the probability distribution of the DGDs is a Maxwellian distribution.

PMD is statistical parameter, and may be defined by three different statistical parameters.

Statistical parameters of interests here are so called central moments that show the deviation of the random variable from the mean:

- The first statistical moment called the mean

- The second central moment, called the variance

According to the G.650 standard PMD may be characterized as follows.

- The second moment (variance) PMD delay P_s is defined as twice the root mean square deviation (2σ) of the time dependent light intensity distribution $I(t)$ at the output of the fiber, deprived of the chromatic dispersion contribution, when a short pulse is launched into the fiber, that is:

$$P_s = 2(\langle t^2 \rangle - \langle t \rangle^2)^{1/2} = 2 \left(\frac{\int I(t)t^2 dt}{\int I(t)dt} - \left(\frac{\int I(t)t dt}{\int I(t)dt} \right)^2 \right)^{1/2} \quad (5.5)$$

t represents the arrival time at the output of the fiber. In practical cases the broadening due to chromatic dispersion must be taken into account to obtain P_s .

- The mean differential group delay P_m is the differential group delay $\delta\tau(\nu)$ between the principal states of polarization, averaged over the optical frequency range (ν_1, ν_2):

$$P_m = \frac{\int_{\nu_1}^{\nu_2} \delta\tau(\nu) c \nu}{\nu_2 - \nu_1} \quad (5.6)$$

Averaging over temperature, time or mechanical perturbations is generally an acceptable alternative to averaging over frequency

- The r.m.s. differential group delay P_r is defined as

$$P_r = \left(\frac{\int_{\nu_1}^{\nu_2} \delta\tau(\nu)^2 d\nu}{\nu_2 - \nu_1} \right)^{1/2} \quad (5.7)$$

PMD coefficient is calculated in two different ways for two separate cases:

- Weak mode coupling (short fibers):

$$PMD_c [ps/km] = P_s / L, P_m / L, \text{ or } P_r / L \quad (5.8)$$

- Strong mode coupling (long fibers):

$$PMD_c [ps/\sqrt{km}] = P_s / \sqrt{L}, P_m / \sqrt{L}, \text{ or } P_r / \sqrt{L} \quad (5.9)$$

Strong mode coupling is mostly observed in installed cables longer than 2 km. Under normal conditions, the differential group delays are random functions of optical wavelength, of time, and vary at random from one fiber to the other. Therefore, in most cases, the PMD coefficient has to be calculated using the square root formula

6 Technology of optical fibers

6.1 Telecommunication windows and generations of fiber optic systems

The telecommunication windows, and the telecommunication system generations were discussed in Chapter 2.

6.2 Attenuation of silica glass fiber

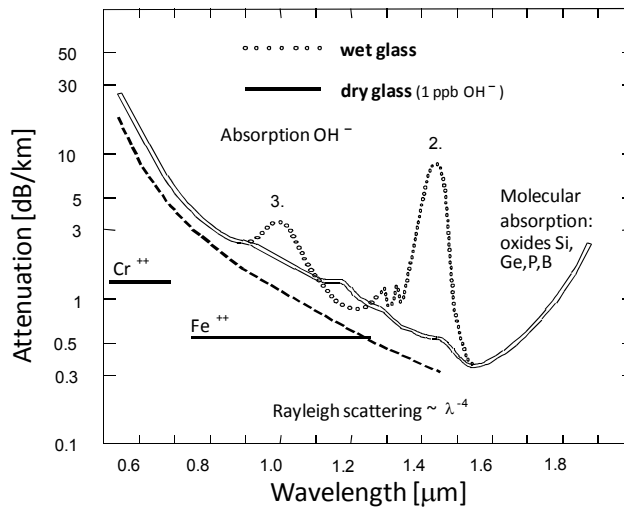


Fig. 6.1 Silica glass fiber attenuation in function of light wavelength.

Fiber attenuation is a gradual decrease in energy (optical power) carried by the lightwave as it propagates along the fiber. Numerical values of attenuation are expressed in the units of [dB / km], which translates into: what part (in decibels, dB) of the initial optical power is lost due to attenuation assuming the light has travelled a path of the length of 1 kilometer (km) inside the fiber. Whereas reasons of attenuation occurrence are common to all silica glass fibers, the attenuation values strongly depend on parameters of a given fiber (e.g. on manufacturing process, fiber type, and others).

We will describe the attenuation of silica glass fiber in two contexts. Firstly, in the context of physical mechanisms standing behind the attenuation. Secondly, in the context of how the attenuation value varies with the wavelength of propagating light.

Three groups of physical mechanisms can be named. They are (Bass, 2001b), (J.-ming Liu, 2005), (Agrawal, 2002):

- intrinsic absorption,
- extrinsic absorption, and
- scattering.

All mechanisms of the types listed above occur with different strength depending on the light wavelength. In telecommunications, we are interested in characterizing the absorption strength

- in the short-wavelength region (ultraviolet and visible), i.e. for lightwaves shorter than about 800 nm,
- in the infrared region, i.e. for lightwaves longer than about 1600 nm, and
- in the near-infrared region, i.e. between 800 and 1600 nm where the telecommunication windows are located.

Optical power lost due to absorption is transformed into heat - fiber's temperature is increased. This temperature change of fiber material can usually be neglected unless we deal with high levels of optical power. Some of the scattering mechanisms include the transformation of light into heat, as well. However, a scattering mechanism we will discuss later in this lecture, only alters the direction of light propagation, thus making some part of optical power propagate out of the fiber core.

The intrinsic absorption is the one that occurs when light interacts with the chemical ingredients (chemical structure) of pure glass. In silica fibers, the intrinsic absorption becomes significantly high (strong)

- in the short-wavelength spectral region (below 800 nm) where it is caused by the electromagnetic field interaction with electrons (electronic absorption), and
- in the infrared spectral region (above 1600 nm) where it is caused by the electromagnetic **field** interaction with chemical bonds (Si-O bonds) that connect the silicon and oxygen atoms (molecular absorption).

Reasons of the extrinsic absorption lie in the interaction of light with impurities contained in glass. Though unwanted, impurities are always present in actual silica fibers. The most significant types of such impurities are:

- ions of the following metals - iron (Fe), nickel (Ni) and chromium (Cr) (see the diagram for spectral ranges of absorption associated with individual ions), and
- the hydroxyl ions (OH-) showing the strongest absorption around 2700 and 4200 nm (the fundamental OH- absorption) and - what is of special interest to telecommunications - absorption around 1380, 950 and 720 nm (the overtone OH- absorption).

All the discussed ions occur in silica fibers due to imperfections of fiber manufacturing processes. In particular, the OH- ions come from water.

Among several other scattering mechanisms, the most pronounced in silica fibers is

- the Rayleigh scattering (i.e. scattering described by Rayleigh's model) caused by silica refractive index inhomogeneities of the sizes much below (<10%) the light wavelength; this type of scattering shows the λ^{-4} dependence (compare the thick dashed line in the diagram).

Finally, from the viewpoint of individual spectral ranges, the absorption and scattering mechanisms we have discussed so far, contribute to the total attenuation of silica fiber as follows (J.-ming Liu, 2005):

- in the short-wavelength range, the Rayleigh scattering is dominant and it outweighs the other factor present in this spectral range, the electronic absorption,
- in the infrared range, only the molecular absorption defines the silica fiber attenuation,
- in the near-infrared range, absorption on OH- ions is a decisive factor; particularly, the low-attenuation (low-loss) spectral ranges in between the neighboring OH- absorption peaks are used as transmission windows in telecommunications; fiber transmission can, however, be significantly degraded within those windows if fiber quality is not high enough.

6.3 Properties of silica glass

For convenience, a summary of the already discussed silica glass-related facts is given in a list below.

- Chemical formula SiO₂
- Lowest fiber loss 0.2 dB/km
- Bandgap of fused silica 9 eV (~137 nm)
- (Pure germania bandedge ~185 nm)
- Infrared edge (vibrational resonances) ~2 mm

- Rayleigh scattering $\sim \lambda^{-4}$ (i.e. its intensity changes proportionally to the -4^{th} power of light wavelength)
- OH⁻ ions infrared absorption: fundamental 2.27 and overtones 1.37, 0.95 and 0.725 μm

6.4 Structure of silica glass

In telecommunication fibers, the silica glass used never consists of a perfectly regular, uniform net (crystal lattice) of silicon (Si) and oxygen (O) atoms. There is always a certain density of lattice defects present in fiber material. The defects, independent of their origin, result in local fluctuations of the fiber material (i.e. the silica-glass) refractive index. Structure of silica glass compared to silica crystal is shown in figure Fig. 6.2.

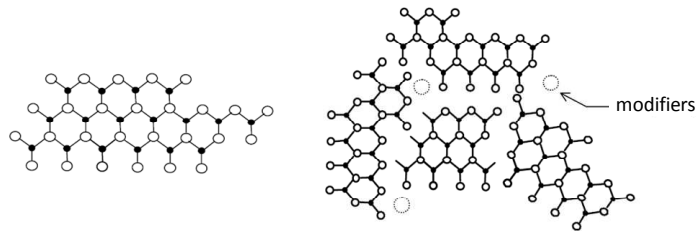


Fig. 6.2 Structure of silica crystal: two dimensional crystal lattice is presented.

Before all, the fiber material atoms are not located at perfectly regular positions because fiber material is not the silica crystal but the silica glass. In general, a perfect regularity of atom geometrical configuration can only be expected in crystals. In glasses, due to the process of melting that glasses undergo when they are produced, the crystal-like regularity is lost.

In the specific situation of the silica glass application in optical fibers, a second source of glass structure irregularities appear. It is the presence of the so called modifiers, i.e. chemical substances (chemical compounds) that are introduced into glass to alter its optical properties. Adding of the modifier substances in the process of fiber manufacturing is called doping and it will be discussed in greater detail in paragraph 6.6.

6.5 Three main steps in fabrication of optical fibers

Optical fibers are fabricated using a number of different methods (technologies). These methods fall into two main categories:

- fiber production from preform, and
- direct fiber production (without preform).

Only methods from the first category are of importance in mass production of silica glass fibers. The second category includes methods that are often used for plastic fibers (e.g. a method of extrusion).

In this lecture we will only focus on the preform-based fabrication technologies. There are three main steps in each preform-based fabrication technology of silica glass fibers:

- manufacturing of the pure glass preform,
- drawing of the fiber from the preform, and
- tests and measurements.

In the following slides, we will explore in more detail how the pure glass preform is manufactured and how the preform is then transformed into the final product – the silica glass fiber.

6.6 Chemicals and chemical reactions

All the preform manufacturing technologies share some basic chemical reactions, which are used for:

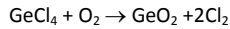
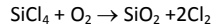
- creating the silica (SiO₂) itself,
- increasing the refractive index of silica, or
- decreasing the refractive index of silica.

The primary chemicals are:

silicon tetrachloride (SiCl₄),

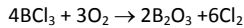
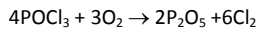
germanium tetrachloride (GeCl₄).

Then, basic chemical reactions of manufacturing of optical glass proceed as follows (Gambling, 2000), (Bass, 2001b), (Agrawal, 2002):



In the first reaction, a white silica powder is created. Before being transformed into glass (vitrified) at a later stage of the preform manufacturing process, this silica powder is often called the soot in the fiber production terminology. In the second reaction, germanium dioxide (GeO₂) is created. When present in silica, germanium dioxide plays a role of a refractive index-increasing dopant.

Two other reactions commonly used in preform manufacturing are:



The reaction substrates are: phosphorus oxychloride (POCl₃) and boron trichloride (BCl₃). Both the reactions create substances that modify the refractive index of silica. Phosphorus pentoxide (P₂O₅) is a refractive index-increasing dopant and boron oxide (B₂O₃) is a refractive index-decreasing dopant.

The possibility of adjusting the silica glass refractive index by means of dopants is a crucial element of the entire silica fiber fabrication technology. This is because the transversal (radial) distribution of preform's refractive index defines the refractive index distribution of a fiber that will later be created (drawn) from the preform. The part of preform's volume that will create the core of the fiber must then have a higher refractive index than the rest of preform's volume (which will create the cladding of the fiber).

6.7 MCVD or IVD

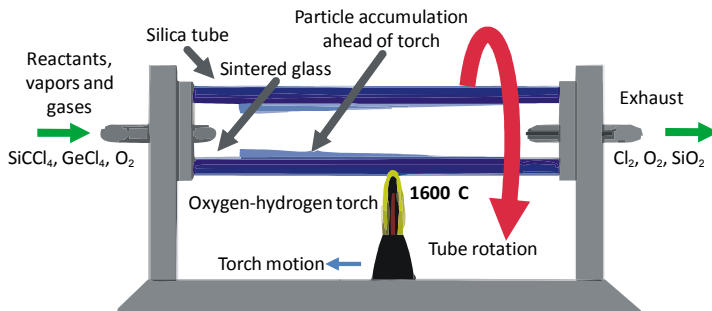


Fig. 6.3 The MCVD preform-manufacturing setup.

In the Modified Chemical Vapor Deposition (MCVD) (also called the Inside Vapor Deposition, IVD) (Paschotta, 2008a), (Wang, Nie, Xu, & L. Liu, 2006), (Agrawal, 2002), a mixture of gaseous reactants is fed into

- a rotating target silica tube
- that is heated by a moving torch,
- and at the end of the process, the tube is collapsed.

At a temperature of 1600°C, the silica soot is deposited on tube walls. Thanks to the rotation, radial symmetry of the deposition is ensured. In turn, longitudinal symmetry of the deposition (i.e. along preform's length) is enabled by the torch movement – it is shifted back and forth on a regular basis. In fact, soot deposition takes place only near the current location of the torch. When the MCVD method is used up to about 100 silica glass layers are deposited.

Once the deposition process is complete, the tube is collapsed at a temperature of 2000°C. This gives the preform its final shape – the remaining void volume within the preform is removed. The collapse process will also be discussed later.

The MCVD technology was developed 1974 by Bell Laboratories.

6.8 OVD

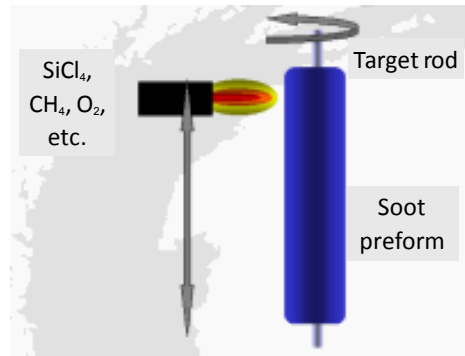


Fig. 6.4 The OVD preform-manufacturing setup.

In the Outside Vapor Deposition (OVD) (Paschotta, 2008a), (Wang, Nie, Xu, & L. Liu, 2006), (Agrawal, 2002), unlike the previously discussed MCVD, the deposition takes place on target's surface. In other words, instead of a silica tube,

- a rotating target rod (mandrel) is used,
- and the deposition is realized by means of a moving burner's flame containing all the chemicals needed;
- finally, the rod is removed and the preform is collapsed.

Materials commonly used for the target rod are: aluminum oxide or graphite. In contrast to the MCVD, where the initial target (silica tube) becomes part of the resulting preform, in the OVD, the initial target is removed before the final preform collapse takes place. Moreover, whereas the MCVD's burner only supplies heat to promote chemical reactions within the tube, in the OVD, the flame leaving the burner also contains all the chemicals required for the deposition.

The OVD technology was developed in 1973 by Corning.

6.9 VAD

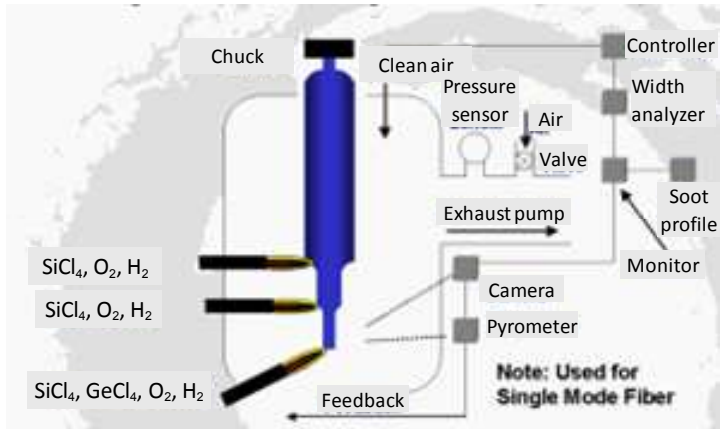


Fig. 6.5 The VAD preform-manufacturing setup.

The Vapor-phase Axial Deposition (VAD) (Paschotta, 2008a), (Wang, Nie, Xu, & L. Liu, 2006), (Agrawal, 2002) borrows from the OVD's idea of depositing the silica soot directly from the burner flame. There are, however, some significant differences, as well. In the VAD

- the preform, besides its rotational movement, is being continuously pulled upwards;
- at preform's bottom, individual layers of the preform material (soot) are deposited from different burners, and
- at preform's top, a ring heater transforms (sinters) the soot into a transparent silica glass.

So, instead of moving a single burner along the preform and simultaneously changing the chemical composition of the burner flame, which was the case in the OVD, the VAD uses several burners that are fixed in their position and in chemical composition of their flames. As an example, consider the bottom-most burner visible in the diagram. Germanium tetrachloride (GeCl_4) is present in the gas mixture supplied to this burner. Thus, the inner-most part of preform's volume will be the one that has the highest refractive index. It is because the source GeCl_4 shows up as germanium dioxide (GeO_2) – a refractive index-increasing dopant – in the burner flame.

There is some additional instrumentation employed in the VAD for monitoring the entire deposition process. In particular, a video camera and a pyrometer are used to directly monitor the current width and temperature of the bottom part of the preform, respectively. Information from these sensors provides feedback enabling the instantaneous adjustments to both the burners' temperature and the pulling speed.

The VAD technology was developed in 1977 by Nippon Telegraph and Telephones. A key advantage of this technology is the lack of the process step present in the two technologies discussed earlier (MCVD and OVD) – the preform collapse.

6.10 Collapse

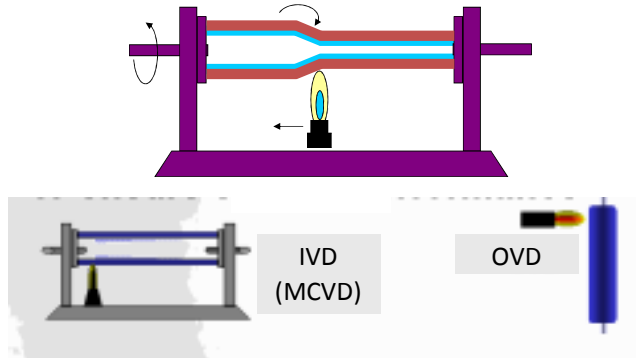


Fig. 6.6 The collapse process setup (top). It is applied to fiber preforms fabricated by means of the MCVD and OVD technologies (bottom).

Both MCVD (IVD) and OVD preforms are collapsed at the process finish. At an elevated temperature, i.e. at 2000°C as compared to 1600°C used during the deposition,

- preform diameter is reduced, thus void volume within the preform is removed;
- also preform material initially being porous, undergoes sintering into its final pore-free form.

The collapsing process is usually carried out in helium atmosphere. This gas easily permeates into the porous material and then, after the gas has exited the material during sintering, the preform is practically pore-free.

A potentially significant disadvantage of the preform collapse lies in the possibility of the creation of fiber centerline defects, i.e. deviations of the fiber core position from fiber's geometrical center. Performance of multimode fibers is especially sensitive to centerline defects because these defects can severely increase the differential mode delay of a multimode fiber.

6.11 Double Crucible method

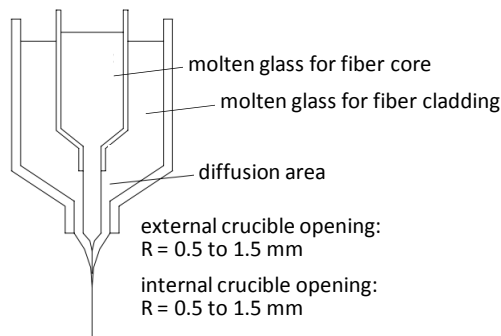


Fig. 6.7 The Double Crucible fiber-manufacturing setup.

A fiber manufacturing method that completely avoids the need of the preform fabrication, is the Double Crucible method. In fact, it was invented and applied before the deposition-based methods we have discussed earlier. In the Double Crucible method

- two containers (crucibles) keep the molten glass of two kinds: the first kind that will create fiber core, and the second one intended for fiber cladding;

- the two materials come into contact with each other near the bottom of the external crucible and they are then drawn in to the final fiber.

The Double Crucible method gives a considerable ease in selecting the fiber material types. However, minimizing the material contamination to the extremely low levels attainable in the deposition-based methods, becomes very difficult.

6.12 Preferred technologies and the biggest manufacturers

A statistical overview related to the market (the leading manufacturers) and to the manufacturing technologies of the telecommunication-grade silica-glass fibers are given in tables Tab. 1.1 and Tab. 1.2, respectively.

Tab. 1.1 Silica-glass fiber biggest manufacturers.

The biggest manufacturers (1996)	
Corning	6 mln km
AT&T (Lucent)	4 mln km
Siecor	2 mln km

Tab. 1.2 Silica-glass fiber preferred manufacturing technologies.

Technology	
OVD	50% growing
MCVD	23% decreasing
VAD	23% growing
PCVD	2%
MCVD-plasma	2%

6.13 Attenuation of a PMMA step-index POF

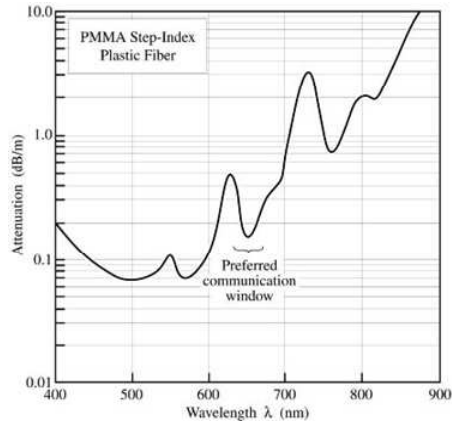


Fig. 6.8 Attenuation of a PMMA step-index plastic optical fiber (after data of Toray Industries Ltd.) (Schubert, 2003).

Around the 650 nm light wavelength, the preferred communication window of the PMMA-based fibers is located. The attenuation is about 150 dB/km, which is a much higher value than that characteristic of the silica-glass fibers. So high an attenuation makes plastic fibers suitable for use in the short-range (several dozen meters) optical data-links only.

As stated above, plastic optical fibers cannot compete with silica-glass fibers in terms of attenuation and also the maximum transmission speeds are relatively lower. Nevertheless, plastic fibers possess several features that are found advantageous in the short-distance computer networking and other applications (Paschotta, 2008b). The features are:

- transmission possible in the visible spectral range,
- relatively large fiber core diameters and high numerical aperture values enable an easy coupling of light into the fiber, and
- plastic fiber installation is by far easier than is the case with silica-glass fibers;
- in particular, the installation can thus be done at significantly lower costs as neither highly trained personnel nor expensive installation equipment is needed.

Of course, due to large core diameters, plastic fiber support the multimode propagation only (which limits the maximum transmission speeds). On the other hand, larger core makes the plastic fiber splicing notably more tolerant of any fiber positioning inaccuracies that may occur during splicing. Moreover, thanks to specific mechanical properties of PMMA, plastic fiber termination does not require any precise cleaving procedures (methods). Simple cutting is sufficient.

Plastic fiber-based optical links were first introduced in the 1960s.

6.14 Plastic fiber fabrication technologies

Ideas of the two different technologies of plastic fiber fabrication are schematically depicted in figure Fig. 6.9.

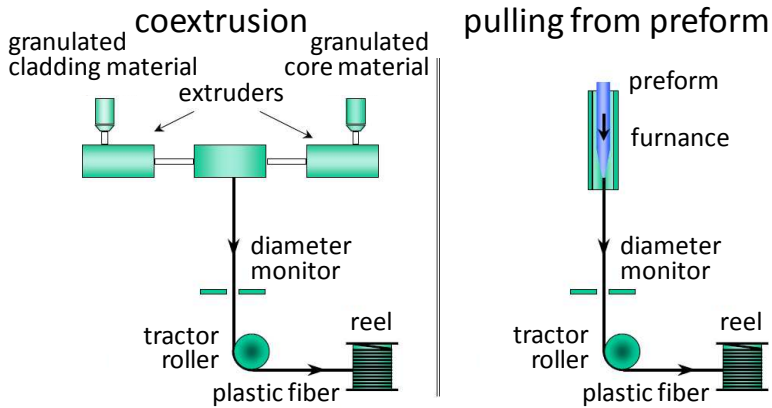


Fig. 6.9 The plastic fiber fabrication setups – coextrusion, and pulling from the preform.

In fact, both these technologies are, to some extent, analogous to the silica-glass fiber fabrication technologies. In the first one, i.e. in creating the plastic fiber by means of the coextrusion, the plastic fiber material is extruded through an orifice (small-diameter hole). The fiber consists of a core and a cladding layer surrounding the core. There are two separate material reservoirs (for the core and the cladding). The elements mentioned above are similar to the double-crucible method discussed in paragraph 6.12. The difference lays in the plastic fiber being extruded by means of applied pressure, and not pulled as is the case in the double-crucible method.

The second plastic fiber fabrication technology uses the preform as the source of the raw fiber material. The plastic fiber is then drawn from the preform much as was the case in the previously discussed preform-based technologies of the silica-glass fibers. The plastic preform refractive index profile is, however, created in a different way. Rather than being deposited layer-by-layer, the refractive index variations are induced within the plastic preform volume by means of a (chemical) process of the copolymerization.

7 Passive devices (fundamentals and examples)

In this chapter, elements of fiber optic link will be discussed. They are: optical fiber cables, couplers, connectors, etc.

7.1 Placement of passive photonics devices

Figure Fig. 7.1 shows a layout of an example network containing both passive elements (red blocks) (but also cables and fibers are classified as passive elements) and active elements (grey blocks). By definition, active elements are those, which process data signals using external energy, e.g. light sources, detectors. Passive elements, in turn, are the ones that do not draw any additional energy, e.g. optical fibers, connectors, couplers, etc.

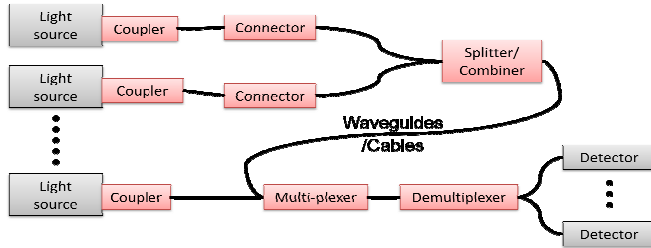


Fig. 7.1 Diagram can represent optochip or WAN. Red and black color indicates passive element of track.

7.2 Properties and classifications of fiber optic link passive elements

List of passive photonic devices:

- Optical waveguides
- Connectors
- Couplers
- Splitters
- Attenuators
- Isolators
- WDM and DWDM multiplexers and demultiplexers
- Filters
- Add-and-drop multiplexers

Properties and parameters:

- Functional parameters
 - reflection,
 - dispersion(s),
 - mode-field diameter,
 - numerical aperture...
- Attenuation
- Back-reflection (ORL)
- Polarization dependence

7.3 Properties and classifications of optical fibers

Optical fibers

- Single mode fibers standard e.g. G-652, SMF-28, Dispersion Shifted Fiber (DSF)
- Multimode fibers, 62.5/125, 50/125, G-651
- Specialty fibers (PM, UV-FIR, EDFA pump fiber)
- POF – Passive Optical Fiber (core diameter ~1mm)

Planar and structured waveguides

- Semiconductor (GaAs, polymers)
- Dielectric (glass, Si, SOI, SiO₂)
- Polymers (PMMA, PS)

Polarization maintaining fibers

- Polarizing fibers
- Polarization maintaining (PM) fibers

One of the polarization maintaining fiber (PMF) types, the Panda PMF, is displayed in figure Fig. 7.2. Panda is manufactured by Alcoa Fujikura Ltd. of Japan. The two stress rods on

either side of the core induce birefringence in the core. This creates a slow axis and a fast axis, i.e. light will travel faster down one axis than the other. The direction that bisects the core and the stress rods is the slow axis. Industry standard is to have connectors aligned to the slow axis. Other PMF types are presented in figures Fig. 7.3, Fig. 7.4, and Fig. 7.5.

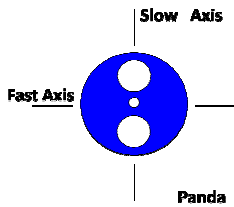


Fig. 7.2 Panda type of PMF (“Single Mode Polarization Maintaining Fiber,” 2010).

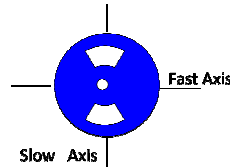


Fig. 7.3 Bow-tie (“Single Mode Polarization Maintaining Fiber,” 2010).

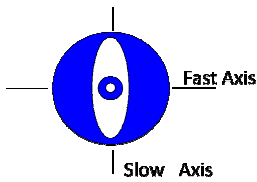


Fig. 7.4 Over-Inner Clad

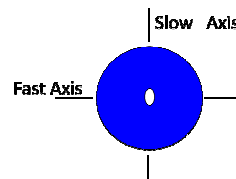


Fig. 7.5 Over Core

PM fibers are primarily used with:

- high performance transmission lasers and modulators in DWDM systems working at 10 Gb/s and above
- fiber lasers and Raman amplifiers
- polarization sensitive devices such as waveguide modulators
- sensor applications (particularly interferometric sensors)

7.4 Properties and classifications of optical fiber cables

Optical cable can contain a single optical fiber as well as multiple optical fibers as shown in figures Fig. 7.6 and Fig. 7.7, respectively. Cables can also be classified according to how optical fibers are placed (packed) within cable structure – either tightly (tight-buffered fiber optic cables) or loosely (loose-tube fiber optic cables). Other classifications consider the following parameters:

- number of fibers
 - Simplex
 - Zip-cord (duplex)
 - Multi-fiber
- technology
 - tight-buffered
 - loose tube
- field of application, working environment
 - distribution, raiser, breakout;
 - indoor, outdoor;
 - short distance, long distance;
 - military grade, oceanic, ...

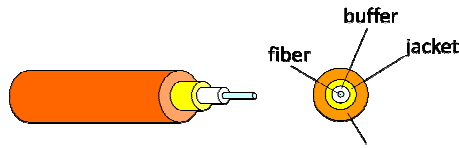


Fig. 7.6 Optical fiber cable – simple type.

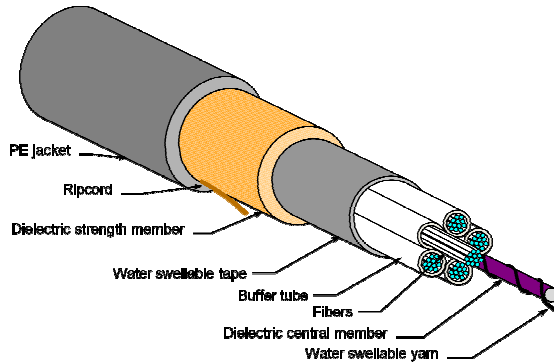


Fig. 7.7 Detailed cross-sectional view of optical fiber cable – multi-fiber type.

7.5 Properties and classifications of fiber optic connectors

A fiber-optic connector joins two fibers together such that light passes from one fiber to the other. It is one of the most critical components of a fiber-optic system (link).

The main requirements are:

- to minimize signal loss, and reflections,
- to provide a connection that is stable both mechanically and optically.

Achievable losses for various connector types are in the range of 0.25 to 1.5dB.

Types of fiber connections:

- connectors (demountable interconnections between fibers and photonics devices)
- splices (permanent connections)
- mechanical splices (connectors with optical parameters similar to splices, but do not require fiber optic splicers)

Every optical fiber connection introduces some additional losses (i.e. losses added to that of the fiber itself). These connector-related additional losses can be classified as intrinsic or external losses.

Intrinsic optical connector losses

- intrinsic – fiber imperfections, uncorrectable
 - core diameter, shape and area Fig. 7.8
 - numerical aperture Fig. 7.9
 - core excentricity Fig. 7.11

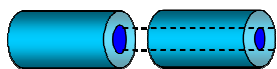


Fig. 7.8 Core area mismatch

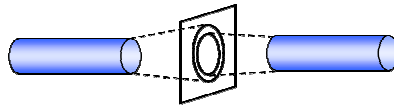


Fig. 7.9 Numerical aperture mismatch

Figure Fig. 7.10 shows losses (attenuation) introduced by a larger-to-smaller butt-joint connection between fibers in the function of core diameter difference. A significant, rapid increase in losses is already visible at small values of the core diameter difference. The connection losses increase becomes linear for difference values of 6% and higher.

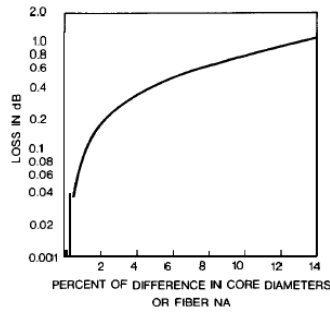


Fig. 7.10 Approximate loss in dB due to larger-to-smaller core diameter difference or fiber numerical aperture difference for two butt-joined optical fibers.

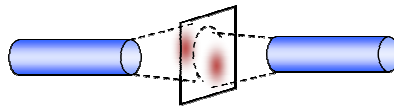


Fig. 7.11 Beam profile mismatch.

External optical connector losses

- external – connector design, minimized by careful design
 - longitudinal separation Fig. 7.12
 - angular misalignment Fig. 7.14
 - lateral offset Fig. 7.16
 - end-face smoothness, flatness, perpendicularity

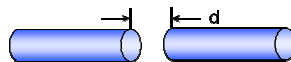


Fig. 7.12 End separation.

Connection attenuation in the function of separation (distance) between fiber ends is visible in figure Fig. 7.13. For high numerical aperture fibers, the strongest impact of the fiber end separation is observed. Then, for lower numerical aperture fibers, the end separation becomes less significant.

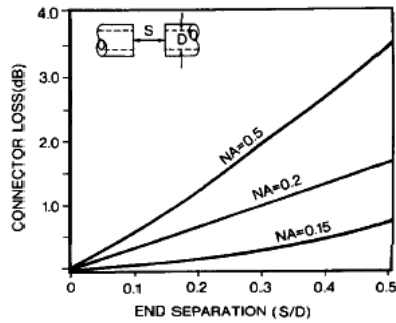


Fig. 7.13 Variation of connector power loss with end-separation distance-to-diameter ratio between two step-index air-gap optical fiber ends for several values of numerical aperture (NA) (Senior & Jamro, 2009).

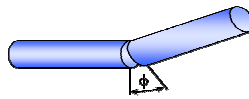


Fig. 7.14 Angular misalignment.

Figure Fig. 7.15 shows how a relatively small difference in fiber ends' angular position can be a reason for noticeable losses. Misalignments as low as several degrees are enough to make the connector loss reach 1dB.

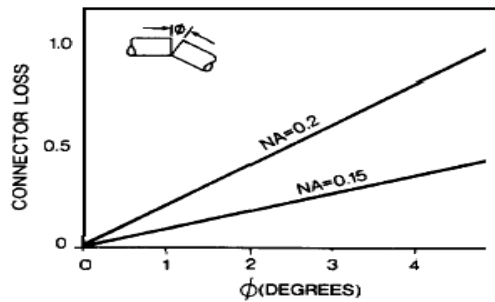


Fig. 7.15 Connector power loss due to axial angular misalignment of the cores of two step-index optical fiber butt-joined ends (Senior & Jamro, 2009).

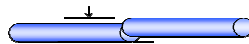


Fig. 7.16 Lateral offset

From figure Fig. 7.17 we can find that shifting of fiber cores in opposite directions by 10% (relative to fibers' core diameter) gives rise to an attenuation of the order of 1dB. Obviously, further increase in lateral core misalignment (displacement) increases the connection losses even further.

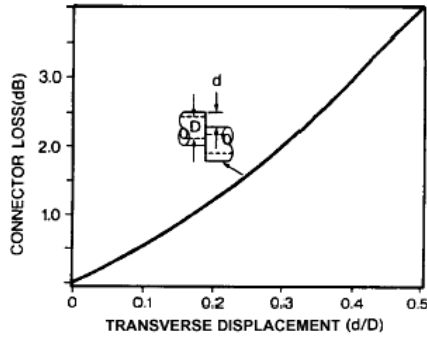


Fig. 7.17 Connector power loss due to transverse (lateral) displacement of the cores of two step-index optical fiber butt-joined ends (Senior & Jamro, 2009).

7.6 Losses

Total value of optical losses in optical links consists of intrinsic losses introduced by link elements, and of back-reflections at boundaries (interfaces) between two different media.

- o Loss introduced by an element of optical link

$$A[dB] = 10 \log \frac{P_{out}}{P_{in}} \quad (7.1)$$

where P_{in} is the optical power fed into the link, and P_{out} is the optical power at link's output.

- o Reflection losses – reflection coefficient at dielectric interface (refraction coefficients n_1 and n_2)

$$R = \frac{(n_1 - n_2)^2}{(n_1 + n_2)^2} \quad (7.2)$$

- o Reflection coefficient expressed in dB is, by definition, the optical return loss (ORL) – it describes what part of the signal returns toward the source.

$$ORL[dB] = 10 \log(R) = 10 \log \left(\frac{(n_1 - n_2)^2}{(n_1 + n_2)^2} \right) \quad (7.3)$$

- o Attenuation caused by reflections (dB) – describes what part of the signal remains in fiber after reflection

$$A = 10 \log \left(1 - \frac{(n_1 - n_2)^2}{(n_1 + n_2)^2} \right) \quad (7.4)$$

Reflection losses at the material-air interface– examples

- o glass $n = 1.5$ $R = 4\%$ or -14dB
- o GaAs $n = 3.2$ $R = 27\%$ or -6 dB
- o Si $n = 4$ $R = 36\%$ or -4 dB

7.7 A simple f-o connector

In telecommunication systems as well as in other optical systems (setups) where connections between fibers need to be utilized, it is important to maintain a possibly low level of

losses introduced by incorrect fiber positioning (fiber misalignments). At the same time, quick and easy fiber connection preparation may also be a vital requirement. Many fiber connection methods have been introduced and standardized. Figure Fig. 7.18 presents one of the simplest methods of fiber connection making. It employs a fluid in which fiber ends are immersed (immersion fluid) to decrease the refractive index difference between fiber core and the surrounding medium (air). Back-reflections at fibers' ends are thus minimized. A disadvantage of this approach are difficulties in connecting / disconnecting the fibers quickly. Because of this, the most frequently used solution is based on furnishing fiber ends with appropriate mechanical connectors (see figure Fig. 7.19), which then allow to connect fibers in a repetitive, quick, and precise manner.

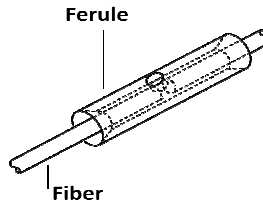


Fig. 7.18 A simple f-o connector with hole for index-matching fluid.

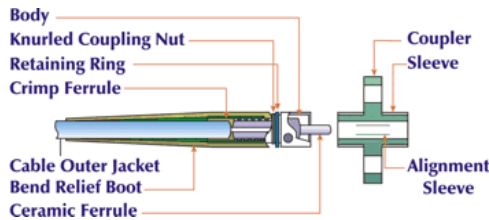


Fig. 7.19 An actual fiber optic connector with a ferrule for fiber alignment ("Fiber Optic Connectors Basics, Styles, Trends," 2010).

Subsequent figures below (Fig. 7.20 – Fig. 7.23) present some of the popular fiber optic connector types. Figure Fig. 7.20 shows a connection in which air fills the gap between fiber ends. It is not a recommended approach as it increases the back-reflection losses as well as losses resulting from geometrical reasons (i.e. from fiber cores' dimensions together with relative position of the cores). The remaining figures present fiber connections in which the physical contact (PC) approach is employed. Minimizing the air gap width leads to a decrease in connection loss down to a level of about -40dB or even less when the angular physical contact (APC) connectors are considered.

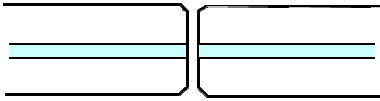


Fig. 7.20 Air Gap (“Fiber Optic Connectors Basics, Styles, Trends,” 2010)

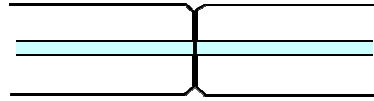


Fig. 7.21 Flat PC (“Fiber Optic Connectors Basics, Styles, Trends,” 2010)

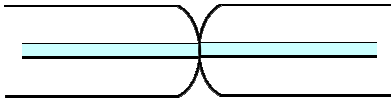


Fig. 7.22 PC (“Fiber Optic Connectors Basics, Styles, Trends,” 2010)

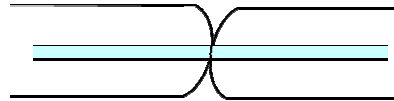


Fig. 7.23 APC (“Fiber Optic Connectors Basics, Styles, Trends,” 2010)

7.7.1 Fiber-optic connector types

There are more than 100 types of fiber optic connectors. Main connector types are described by TIA/EIA-604 standards. They are called Fiber Optic Connector Intermateability Standards (FOCIS) and are published with a document number format TIA-604-XX. To date, the following FOCIS documents exist:

- FOCIS 1: Biconic
- FOCIS 2: ST
- FOCIS 3: SC
- FOCIS 4: FC
- FOCIS 5: MTP/MPO
- FOCIS 6: Panduit FJ
- FOCIS 7: 3M Volition
- FOCIS 8: Mini-MAC (Withdrawn)
- FOCIS 9: Mini MPO (Withdrawn)
- FOCIS 10: Lucent LC
- FOCIS 11: Siecor SCDC/SCQC (not yet approved)
- FOCIS 12: Siecor/Amp MT-RJ
- FOCIS 15: MF
- FOCIS 16: LSH (LX-5)

In fiber optic systems, the most frequently used connectors were the ST (Single Termination) and the SC (Subscriber Connector) connectors visible in figures Fig. 7.30 and Fig. 7.29, respectively. Both the dimensions (form factor) and the connection precision of most of the fiber connector types are at acceptable levels. The ST connectors feature a circular casing and the SC connectors use a rectangular one. Both the connector types use a bayonet connection mechanism. Additionally, there are also the duplex-type SC connectors dedicated for optical networks (links) in which the transmit and receive channels are separated (into separate fibers). The duplex-type SC connectors make the installation of such optical links much less error-prone. In figures below, there are several of the fiber optic connector types most commonly used in telecommunication systems and in other optical systems setups. Dimension and some construction details of the three most popular types are shown in figure Fig. 7.35.

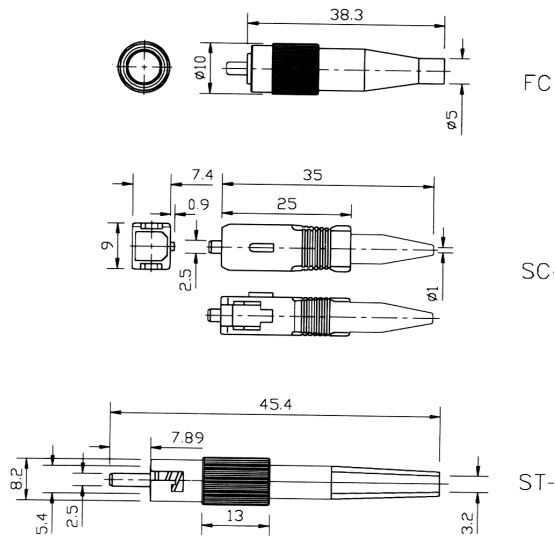
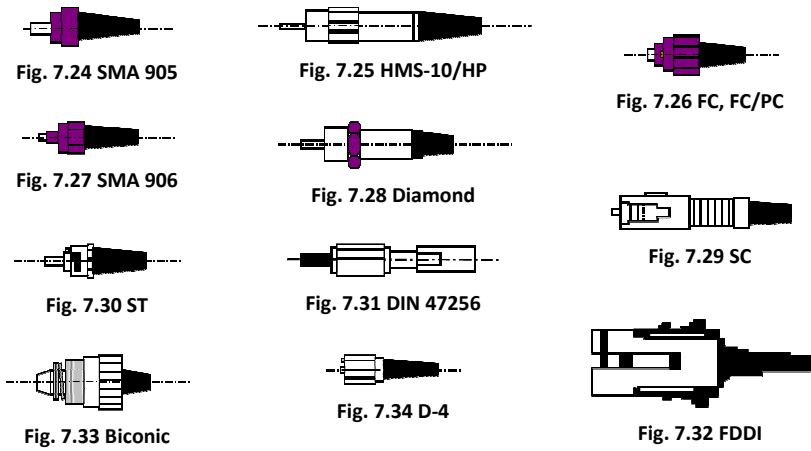


Fig. 7.35 The three main connector types.

For the PC-type (physical contact) connectors it is of major importance that optical fiber is precisely held in a fixed position regardless of the ambient temperature changes or mechanical vibrations. Otherwise, a correct contact between the connected fibers could not be ensured. In the PC-type connectors, optical fiber is fastened inside a small, rigid tube called a ferrule. Because fiber and ferrule diameters are precisely matched (and an adhesive is used), fiber's position is properly fixed (see figure Fig. 7.36). In figure Fig. 7.37, some statistical data concerning the FC-PC connector properties are given. As we can see in the respective diagrams, values of the connection loss (insertion loss) and the back-reflection loss (return loss) are at the level of -50dB and 0.15dB, respectively.

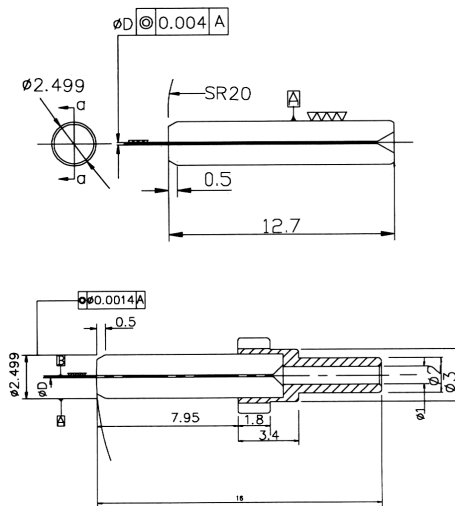


Fig. 7.36 Details of ferrule construction (FC-PC).

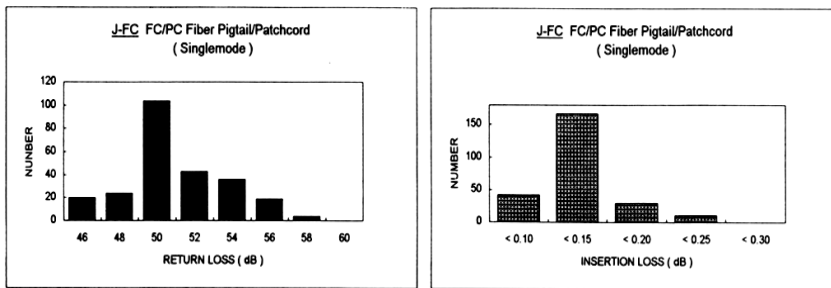


Fig. 7.37 Return and insertion losses for FC/PC (Fiber Pigtail/Patchcord) joint.

7.7.2 Small Form Factor (SFF) connectors

In telecommunication systems of large integration, dimensions of single connector plays a key role in minimizing the size of fiber optic distribution box. Standard connector types are relatively big compared to a single fiber or to other switching elements. Thus, these are the connector dimensions, which often determine the amount of space needed to accommodate an optical system.

Comparison of standard and small form factor (SFF) connector dimensions (FC and LC) are shown in Fig. 7.38.

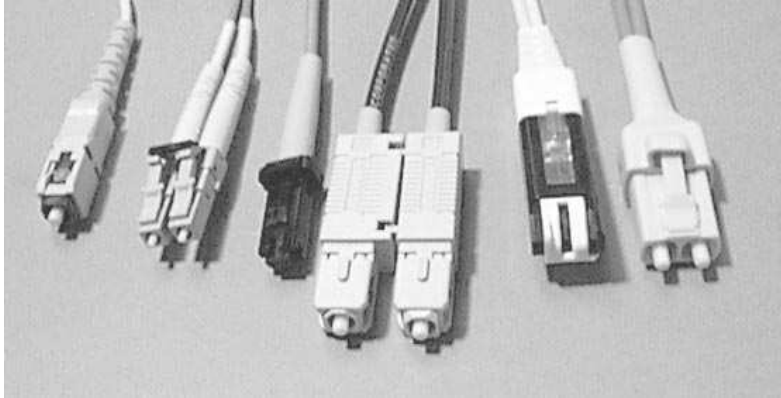


Fig. 7.38 From the left: SC-DC, LC, MT-RJ, Duplex S.C.(for comparison), Volition, and Opti-Jack (“Fiber Optic Connector Reference,” 2010).

7.7.3 Connector’s technology

In order to ensure the optical fiber is maintained by a connector in a fixed, precisely adjusted position regardless of ambient conditions (temperature, humidity, etc.), much care must be taken during the technological process of the connector production (connector assembly process). In the first two process steps, optical fiber is fastened to the ferrule hole with an adhesive. Precision and quality of adhesion will then be a decisive factor of whether the fiber position inside the connector is maintained despite varying environmental conditions over an extended period of time. In subsequent steps, polishing of fiber end is performed. Quality of polishing affects the back-reflection loss of the final product. International standards precisely define the parameter values that must be attained by a connector in order to avoid the creation of an excessive air gap between the fibers (fiber ends) being connected.

The connector assembly process steps are listed below:

- Epoxy glued, cured in room temperature (overnight) or in ovens (minutes)
- HotMelt (3M) glue already in place, softened during installation
- Prepolished, ready for splicing (UniCam®)
- Crimp and polish (LightCrimp AMP)

7.8 Mechanical splices

Besides fiber optic connectors, there are also the so called mechanical splices that can be used for connecting the optical fibers. Thanks to a rigid structure, mechanical splices are able to stably hold fibers at their prescribed positions, thus maintaining efficient fiber-to-fiber light coupling. Unlike the standard fiber optic splices, mechanical fiber optic splices are reusable. They are also easy to install and, consequently, lower costs and shorter installation times are involved. Mechanical splice disadvantages are losses, especially the back reflections, being significantly higher than that characteristic of fiber optic connectors. It is because of a thicker air gap present in mechanical splices. Also not all commercially available mechanical splice solutions ensure sufficient connection stability under varying environmental conditions.



Fig. 7.39 Elastomeric Lab Splice. Allows hundreds of uses.



Fig. 7.40 3M Fibrlok. $il < 0.2\text{dB}$, $fr > 7.75\text{ lbs.}$ $orl - 35\text{dB}$. V-groove technology - no epoxy. Thermal stability of -400°C to 800°C $il -$ insertion loss, $fr -$ fiber retention, $orl -$ optical return loss.

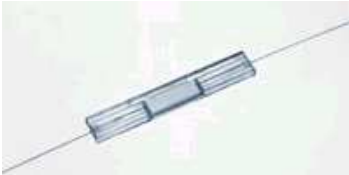


Fig. 7.41 AMP Corelink. $sl 0.15\text{dB}$ on $125\mu\text{m}$ fiber.



Fig. 7.42 Siemon Ultra Splice. $sl - 0.2\text{dB}$, $fr > 2\text{ lbs.}$



Fig. 7.43 Corning Cable System CAM Splice. 0.5dB .

7.9 Other types of optical link passive elements

7.9.1 Technology and construction of optical splitters/ couplers

Optical splitters are devices that are used to divide a single optical signal (beam) into two or more optical signals. In telecommunication systems, splitters are employed when optical signal is supposed to be delivered to multiple locations. Device performing an inverse function, is the optical coupler in which optical signals coming from multiple fibers are merged and then fed into a single output fiber. Both the devices share a common principle of operation – the evanescent coupling. Optical fiber modal field is not completely bounded within fiber core, it rather extends into fiber cladding as well. The part of modal field outside the core (field tails) is an evanescent wave (i.e. its power vanishes exponentially along fiber radius). Now, when cores of two different fibers are brought together close enough, gradual exchange of optical power will take place due to tails of both the modal fields each one penetrating the opposite fiber's core. It is how evanescent coupling works and, in fact, how the discussed splitters and couplers are constructed. Some more construction (fabrication) details are discussed below.

One of the methods of fiber optic coupler fabrication is described in figure Fig. 7.44. Two fibers are overlapped after their claddings have been partially removed by polishing.

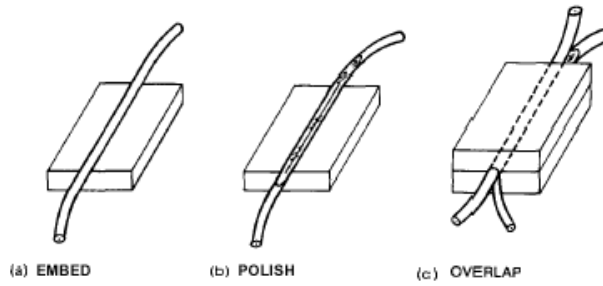


Fig. 7.44 Steps in fabricating a polished fiber optic coupler.

Figure Fig. 7.45 shows a different method of fiber optic coupler fabrication. Here, core proximity is achieved by means of thermal fusion.

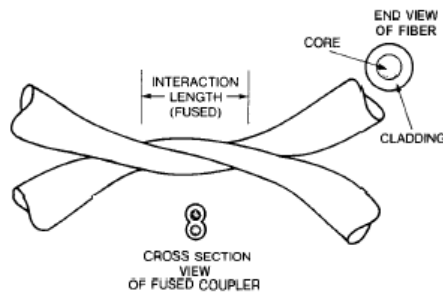


Fig. 7.45 Thermally fusing couplers.

7.9.2 Polarization controllers

A tri-waveplate controller (figure Fig. 7.46) consists of a half-wave plate sandwiched between two quarter-wave plates, with all three plates free to rotate independently about the optical beam. The first quarter-wave plate converts the light beam of generally elliptical polarization state into a linear polarization state. The half-wave plate then rotates the linear polarization state of the optical beam to a desired orientation. Finally, the second quarter-wave plate converts the linear polarization into any desired polarization state. The wave plates are sensitive to light beam's wavelength because a wave plate is half-wave (or quarter wave) only if the relative retardation between the slow and fast axes is half (or quarter) of the optical beam's wavelength. Consequently, the tri-waveplate controller is inherently sensitive to wavelength.

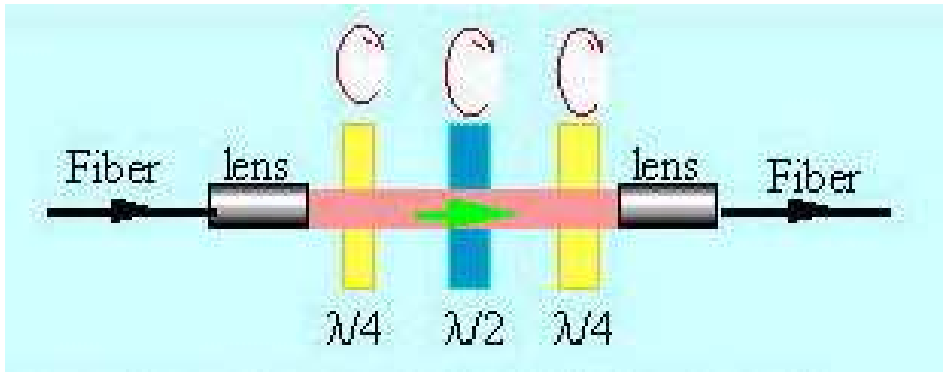


Fig. 7.46 Polarization controllers – classical solution (“Harness Optical Polarization with Ease and Elegance,” 2008).

A Lefevre controller (figure Fig. 7.47) operates on the same physical principle as the tri-waveplate controller, except that the waveplates are made of fiber coils and the signal beam does not travel in free space. However, it also shares the same limitation of wavelength sensitivity.

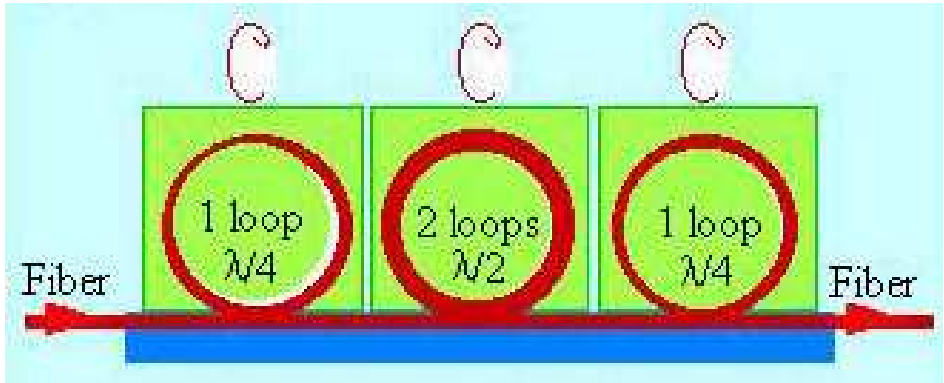


Fig. 7.47 Polarization controllers – fiber solution (“Harness Optical Polarization with Ease and Elegance,” 2008).

The Yao (commercially known as PolarITE™) controller (figure Fig. 7.48) uses a rotatable fiber squeezer to create a waveplate of variable retardation and can convert an arbitrary polarization state into any desired polarization state. It operates in principle like the Babinet-Soleil compensator and shares the same advantage of wavelength insensitivity.

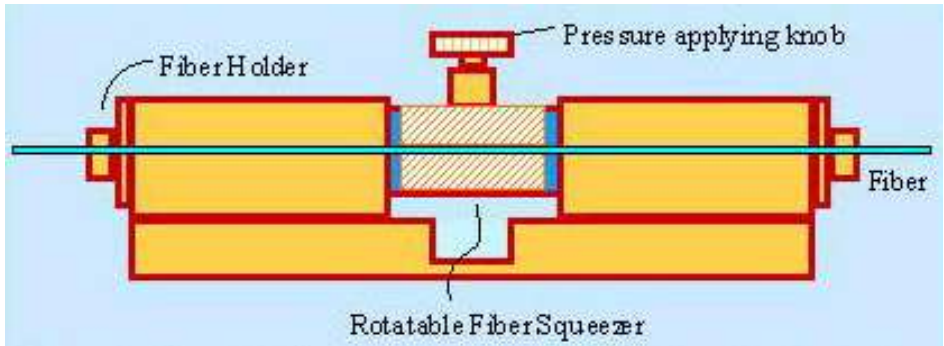


Fig. 7.48 Polarization controllers – fiber solution (“Harness Optical Polarization with Ease and Elegance,” 2008) (“Polarization Controller, Manual,” 2010).

7.9.3 Fiber Bragg gratings in optical communications

In telecommunication systems (especially the (D)WDM ones) there arises a need for selecting a desired wavelength out of multiple wavelengths that are simultaneously present in light beam. Such an operation is usually realized by means of an optical fiber in which Bragg grating of precisely controlled (designed) properties has been induced. The Bragg grating acts as an optical filter that extracts light of the desired wavelength(-s) from the entire optical transmission carried by an optical link. What is also important, other frequencies present in the transmission, are passed through the grating unaffected (see figure Fig. 7.49).

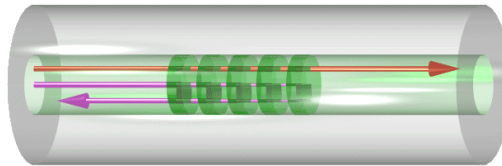


Fig. 7.49 Fiber-optic Bragg grating (DWDM filter) (“Basics of Fiber Bragg Grating,” 2010) (“Harness Optical Polarization with Ease and Elegance,” 2008).

7.9.4 Lenses

Geometrical path along which the light beam propagates, depends on what is the spatial distribution of the propagation medium refractive index. For example, graded-index (GRIN) lenses (figure Fig. 7.50) are often used to focus light. Thanks to the refractive index varying along the GRIN lens radius, it is possible to make the output lightwave focus at a prescribed distance behind the lens end-facet (the total length of the lens also needs to be properly adjusted). Another example is a telecommunication graded-index fiber (figure Fig. 7.51). The refractive index reaches its maximum value at fiber center (fiber axis), and it gradually decreases along fiber radius. This type of the refractive index transversal profile, if designed and manufactured properly, allows light beams within the fiber to propagate along sinusoidal paths. This, in turn, can significantly decrease the light beams’ interaction with fiber cladding. In multimode step-index fibers, excessive level of such an interaction severely limits the maximum transmission speeds attainable. This problem will be discussed in greater detail in the chapter devoted to optical fiber dispersion.

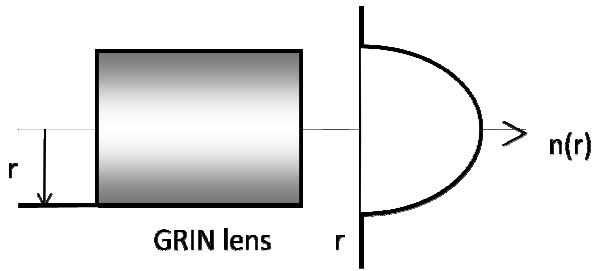


Fig. 7.50 Gradient index (GRIN) lenses, refractive index distribution

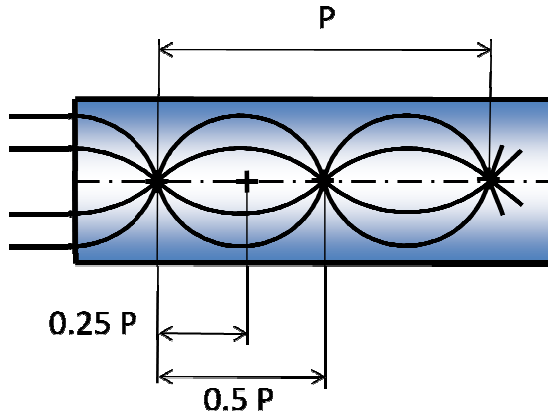


Fig. 7.51 Microlens in fiber.

7.9.5 Multiplexers

In the WDM telecommunication systems, where many lightwave frequencies are transmitted in a single physical channel (single fiber), devices are needed which collect optical signals from multiple physical channels (fibers) and couple them into a single output channel (fiber). Devices of the functionality described, are called the optical multiplexers. The working principle of an optical multiplexer is schematically shown in figure Fig. 7.52. Probably the simplest device that can realize the optical multiplexer (and demultiplexer) functionality, is the prism. However, prism-based solutions are not utilized in fiber optic telecommunications. It is because spatial separation of light beams that only slightly differ in frequency, is not effective enough when it is realized with the prism. Instead, the so called optical add/drop multiplexers (OADMs) are utilized. Their construction is usually based on optical fibers. OADM operation is schematically depicted in figure Fig. 7.53. Generally speaking, optical add/drop multiplexers enable the extraction (the “drop” function) of the desired optical frequencies (wavelengths), i.e. WDM data channels, from the entire optical transmission, i.e. from all the WDM data channels being transmitted. Then, if such a functionality is needed, an OADM allows another data streams to be launched (the “add” function) into the “empty” (previously dropped) WDM channels.

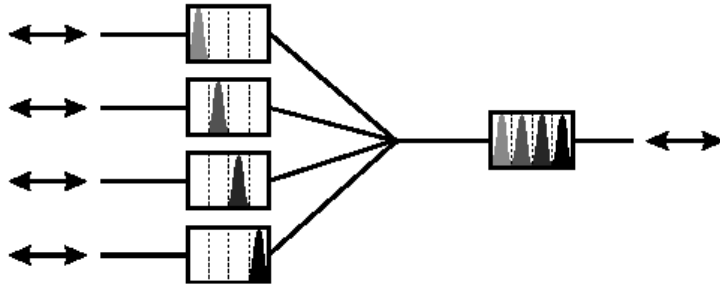


Fig. 7.52 Devices that allow mixing several (up to 100s) wavelength channels in one fiber.

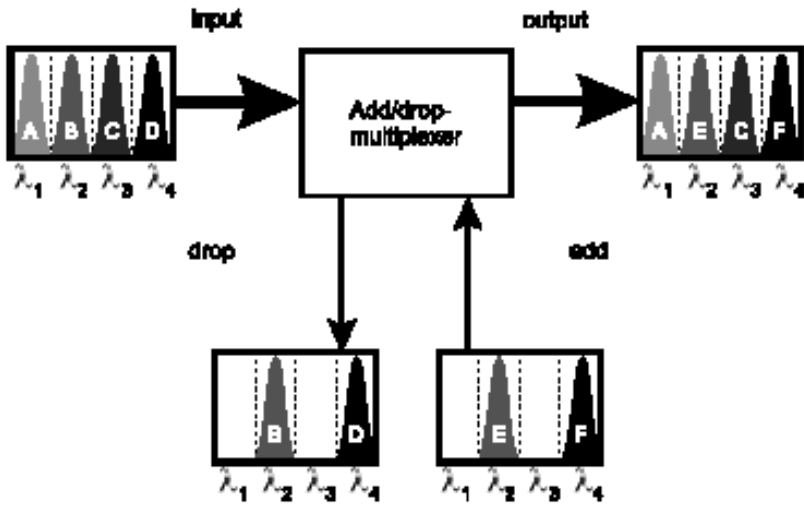


Fig. 7.53 Adding and dropping information into optical transmission path without disturbing other channels.

An example of a fabricated DWDM multiplexer structure is visible in figure Fig. 7.54. The DWDM channel multiplexing is performed in the following way. Four input planar waveguides supply the optical signals to a free-space propagation area where all the signals interfere. The resulting optical field enters an array of specially designed planar waveguides – neighboring waveguides differ in length by ΔL . Thus, optical signals propagating along these waveguides acquire different phase shifts before they enter the second free-space propagation area. The phase shifts are adjusted (by an appropriate selection of ΔL) so that optical interference in the second area results in the desired optical frequencies being coupled to their respective output waveguides.

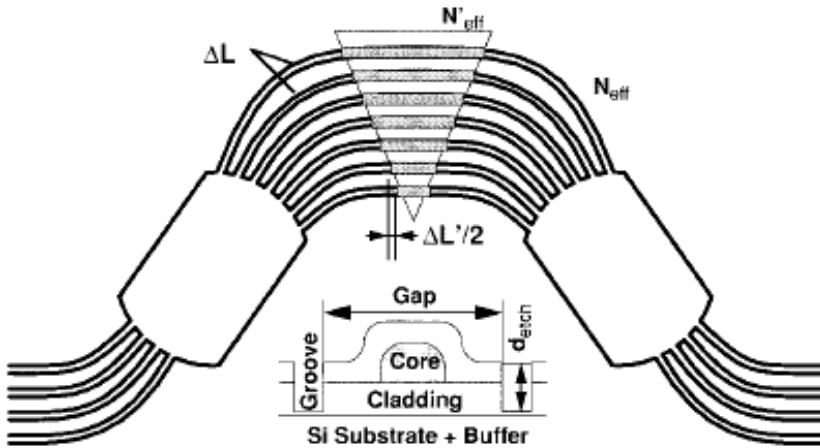


Fig. 7.54 Arrayed waveguide grating with stress release grooves for birefringence compensation. The SiO₂-on-Si waveguide cross section is shown in the inset (Nadler, Wildermuth, Lanker, Hunziker, & Melchior, 1999).

8 Active devices – telecom sources and detectors

8.1 List of active photonic devices

1. Lasers and light emitting diodes
2. Detectors
3. Amplifiers
4. Modulators
5. Switches
6. Tunable filters
- + *Passive devices*
- Σ. Integrated optoelectronic circuits

8.2 Waveguide light sources - classification

In fiber-optic telecommunications, the most frequently used light sources are electroluminescence diodes (LEDs) and lasers. Their general classification is given below.

Light emitting diodes (LED)

- surface emitting diodes
- edge emitting diodes
- RCE (resonance cavity enhanced) LEDs

Lasers (LD)

- FP (Fabry-Perot) lasers
- DFB (distributed feedback) and DBR (distributed Bragg reflector) lasers
- VCSEL (vertical cavity surface emitting) lasers
- waveguide lasers

8.3 LED construction

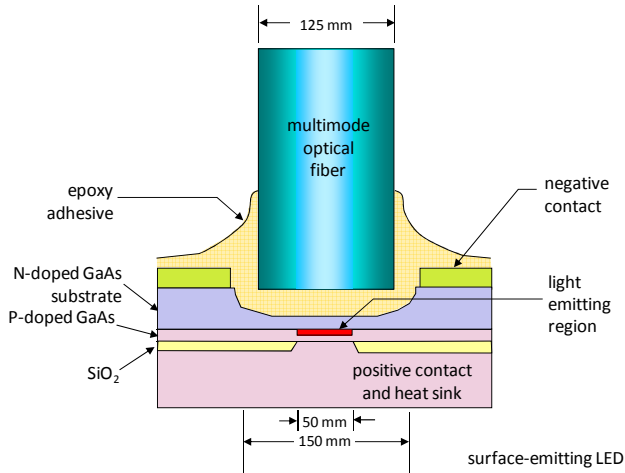


Fig. 8.1 Burrus-type surface diode construction (based on (Siuzdak, 1999)).

Among a number of LED structures, three of them are practically utilized in fiber-optic telecommunications: surface diode, edge diode, and superluminescence diode (Siuzdak, 1999). Because of their: low cost, low power consumption, and long lifetime, these electroluminescence diode types meet the light source requirements for fiber-optic telecommunications. Moreover, they can be modulated at frequencies up to 100 MHz, which is a sufficient value in majority of telecom applications (Mitschke, 2010).

The Burrus-type surface diode is shown in Fig. 8.1. Characteristic of this construction is a dimple in the N-doped GaAs substrate. The dimple causes a decrease in absorption of the generated light within its volume, and enables a minimum distance between the light-generating structure and the optical fiber. Structures of this type show a low thermal impedance in the active region, thus allowing higher electric current density and higher luminance (Siuzdak, 1999). From the technical point of view, it is of big benefit to use the epoxy resin for coupling the multimode optical fiber to the LED structure. An optically justed and mechanically robust connection is created in this way, and light coupling from LED's active volume directly to fiber is ensured. The use of other, more complicated, and often ineffective coupling techniques is eliminated as well.

8.4 Laser – definition

Consecutive enhancements in the fiber optic telecommunications have exerted a constant pressure towards increasing the light source performance in terms of:

- low beam divergence,
- low spot size at focus,
- high monochromaticity,
- high total power, power density and luminance,
- short pulse duration.

These are lasers, which meet all the requirements above.

The name – laser – is an acronym for Light Amplification by Stimulated Emission of Radiation (Silfvast, 2004).

8.5 Laser – principle of operation

The radiation emission by a laser (lasing action) requires the following conditions to be fulfilled:

1. Presence of metastable states (ms)
2. Energy pumping (to put atom into ms)
3. Population inversion
4. Stimulated emission
5. Optical feedback (FB)

8.6 Population inversion

There are three basic processes in the light-matter interaction. All of them result in a change of the quantum state of an atom, ion or particle. The processes are:

- absorption,
- spontaneous emission,
- stimulated emission.

In absorption, a photon becomes absorbed by an atom, and the atom transits from its basis state to an excited state. The second process, spontaneous emission, is a spontaneous transition of an atom from a higher-energy state to a lower-energy state. This transition results in a photon being emitted by the atom (photon emission). Properties of the emitted photon are completely uncorrelated (incoherent light is generated) (Siuzdak, 1999). Finally, the last light-matter interaction process, stimulated emission, also includes the photon emission and atom's transition from a higher- to a lower-energy state. In this process, however, the transition does not occur spontaneously. It is instead triggered by an external photon whose energy, which is important, equals the energy difference between the higher- and the lower-energy state.

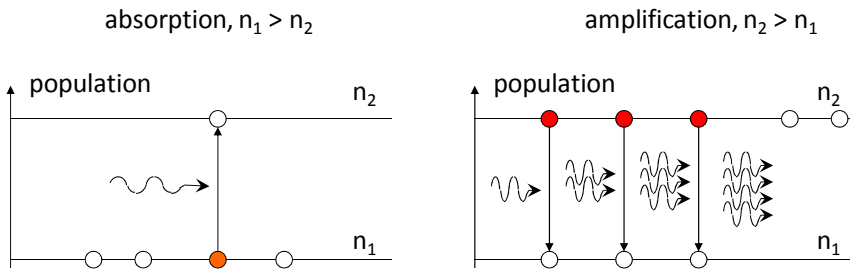


Fig. 8.2 Absorption, emission and illustration of population inversion (based on (Siuzdak, 1999)).

8.7 Optical feedback – Fabry-Perot resonator

For exciting the atoms' electrons from their basis state (lowest-energy level) to an excited state (higher-energy level), a strong external light source is used, the so called optical pump. Pump's light wavelength must be chosen appropriately. Within the laser's active volume, spontaneous emission results in light amplification, i.e. in an increase in the number of photons having identical properties. Besides the amplification, for the lasing action to take place also an appropriate feedback mechanism is needed. A positive-feedback setup most commonly used in lasers is the Fabry-Perot cavity. It is usually realized by means of two mirrors M_1 , M_2 placed at opposite ends of the active medium. The light undergoes multiple reflections off the mirrors, and additional photons are generated each time light passes through the active medium. The M_2 mirror is a semitransparent one, thus allowing part of the amplified radiation (light) to exit the cavity. It is important to note that the positive feedback only occurs when lightwaves that propagate in the same direction, after multiple reflections are in phase i.e. interfere constructively (lightwaves being out of phase would cancel each other, would interfere destructively) (Siuzdak, 1999).

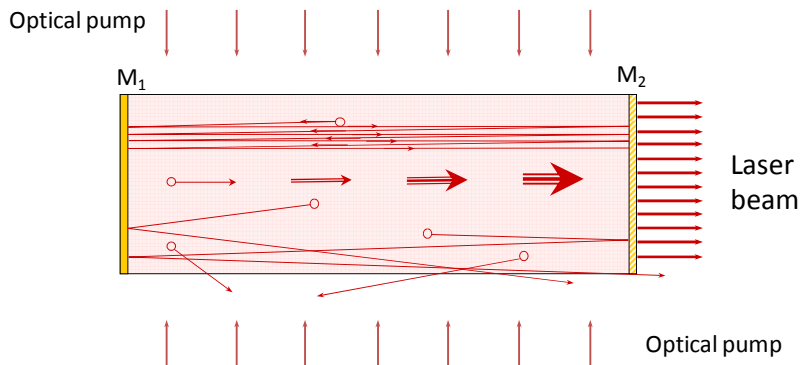


Fig. 8.3 Fabry-Perot resonator serving as an optical feedback element for the laser.

8.8 Lasers – classification

Considering the lasing medium types, lasers can be divided as follows:

1. Solid state lasers: lasing medium placed in a solid state matrix. Examples: neodymium laser-YAG <Yttrium Aluminum Garnet> 1.064 μm , ruby laser
2. Gas lasers
 - a. Atomic He-Ne, 632.8 nm
 - b. Molecular CO_2 , 10.6 mm
 - c. Ion Ar^+ , main wavelengths 488, 514 nm
 - d. Excimer (ionized fluorides of noble gases) UV sources
3. Dye lasers (*liquid*) Liquid solution of organic dye. Possible wavelength tuning (VIS, NIR). Tuning range depends on selected dye – for Rhodamine 6G \rightarrow 0.570 - 0.650 μm .
4. Semiconductor lasers (LD)

8.9 Pumping in semiconductor lasers: p-n junction current

In semiconductors, the population inversion, which is needed for the lasing action to occur, is attained by the injection of electrons into the conduction band. It can be realized in a p-n junction by means of a strong doping of both the materials having different conduction types. At high densities of injected carriers (electrons), an active region in the junction is formed where the population inversion takes place. Stimulated emission of radiation is possible there. Note that laser diodes (semiconductor lasers) can only be made of semiconductors possessing the direct bandgap (direct energy gap). They are e.g.: GaAs, InGaAs, GaN, InGaAsP. Lasers can not be made of indirect bandgap semiconductors, like e.g.: Si, Ge.

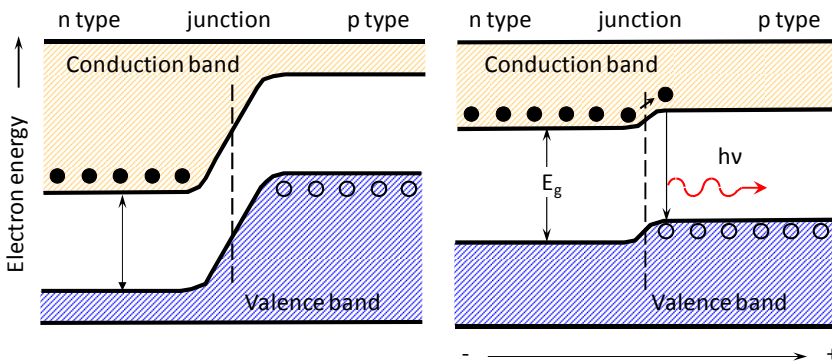


Fig. 8.4 Recombination of electron-hole pair and emission of a photon.

8.10 Simple semiconductor laser (homostructure)

Early semiconductor lasers were based on the homojunction structure and could only work at low temperatures. The p-n junction was created within a single crystal of a semiconductor material. Cavity mirrors in such lasers are usually created as cleavage planes of the semiconductor crystal or as properly polished and sputtered surfaces of the active layer. Low dimensions and a weakly defined generation volume result in a relatively low coherence of the emitted radiation.

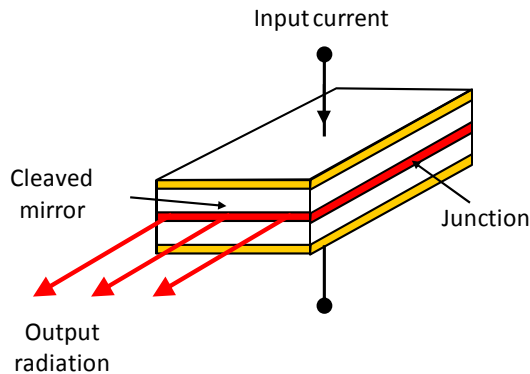


Fig. 8.5 Cross-section of a homojunction laser diode (based on (Mitschke, 2010)).

8.11 Heterostructure laser (cross section)

Heterojunction (heterostructure junction) is a junction made of semiconductors having different energy gaps (bandgaps), like e.g.: GaAs and $\text{Al}_x\text{Ga}_{1-x}\text{As}$, where x is a molar fraction describing the aluminum content. In heterostructure junctions that contain semiconductors of the same conductivity types (n-n or p-p), density of minority carriers can be reduced. This enables the radiative recombination to be bound within a small active volume. In turn, heterojunctions consisting of different conduction-type semiconductors show better carrier injection efficiency.

An example of the heterojunction laser is a laser incorporating the so called buried layer (BH – buried heterostructure). In this case, light is guided within a waveguide formed along the junction. The waveguide is created by introducing step-like variations in semiconductor's refractive index. The refractive index difference of the order of 0.2 – 0.3 strongly bounds the emitted mode, which leads to a high stability of mode's spatial distribution, and consequently to the generation of only one lateral mode in this type of laser structures (Siuzdak, 1999).

Moreover, threshold currents in this kind of lasers are usually low (on the level of 10-20 mA), and the optical power is linearly related to the driving current (no nonlinearities).

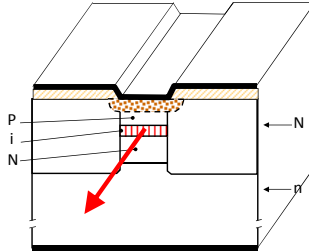


Fig. 8.6 Structure of a buried double-heterostructure laser (based on (Hunsperger, 2009)).

8.12 Astigmatism of semiconductor laser beam

Unlike the case of electroluminescence diodes (LEDs), the directional characteristics of laser radiation is relatively narrow. It strongly depends on the dimensions of the light-emitting surface, and the optical power distribution changes along the distance from this surface. Angular divergence of laser beam in far field (i.e. at a large distance from the emitting surface) is determined by the diffractive properties of light, and, using the symbols shown in Fig. 8.7, equals λ/w and λ/l in the horizontal and vertical direction, respectively.

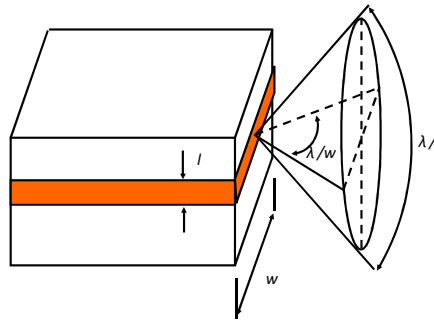


Fig. 8.7 Cross-section of a laser beam emitted from the edge of the semiconductor laser (based on (Siuzdak, 1999)).

8.13 Semiconductor laser types

According to their structure, semiconductor lasers can be grouped as follows:

- Homostructure lasers, threshold current (300 K) 30000 - 50000 A/cm²
- Single heterostructure (300 K) 6000 - 8000 A/cm²
- Double heterostructure (300 K) 500 A/cm²
- GRIN SCH (Graded-index separate confinement heterostructure), threshold current ~ 30 mA
- Mirror type: FP, DFB, DBR
- VCSEL (Vertical Cavity Surface Emitting Laser), threshold current ~ 1 mA

8.14 DFB Laser

Contemporary transmission systems often require the single-mode laser operation (to minimize dispersion). Although the semiconductor lasers discussed above are able to ensure this kind of operation, their modal selectivity is not sufficient due to the type of the feedback

mechanism employed (the Fabry-Perot cavity). A needed improvement in this regard is offered by lasers employing a distributed feedback. The longitudinal mode selectivity is greatly enhanced in this type of laser structures. There are two groups of lasers employing the distributed feedback mechanism, they are: the distributed feedback (DFB) lasers and the distributed Bragg reflector (DBR) lasers.

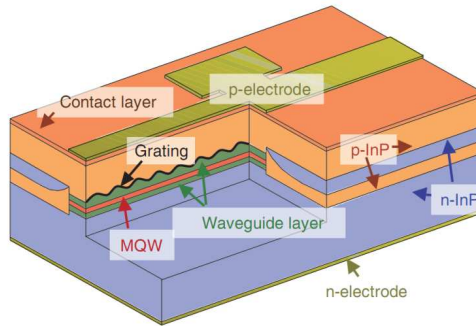


Fig. 8.8 Cross section of the DFB laser (Sato, Mitsuhara, & Kondo, 2009).

8.15 DFB Laser schematic

In a DFB laser, feedback is supplied by periodic refractive index variations within a waveguide placed below or above the active layer. Feedback occurs in a distributed manner, i.e. at all the refractive index changes along the entire cavity length. The distributed feedback's characteristic shows a single maximum determined by the grating period and it is located at $\lambda_0 = 2\Lambda n_{\text{wvg}}/v$, where Λ – grating period, n_{wvg} – refractive index of the waveguide, $v = 1, 2, 3, \dots$

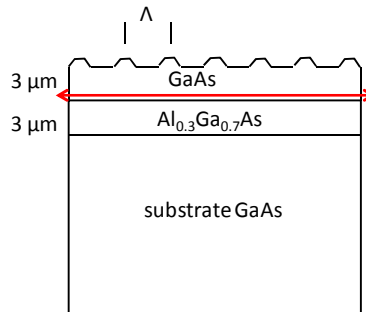


Fig. 8.9 Principle of operation and cross section of the DFB laser.

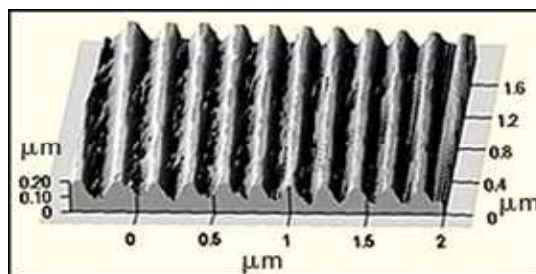


Fig. 8.10 SEM (Scanning Electron Microscope) picture of a Bragg grating utilized in the DFB laser.

8.16 VCSEL Laser

The next semiconductor laser structure utilized in fiber-optic telecommunications is the one employing a vertical optical resonator – the Vertical Cavity Surface Emitting Laser (VCSEL). The VCSEL structure is completely different from that of the classical Fabry-Perot resonator-based structures. The active layer is bound from top and from bottom with multilayer reflectors. The multilayer reflectors act as selective mirrors just like mirrors used in the DBR lasers. In such a structure, the cavity (resonator) is very short, usually shorter than the emitted light wavelength, and this enforces the single-mode operation of the laser (Mitschke, 2010). Thanks to a small volume of the resonant cavity, VCSELs attain low threshold current levels and high efficiency. Vertical emission is a significant advantage as well. In addition, VCSEL laser production costs are relatively low.

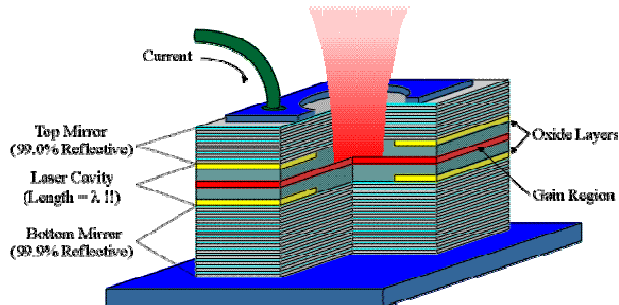


Fig. 8.11 Cross section of the vertical cavity surface emitting laser (VCSEL) (Giovanni, 2010).

8.17 Beam profiles of VCSEL and edge-emitting lasers

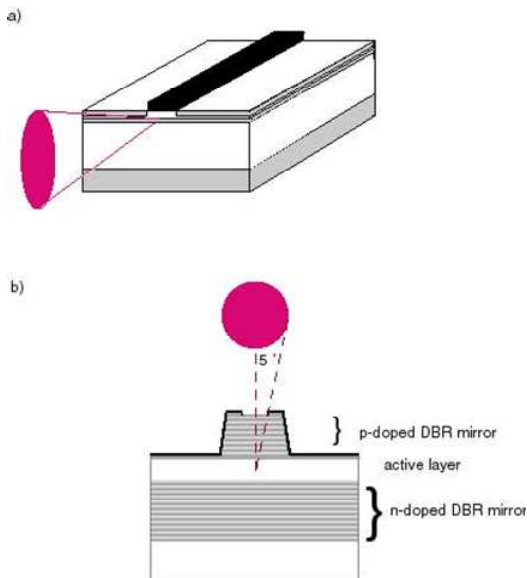


Fig. 8.12 Comparison of cross sections of the beams emitted from the edge emitting laser (a) and the VCSEL (b) (based on (Milligan, 2004)).

VCSEL lasers generate a light beam of more advantageous geometrical profile than that of beams generated by the edge lasers. It should be noted that the edge laser beam profile is

elliptical, and shows an angular divergence strongly dependent on the light-emitting surface dimensions. In VCSEL lasers, due to a circular internal aperture, the propagating light beam has a conic shape. The cone's base is circular and the divergence angle has a value of about 5°.

8.18 Optical Laser parameters

Lasers are commonly characterized with the following optical parameters:

- center wavelength,
- FWHM, spectral line spread,
- beam divergence.

8.19 Center wavelength and FWHM

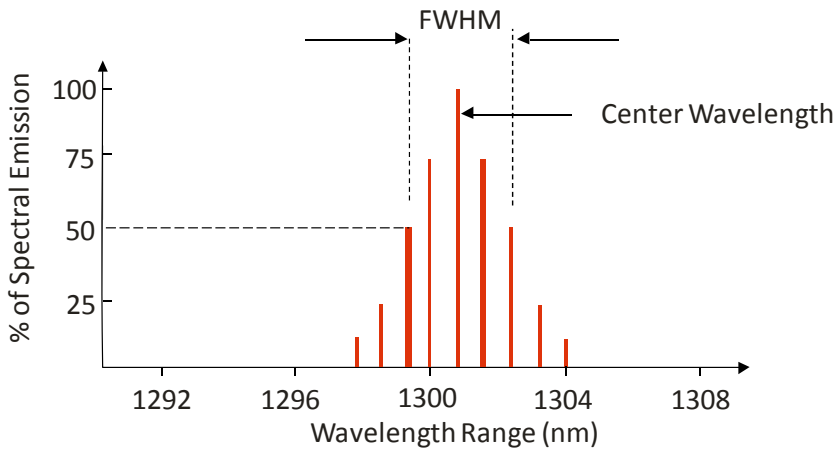


Fig. 8.13 Modal spectrum of light emitted by edge emitting laser. Shown are FWHM and the center wavelength(“Illustrated Fiber-Optics Glossary,” 2010).

Center Wavelength: In a laser, the nominal value central operating wavelength. It is the wavelength defined by a peak mode measurement where the effective optical power resides - Fig. 8.13. In an LED, the average of the two wavelengths measured at the half amplitude points of the power spectrum (“Illustrated Fiber-Optics Glossary,” 2010).

8.20 Laser Classifications (Safety Classes)

Laser classification according to the operational safety is (DeCusatis, 2008):

- Class I - lasers cannot emit laser radiation at known hazard levels.
- Class I.A. - special designation that applies only to lasers that are "not intended for viewing," such as a supermarket laser scanner. The upper power limit of Class I.A. is 4.0 mW.
- Class II - low-power visible lasers that emit above Class I levels but at a radiant power not above 1 mW. The concept is that the human aversion reaction to bright light will protect a person.
- Class IIIA - intermediate-power lasers (cw: 1-5 mW), which are hazardous only for intrabeam viewing. Most pen-like pointing lasers are in this class.
- Class IIIB - These are moderate-power lasers.
- Class IV - high-power lasers (cw: 500 mW, pulsed: 10 J/cm²), which are hazardous to view under any condition (directly or diffusely scattered), and are a potential fire hazard and a skin hazard.

The safe optical power level depends on the emitted light – the shorter the light wavelength, the lower the allowable optical power. The safe optical power also depends on the device configuration.

8.21 Detector – definition

Person or thing that detects.
UV detectors, IR detectors, ...
telecommunications detectors, ...

8.22 Optical-to-electrical converters

In case of fiber-optic telecommunications, when we say “detector”, we think of an optical-to-electrical (O/E) converter: a device used to convert optical signals to electrical signals. Also known as OEC



8.23 Detectors – main classification

In terms of the physical principle standing behind the photodetector’s operation, photodetectors fall into the following categories:

- Quantum detectors
A photodetector in which an electrical charge is produced when incident photons change electrons within the detecting material from nonconducting to conducting states. E.g. photoconductive detector; photovoltaic cell.
- Thermal detectors
The functional process includes absorption of infrared radiation, which causes a temperature change, consequently altering the physical properties of the detector’s elements.

8.24 Detectors sensitivity

One of the most prominent parameters characterizing the photodetectors utilized in fiber-optic telecommunications, is the photodetector spectral sensitivity. It informs about the detection spectral range and detection sensitivity available to a detector under consideration. Thermal detectors are characterized with a constant (but relatively low) sensitivity within a broad spectral range. These features make the thermal detectors a particularly versatile solution. For a specific device type, quantum detectors are usually a more efficient solution. Despite having a narrower detection spectral range, quantum detectors significantly outperform thermal detectors in terms of sensitivity. A comparison between the detection sensitivity of thermal detectors and silicon-based quantum detectors (an ideal and an actual device) is shown in figure Fig. 8.14.

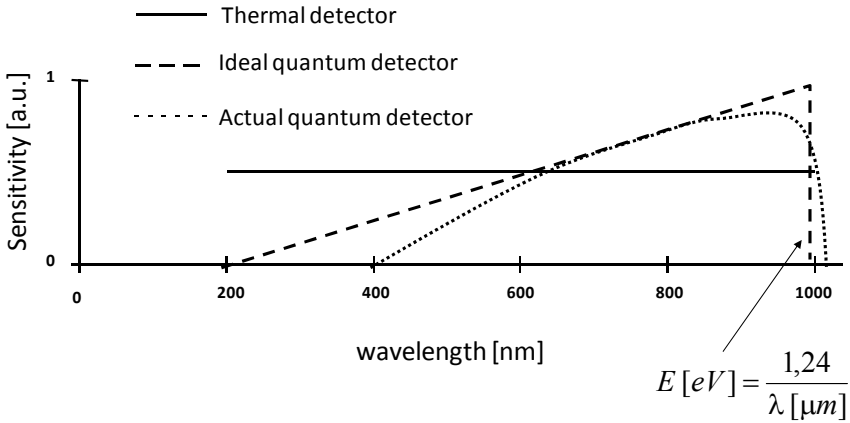


Fig. 8.14 Comparison of spectral sensitivity of quantum and thermal detectors (based on (Senior & Jamro, 2009)).

8.25 Quantum efficiency

In most cases, the quantum detectors utilize the carrier photogeneration in a reverse biased p-n junction. Carrier pairs (electron-hole pairs) generated by photons, are being separated within the junction by an electric field – the electric current (photocurrent) occurs. Photocurrent intensity I_p is directly proportional to the optical power P_{in} reaching the detector (Senior & Jamro, 2009)

$$I_p = RP_{in} \quad (8.1)$$

where R is the detection sensitivity [A/W] of the detector.

Detector's sensitivity is associated with its quantum efficiency η , which is defined as

$$\eta = \frac{\text{number of generated electrons}}{\text{number of incident photons}} = \frac{I_p/q}{P_{in}/h\nu} = \frac{h\nu}{q} R \quad (8.2)$$

Thus, sensitivity

$$R = \frac{\eta q}{h\nu} \approx \frac{\eta \lambda}{1.24}, \quad (\nu = c/\lambda) \quad (8.3)$$

where $l = [\text{mm}]$, $q = 1.602 \cdot 10^{-19} [\text{C}]$, $c = 3 \cdot 10^8 [\text{m/s}]$, $h = 6.62 \cdot 10^{-34} [\text{J.s}]$.

8.26 Detectors – other classifications

There are multiple different classifications possible of fiber-optics detectors. Some of them are given below.

Detector can be classified according to:

- Physical principle of operation (thermal, quantum)
- Applications (telecommunications, ..., astronomy)
- Design (single elements, ..., arrays, CCD)

Other, designer specific classifications:

- Spectral sensitivity
- sensitivity (photon counters, ..., power detector)
- material (metal, semiconductor, dielectric)

- price (photoconductor → photodiode → photomultiplier)

8.27 Absorption coefficient of semiconductors

Quantum efficiency is also related to the absorption coefficient of material of which detector is constructed. Absorption of semiconductor materials depends on light wavelength as shown (for selected semiconductors) in figure Fig. 8.15. For wavelengths exceeding some threshold value, absorption coefficient falls down to zero. The mentioned threshold value of light wavelength is called the absorption edge wavelength. For lightwaves longer than that of the absorption edge wavelength, photon energy is lower than the bandgap energy of given semiconductor material. This, in turn, prevents the electron-hole pairs (photo)generation, thus there is photocurrent flow and the detector cannot work.

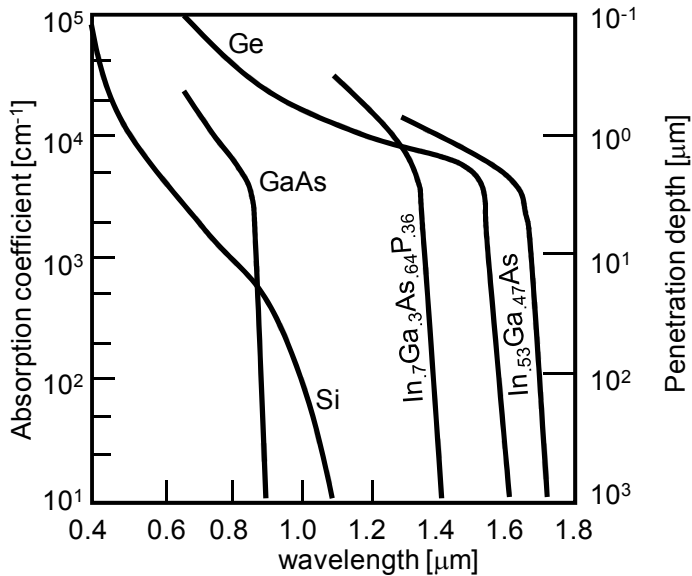


Fig. 8.15 Absorption coefficient of selected semiconductor materials in the function of light wavelength (Senior & Jamro, 2009).

8.28 PIN photodiode

A photodetector type commonly used in fiber-optic telecommunications is the PIN photodiode. It differs from the classical photodiode by an additional semiconductor layer. Whereas classical photodiodes employ the p-n junction, PIN photodiode structures contain an additional layer of undoped semiconductor (this layer is usually called the intrinsic region) (an intrinsic semiconductor is a pure semiconductor without any significant dopant species present) inserted between the p-doped layer and the n-doped layer. Thanks to the intrinsic layer (region), width of depleted region within diode is increased. The undoped semiconductor possesses a high electric resistance. This makes the voltage drop (electric potential difference) across the intrinsic layer to be relatively high. Photocurrent contribution coming from (electric) carriers drift (drift velocities are much higher than diffusion velocities) dominates here and is the reason for high operating speeds of PIN photodiodes (DeCusatis, 2008).

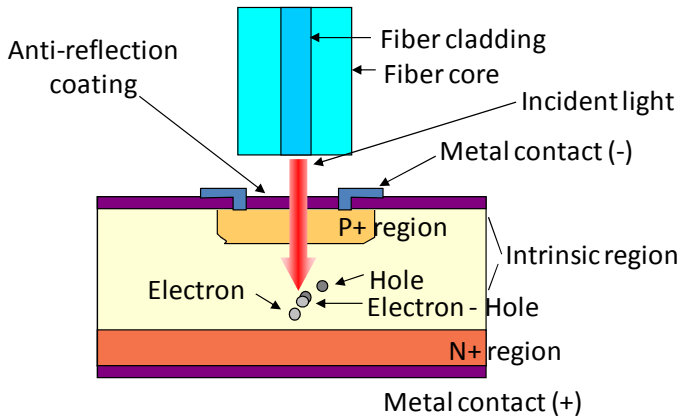


Fig. 8.16 Cross section of a PIN photodiode structure (based on ("Illustrated Fiber-Optics Glossary," 2010)).

8.29 APD photodiode

Another photodetector type utilized in fiber-optic telecommunications is the APD (Avalanche Photodiode) photodiode. APD internal structure is presented in figure Fig. 8.17. APD diodes incorporate an additional layer in which electric field of a high intensity arises after appropriate external voltage is applied. Kinetic energies of electrons and holes within this layer, can reach values that are sufficient for the generation of new electron-hole pairs. This is called the avalanche effect. In avalanche photodiodes (APDs), a single carrier generated via photon absorption (a photogenerated carrier) can, thanks to the avalanche effect, generate additional, secondary carriers, which eventually leads to an increase in the electric current flowing through the photodiode. Disadvantages of APD photodiodes are the need for a specialized biasing circuitry (usually 100-400 V) and a significant temperature dependence of the avalanche effect coefficient (Siuzdak, 1999).

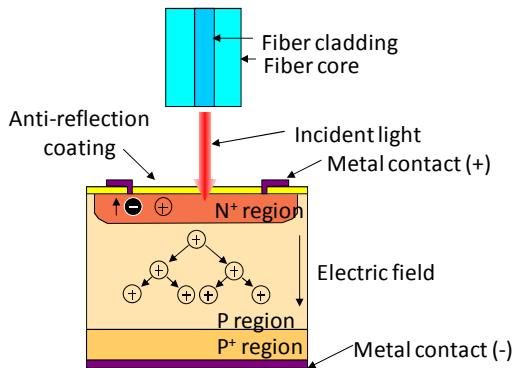


Fig. 8.17 Cross section of an APD photodiode structure (based on ("Illustrated Fiber-Optics Glossary," 2010)).

8.30 Other types of semiconductor detectors

Besides the PIN-type and APD-type photodiodes, there are also many other construction variants of photodetectors used in fiber-optic telecommunication. Figure Fig. 8.18 shows four, most frequently used constructions.

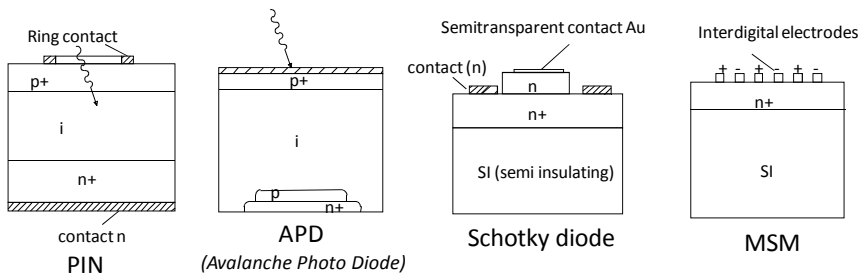


Fig. 8.18 Semiconductor detector types utilized in fiber optic telecommunications.

8.31 Photodiode parameters

Among parameters describing the photodiodes, the most significant are:

1. Sensitivity
2. Spectral response
3. Capacitance
4. Dark current

8.32 Dark current

Dark current is the induced current that exists in a reversed-biased photodiode in the absence of incident optical power. Usually caused by the shunt resistance of the photodiode. A bias voltage across the diode (and the shunt resistance) causes current to flow in the absence of light.

8.33 Receiver Sensitivity

Receiver sensitivity is the minimum acceptable value of received power needed to achieve an acceptable BER or performance. It takes into account power penalties caused by use of a:

- transmitter with worst-case values of extinction ratio, jitter, pulse rise times and fall times,
- optical return loss,
- receiver connector degradations, and
- measurement tolerances.

8.34 BER

Bit error rate (BER) is the fraction of bits transmitted that are received incorrectly.

The bit error rate of a system can be estimated as follows (“Illustrated Fiber-Optics Glossary,” 2010):

$$BER = Q \left[\sqrt{\frac{I_{MN}^2}{4N_0B}} \right] \quad (8.4)$$

Where N_0 is the noise power spectral density [A^2/Hz], I_{MIN} is the minimum effective signal amplitude [A], B is the bandwidth [Hz], and $Q(x)$ is the cumulative distribution function (assumed to be the Gaussian distribution).

8.35 Dispersion penalty

The result of dispersion in which pulses and edges smear making it difficult for the receiver to distinguish between ones and zeros. This results in a loss of receiver sensitivity compared to a short fiber and measured in dB.

The equations for calculating dispersion penalty are as follows (“Illustrated Fiber-Optics Glossary,” 2010):

$$\tau = \omega \cdot D_{\lambda} \quad [ps/km] \quad (8.5)$$

$$f = \ln(4)/(\tau \cdot \pi) \quad [Hz/km] \quad (8.6)$$

$$F_f = f/L \quad [Hz] \quad (8.7)$$

$$\eta_L = c \cdot (F_R/F_f)^2 \quad (8.8)$$

$$dB_L = 10 \cdot \log(1 + \eta_L) \quad [dB] \quad (8.9)$$

where meanings of the symbols used are: ω – laser spectral width [nm], D_{λ} – fiber dispersion [ps/nm/km], τ – system dispersion [ps/km], f – bandwidth-distance product of the fiber [Hz·km], L – fiber length [km], F_f – fiber bandwidth [Hz], C – a constant equal to 0.5, F_R – receiver data rate [b/s], and dB_L – dispersion penalty [dB].

8.36 Spectral characteristics of semiconductor photodiodes

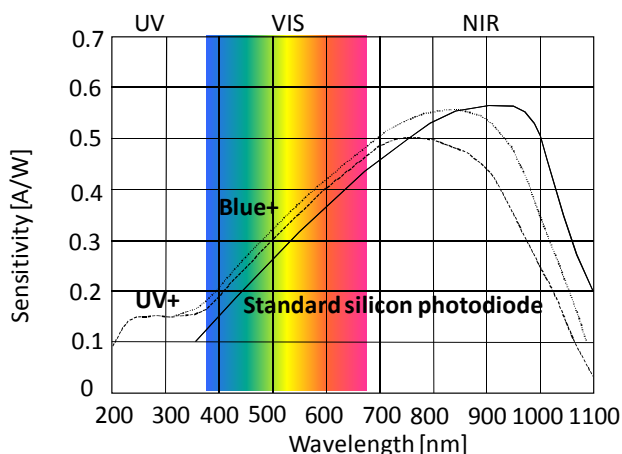


Fig. 8.19 Spectral sensitivity of silicon photodiodes.

Spectral characteristics show photodetector sensitivity in the function of light wavelength. Shapes of individual curves are strictly connected with material being used in the detector and with absorption characteristics of this material. In figure Fig. 8.19 there are shown spectral characteristics of three silicon-based photodiode types: standard, UV+ and Blue+. All the presented characteristics are similar in shape and all sensitivity maxima lay in the near infrared (NIR) spectral range. By changing the doping level (of silicon) and the geometry of individual layers it is possible to “tune” photodiodes, i.e. to adjust their spectral characteristics in order to match the requirements of concrete applications. Such an adjustment may for example be the extending of photodiode’s characteristics to reach the UV spectral range.

8.37 Detector sensitivity specified in power units (W or dBm)

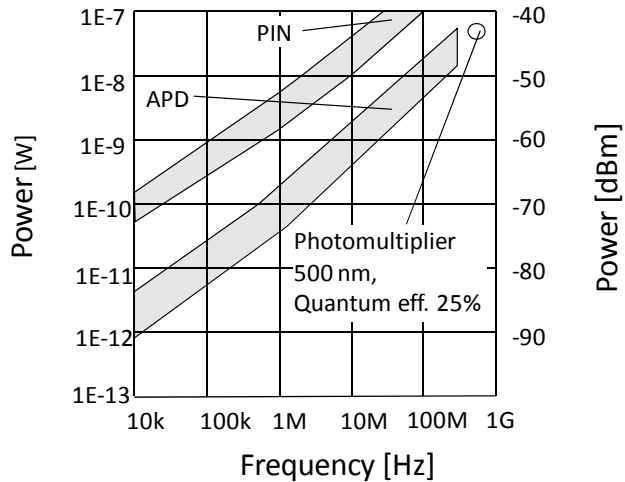


Fig. 8.20 Sensitivity of photodetector expressed in units of power.

Plot in figure Fig. 8.20 compares the sensitivities of PIN and APD photodetectors in the function of the modulation frequency. Scales in both the W and dBm optical power units are shown. In addition, sensitivity of a 500 nm central wavelength, 25% quantum efficiency photomultiplier is shown. All the characteristics assume: SNR = 5, BER = 10^{-9} .

8.38 Receiver module

Receiver: A terminal device that includes a detector and signal processing electronics. It functions as an optical-to-electrical converter (“Illustrated Fiber-Optics Glossary,” 2010).

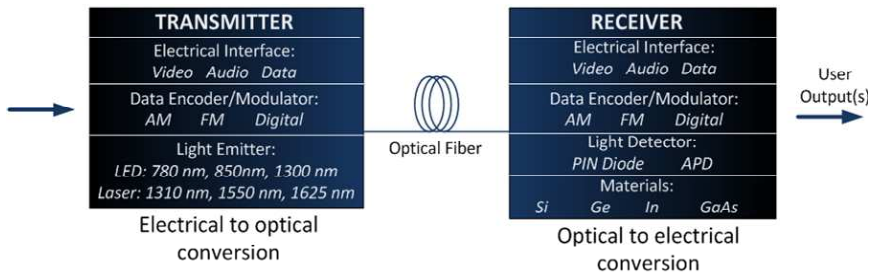


Fig. 8.21 Schematic diagram of telecommunication transmitter and receiver modules.

9 Connecting of passive and active photonic elements

9.1 Introduction

In optoelectronics the package accounts for 60 to 80 percent of current manufacturing expenses in component assembly (in microelectronic the proportion is reversed).

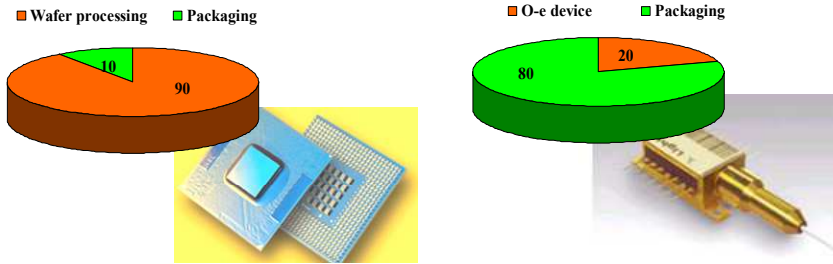
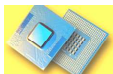


Fig. 9.1 Manufacturing expenses of electronic and optoelectronic circuits

Development of packaging technologies is crucial for the development of integrated optoelectronic.

Packaging is a sequence of technologies that involve:

- connecting,
- protecting,
- and manufacturing of the devices.



Microelectronics devices	Optoelectronic devices
<ul style="list-style-type: none"> • high frequency design • optimized automatic assembly • planar design • electrical connection • components easily recognized (with metal lines as the references) 	<ul style="list-style-type: none"> • high frequency design • optimized for manual assembly • 3D design, difficult visual inspection • electrical and optical connections • fiducial markings necessary to enable visualization and recognition of some elements

Fig. 9.2 Micro versus optoelectronic packaging - similarities and differences

Optoelectronic device fabrication includes the following steps:

- Wafer processing
- Thin film processing
- Device and subassembly packaging
- Fiber handling and alignment
- The finishing steps: tuning, adjusting and testing

The optoelectronic technology is very challenging. It involves multiple, proprietary fabrication techniques and processes involved, coupled with a lack of package and material handling standards.

In the figure below a complete assembly process of optoelectronic devices is presented.

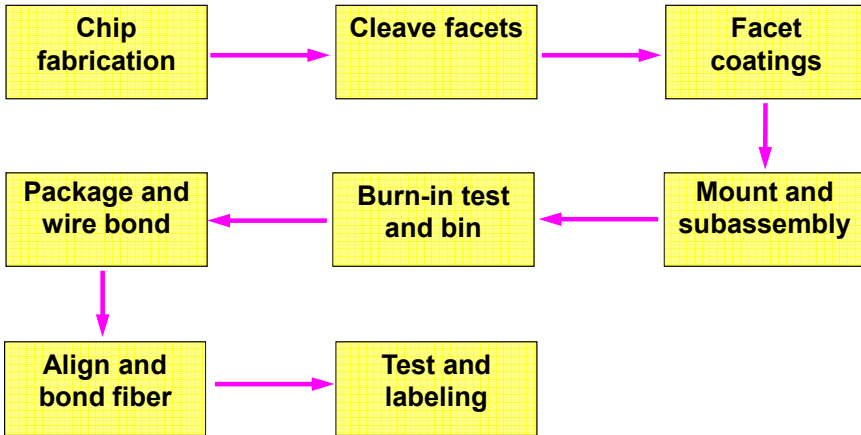


Fig. 9.3 Optoelectronic devices assembly process

The main technologies used for optoelectronic device assembly are listed in the following table:

Tab. 9.1 Technologies for optoelectronic device assembly

Process	Description
Eutectic component attach (for heat dissipation)	In-situ pulse heat, Au-Sn preform
Epoxy component attach	Electrically conductive and nonconductive adhesives
Wire bond	Au wire (25µm diameter), Au ribbon (75µm wide)
Fiber alignment	Passive or active
Active component alignment	Laser, detector, lens, fiber

9.2 Optics of optoelectronic packaging

The critical factor in optoelectronic device packaging is efficient light coupling. Optical loss factors include:

- Efficiency of power transfer (insertion loss)
- Reflections reduction (back reflection)

Usually computer modeling is required prior to fabrication process. Modeling methodology depends on device dimensions. Wave optics or ray optics approach is selected accordingly.

Power density profile of guided light beams can be approximated by Gaussian function:

$$p(r) = p(0) \exp\left\{-2\left(\frac{r}{w_0}\right)^2\right\} \quad (9.1)$$

$2w_0$ is called the mode-field diameter (MFD) - It is diameter at $e^{-2} \sim 13.5\%$ of P_{\max}

$$\frac{MFD}{CD} = A + B \left(\frac{\lambda}{\lambda_c} \right)^D \quad (9.2)$$

A, B, C, D = empirical parameters, λ_c – mode cutoff wavelength

9.3 Classifications and packaging systems

Approach towards optoelectronic devices assembly changes over time.

1. Early days - manual assembly
2. Contemporary - semiautomatic or automatic assembly; small or medium scale production
3. The future - fully automatic assembly; massive scale production; short time to market for new components

Nowadays optoelectronic packages are complex devices themselves - composed of optical, microwave and thermal elements – optoelectronic packaging adding to this complexity. Because of this complexity new diagnostic methods will be necessary for optoelectronic devices and packages. Diagnostic methods for optoelectronic packaging:

- Operational properties
 - optical (power/sensitivity, coupling efficiencies, optical bandwidth)
 - electrical DC
 - electrical RF
 - Structural properties (conformity with design detail, internal cracks and voids)
 - Thermal properties
- It should be noted that 3D visualization is required for optical and optoelectronic elements of the package.

Contemporary optoelectronic packaging systems can be classified according to the manual labor included.

Tab. 9.2 Optoelectronic packaging - classification according to the packaging system design

	Alignment type	Notes
1	Passive	Possible very high adjustment accuracy. Inexpensive equipment. Different dies are needed for different application .
2	Active	Universal equipment, can be expensive if high precision is required. Feedback during positioning guarantees device performance.
3	Mixed	

Below an example of mixed optoelectronic packaging is shown. Schematic shows the construction of the package and the principle of the mixed packaging (note infrared die-bonding).

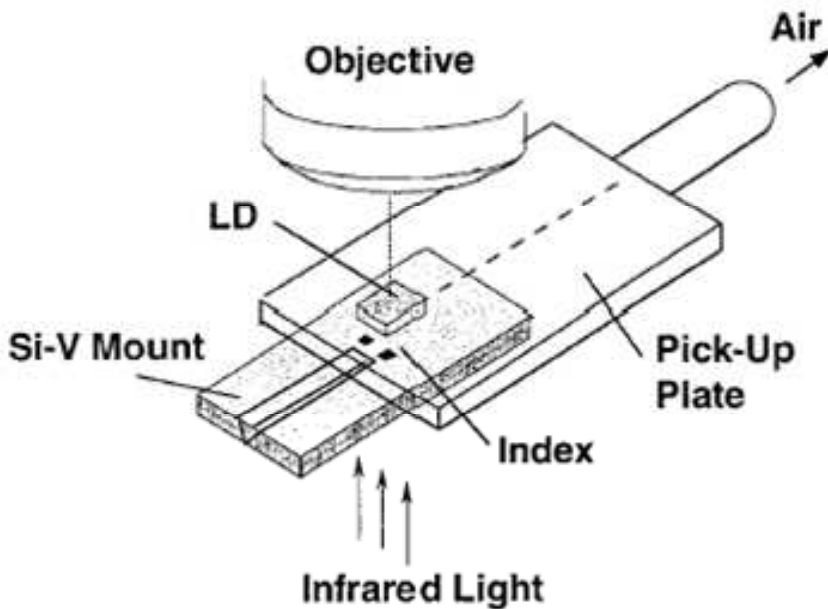


Fig. 9.4 Example of mixed optoelectronic packaging

9.4 Optoelectronic package requirements

The table below summarizes optoelectronic devices that will require dedicated packages design and technology.

Tab. 9.3 Different types of photonics devices to be packaged

	Device	types	applications
1	Laser diodes	FP, VCSEL, DFB, DBR	Telecommunications, datacom., sensors, automotive industry.
6	Detectors	Mainly semiconductor	All kinds of systems
2	DWDM multiplexers and switches	Grating, waveguide, FBG	High speed fiber optic transmission (SM)
3	Filters	Interference, FBG	High speed fiber optic transmission (SM), sensors
4	Couplers	Fused, integrated optics	Fiber optic systems of all kinds. SM, MM, POF fibers.
5	Isolators	Magneto-optic rotators	High speed telecom. In connection with high quality lasers.

6	Optoelectronic integrated circuits		Advanced systems
---	------------------------------------	--	------------------

Optoelectronic package design depends on the functionality of the device being packed. Different constructions and respective requirements are collected in the following table.

Tab. 9.4 Design type and package requirements

	Construction class	Requirements
1	Free space	Lenses, beam collimation, (micro)optical beam-forming elements
2	Waveguides	But-coupled waveguides, high adjustment accuracies
3	Photonics devices arrays	Thermal problems arise for emitting devices. High packaging density (new connector styles may be required – e.g. SFF connectors).

The table below specifies requirements of optoelectronic packaging according to area of application.

Tab. 9.5 Application and package requirements

	Application	Packaging requirements
1	Telecommunications	Mainly SM fibers, very high accuracy, 20+ years working time
2	Datacom., networks	High accuracy and reliability, SM and MM fibers, in the future possibly POFs in massive market (FTTH)
3	Automotive industry	Very high reliability, lower accuracy.
4	Medicine	Special material requirements
5	Sensors	Custom parameters, system dependent.

9.5 Assembly conditions

There are specific conditions and requirements specific for optoelectronic packaging, such as accuracy, geometry and method of alignment or thermal requirements. In the following table the assembly conditions related to the optical path are listed and specified.

Tab. 9.6 Optoelectronic packaging - assembly conditions

	“Optical-path” Assembly-Conditions	Requirements
1	Accuracy	<1 μ m for SM systems, >1 μ m for MM systems. 10 up to 100 μ m for POFs and automotive applications.

2	Alignment (levels of freedom)	X, Y, Z with different accuracies in different directions. Φ (angle).
3	Alignment method	Visual (microscope, camera, image processing) or infrared (“see through the surface”, observation of “hot” active transmission devices (near infrared).
4	Other assembly issues	Optical connection efficiency Electrical (electronic protection, ESD) Thermal Hermetization

In systems with hierarchical structure, hierarchy level may influence packaging – summary of related issues is given in the table below.

Tab. 9.7 Communication system level packaging hierarchy

Level	Contents general	Contents optical	Interconnection distance
1. System level	System service functions	Network interconnections	≈ 100 m
2. Cabinet level	Functioning of the system on the rack	Cabinet level interconnection	~ 10 m
3. Unit level	Interconnection between packages	Interconnection between modules	< 1 m
4. Board level	Board functioning. Power supply	On-board device interconnections and signal transmission	~ 10 cm
5. Fiber level	Placement	Optical fiber placement	~ 1 cm
6. Beam level	Stability, precision	Beam focusing	~ 1 μ m

9.6 Generic optoelectronic package

Design of an optoelectronic package depends of a specific application. However, certain elements are common for different packages. Diagram of a generic optoelectronic package, comprising all basic elements is presented in the following picture.

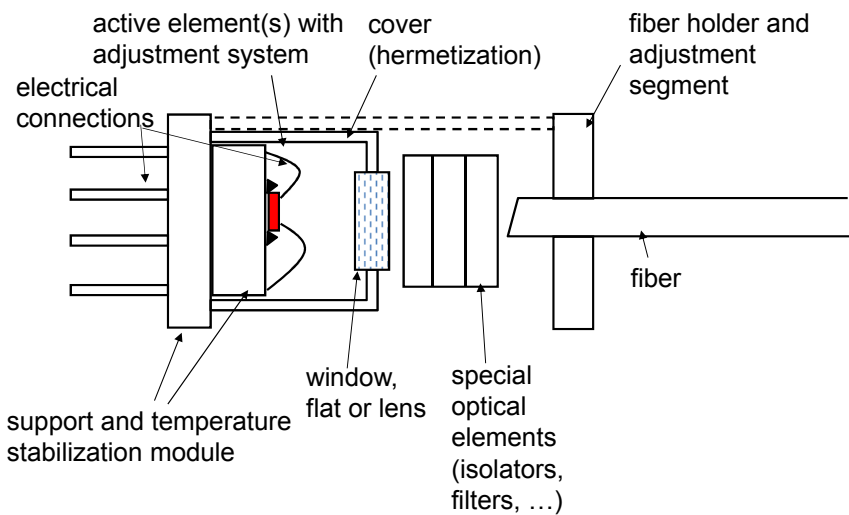


Fig. 9.5 "Generic" optoelectronic package

9.7 Design solutions

Probably the most important issue in packaging of fiber-optical devices is efficiency of light coupling between optical fiber and an active device, e.g. coupling between a laser-chip and single mode fiber. Several solutions to this problem are illustrated in the following two figures.

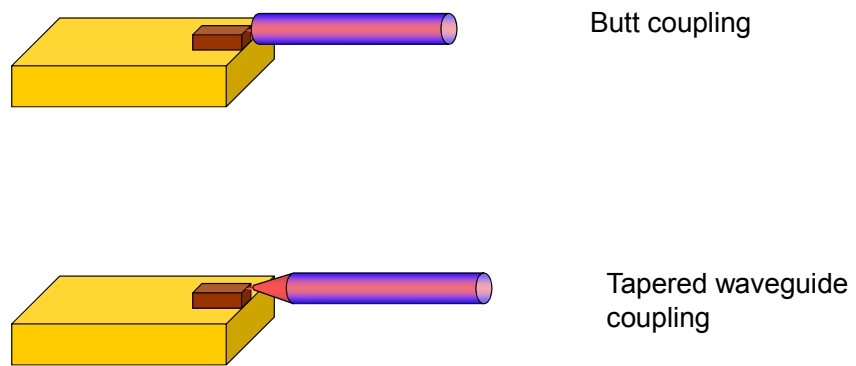


Fig. 9.6 Comparison of different LD – fiber coupling techniques

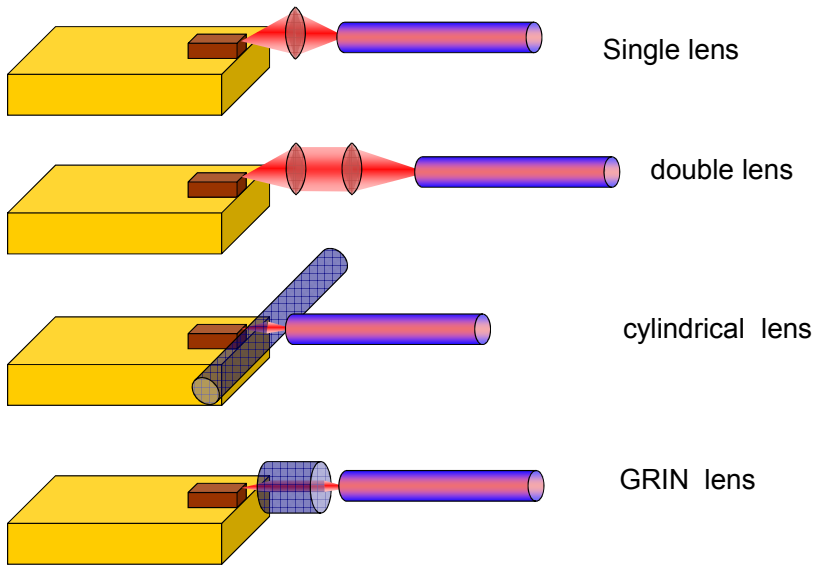


Fig. 9.7 LD coupling with lenses possibilities

9.8 Some notes about materials

Materials for packages should be selected according to application area of the packaged device. Below is a list of selection criteria of the materials

- Temperature properties (resistance, stability, resistance above 100C, 200C for short time, thermal coefficients of expansion)
- Optical properties (attenuation, refractive index)
- Mechanical properties
- Manufacturability
- Environmental resistance (weatherability)
- Price, availability

Selection criteria should also include envisioned application area of the devices.

- Telecommunications systems. High performance, very high reliability and longevity (up to 30 years), very high unit price. Based on metal, glass, ceramic
- Access network systems. High performance and reliability, medium life times (10 years). Low unit price. Based on polymer materials.

10 Dispersion of optical fibers

10.1 Dispersion

By a general definition, dispersion is any phenomenon in which the velocity of propagation of an electromagnetic wave is wavelength dependent.

In communication technology, dispersion is used to describe any process by which an electromagnetic signal propagating in a physical medium is degraded because the various wave components (of different frequencies and wave vectors) have different propagation velocities

10.2 Dispersion in optical fibers

In optical fiber communications dispersion relates to a few well defined fiber parameters, namely:

- Mode dispersion [200-800 MHz·km]
- Chromatic dispersion [0-20 ps/km·nm]
 - Material disp.
 - Waveguide disp.
- Polarization dispersion ≤ 0.2 [ps/km^{1/2}]

Mode dispersion (modal dispersion, intermodal dispersion) is characteristic of multimode fibers only. Different propagating modes of multimode fiber have slightly different propagation constants. In other words, lightwave propagation velocity varies depending on which mode light propagates in. The most frequently used mode dispersion unit of measure is [MHz·km]. This unit emphasizes the impact of the mode dispersion on a maximum frequency (data rate) that can be transmitted over the given fiber. For example, 200 MHz·km indicates: over a fiber that is 1 kilometer (km) long, data stream of the frequency 200 megahertz (MHz) can be transmitted. If the length of the fiber is increased to 2 kilometers, then the maximum data stream frequency will be 100 megahertz.

Chromatic dispersion is a collective name for the next two types of dispersion – material dispersion and waveguide dispersion. Unlike mode dispersion where lightwave propagation velocity depends on the propagating mode number, in the chromatic dispersion, velocity of light within waveguide depends on light wavelength. Chromatic dispersion is measured (expressed) in the units of [ps/km·nm]. For example, 90 ps/km·nm means: two wavelengths that differ by 1 nanometer (nm) will have a differential delay of (will be delayed to one another by) 90 picosecond (ps) after traveling a one-kilometer (km) length of fiber.

Material dispersion directly results from the fiber material's refractive index being dependent on light wavelength. In the normal dispersion regime, found in most materials, within spectral ranges of low absorption, refractive index decreases as wavelength increases.

Waveguide dispersion originates solely from the fact that light propagation takes place within fiber (waveguide). Waveguide dispersion is independent of waveguide's material optical properties. Optical field properties (shape, propagation constant) of a propagating mode change with wavelength.

Polarization dispersion is caused by fiber's birefringence, i.e. different propagation velocities (different propagation constants) experienced by lightwaves polarized in orthogonal directions. In real-world fibers, a linearly polarized lightwave, i.e. polarized in only one of the two orthogonal directions, will "split" into lightwaves propagating in two orthogonal polarizations. The polarization initially absent will be excited because of inhomogeneities in fiber's cross-section. These inhomogeneities are fluctuations in fiber material's refractive index, and in stress locally exerted on fiber. Polarization dispersion unit of measure is [ps/km^{1/2}]. For example, 0.2 ps/km^{1/2} in a 100 km long fiber means a 2 picosecond (ps) differential delay between orthogonal polarizations after a propagation distance of 100 kilometers (km) ($0.2 * 100^{1/2} = 2$).

10.3 Mode dispersion. Pulse broadening in step index fiber

In multimode fibers, besides the chromatic dispersion also occurs the so called mode dispersion. Mode dispersion results from different values of group velocity at which individual optical modes propagate within fiber. Even an ideally monochromatic optical signal (signal containing light of only one wavelength, which is only possible in theory), once it is coupled into a multimode fiber it will be affected by the mode dispersion. It is because multiple optical modes will be excited in fiber by the input signal. Each one of the excited modes will then reach output optical detector at a slightly different time. This phenomenon can be explained within the framework of geometrical optics (ray optics) as shown in figure Fig. 10.1. From the schematic depiction of light ray propagation paths we can see that different modes travel different distances before they reach the detector. As an result, data pulse temporal broadening occurs.

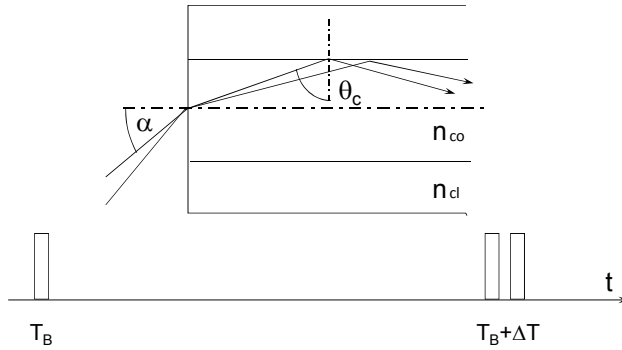


Fig. 10.1 Geometrical optics explanation of the mode dispersion. Portions of the input optical pulse energy propagate as different waveguide modes. As propagation path lengths of the modes differ, propagation times are also different – temporal pulse broadening occurs.

10.4 Dispersion of single mode fiber

The general remarks concerning the chromatic dispersion (from paragraph 10.2) are shown in greater detail in figure Fig. 10.2.

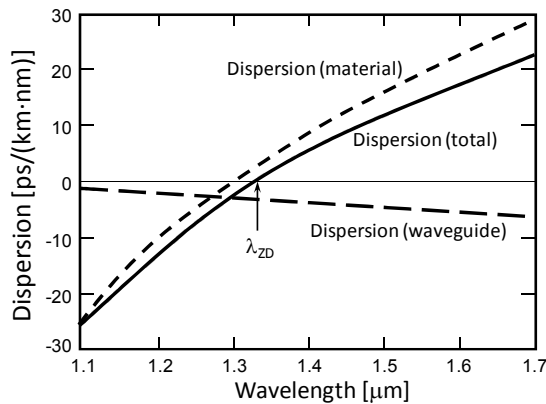


Fig. 10.2 Dispersion of single mode fiber. Both the contributions of the chromatic dispersion – the waveguide dispersion and the material dispersion – show opposite types of wavelength dependence (Agrawal, 2002).

In fact, both the contributions of the chromatic dispersion show opposite types of wavelength dependence. Whereas material dispersion values increase with light wavelength, the waveguide dispersion tends to lower values at the same time. A wavelength denoted as λ_{ZD} in figure Fig. 10.2, for which both the above dispersion types cancel, is called the zero-dispersion wavelength. Its spectral location can be adjusted by a proper fiber cross-section design (geometry, material doping). Zero-dispersion wavelength can e.g. be located within the second telecommunication window (i.e. around $1.3 \mu\text{m}$) thus making the fiber show both low attenuation and low dispersion – a solution especially useful in long-haul fibers.

10.5 Dispersion shifted fibers (DSF)

Considering the spectral distribution of chromatic dispersion values, three types of telecommunication optical fibers are used:

- fibers showing standard dispersion,

- dispersion shifted fibers, and
- dispersion-flattened fibers.

All three cases are presented in figure Fig. 10.3.

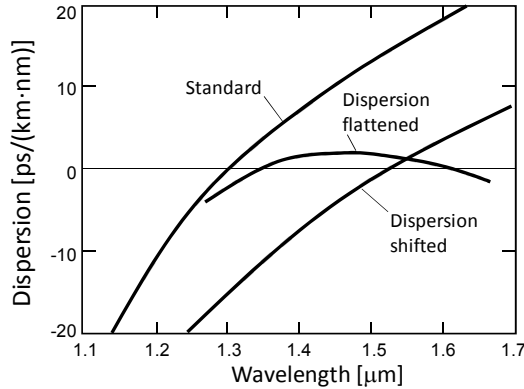


Fig. 10.3 Dispersion characteristics types found in the telecommunication silica-glass fibers (Agrawal, 2002).

In dispersion shifted fibers, the zero-dispersion wavelength lies within the third telecommunication window. However, the general character of the dispersion spectral distribution remains similar to that of normal dispersion. This is changed in dispersion-flattened fibers where dispersion distribution is significantly different. It is designed to be flat thus able to maintain low dispersion values over a relatively broad spectral range.

In silica-glass single-mode fibers, the zero-dispersion wavelength location within the third telecommunication window (i.e. the case of standard dispersion) can be achieved using the simplest fiber cross-section structure, the step-index fiber. Achieving dispersion flattening or dispersion shifting requires the utilization of more sophisticated fiber cross-section structures (i.e. more sophisticated types of refractive index distributions along fiber radius). For example, refractive index distribution can then be designed to have several maxima and minima along fiber radius, which is in contrast with only one step-like change present in step-index fibers.

10.6 Dispersion of optical fibers

Below, there is a summary of the typical values of the dispersion-related parameters. All the values are given for the telecommunication silica-glass fibers of various types.

Bandwidth of multimode fibers [MHz·km]

- 850 nm 400-800 (50/125) 160-400 (62.5/125)
- 1300 nm 400-1500 300-1200

Chromatic dispersion of singlemode fibers [ps/km·nm]

- 1285-1330 nm ≤ 3.5
- 1550 nm ≤ 18

Polarization-mode dispersion

- PMD of the fiber ≤ 0.2 [ps/km^{1/2}]

Meanings of the individual parameters together with the units of measure being used, were explained in the paragraph 10.2.

10.7 Methods for chromatic dispersion measurements

The following paragraphs of this chapter are based on the ITU standard: ITU-T G.650 “Definition and Test Methods for the Relevant Parameters of Single-Mode Fibers” - Series G:

Transmission Systems and Media, Digital Systems and Networks Transmission Media Characteristics - Optical Fiber by International Telecommunication Union.

The ITU-T G.650 standard provides information concerning the recommended methods (techniques) to be used for the determination of the fiber chromatic dispersion. In particular, directives are given on how measurement setups should be constructed. A review of the setups will be given in subsequent paragraphs. Here, let us list the measurement methods recommended by the ITU standard. The methods are:

- Reference test method: The phase-shift technique
- First alternative test method: The interferometric technique
- Second alternative test method: The pulse delay technique

The method designations (reference, first alternative, ...) come from the discussed standard.

All the three methods listed above, despite certain differences, share a common idea of how, in fact, they derive the fiber chromatic dispersion. In short, the idea is as follows:

- to measure the light pulse time delay τ in the function of light wavelength λ ; in other words, light pulse propagation times in fiber of a given length (e.g. 1 km) are measured at several (usually four to eight) light wavelengths;
- then, based on the measurement data points (i.e. time delays measured above), an analytic form of the relation $\tau(\lambda)$ is found (by a numerical fitting procedure);
- finally, the chromatic dispersion coefficient D is found by simply calculating the first derivative of $\tau(\lambda)$, i.e. $D = d\tau(\lambda)/d\lambda$; by definition, the chromatic dispersion coefficient informs on how much the pulse time delay (τ) changes when light wavelength (λ) is changed by a unit value (usually 1 nm); this is why the derivative of $\tau(\lambda)$ in respect to λ is calculated.

Note that the need for finding an analytic form of $\tau(\lambda)$ actually results from the small number of light wavelength values at which measurements are made. This number is determined by the measurement device construction, i.e. by how many different light sources the device contains. An example of the analytic expression for $\tau(\lambda)$ will be discussed in paragraph 10.11.

10.8 Reference test method: The phase-shift technique

This is the reference method characteristics as stated by the ITU standard:

- The fiber chromatic dispersion coefficient is derived from the measurement of the relative group delay experienced by the various wavelengths during propagation through a known length of fiber.
- The group delay is measured in the frequency domain, by detecting, recording and processing the phase shift of a sinusoidally modulated signal.
- The chromatic dispersion may be measured at a fixed wavelength or over a wavelength range.

10.8.1 Measurement setup

Configuration of a measurement setup recommended to be used in the reference method, is shown in figure Fig. 10.4.

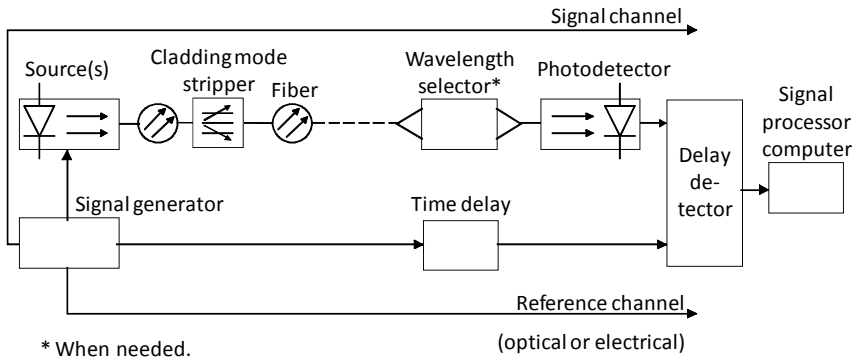


Fig. 10.4 Block diagram of a measurement setup recommended for the reference method of chromatic dispersion measurements ("Recommendation ITU-T G.650 (04/1997)," 1997).

The delay detector visible in the figure measures the relative phase shift between the optical signal that has passed the fiber under test, and the electrical signal of reference. Both the signals are modulated sinusoidally. The phase shift (φ) is then converted into the time delay (τ) with the formula $\tau = \varphi / (2\pi f)$, where f is the modulation frequency.

The optical source: Laser diodes, {laser diode array}, wavelength tunable laser diodes (WTL) {e.g. an external cavity laser (ECL)}, LEDs or broadband sources, (e.g. an Nd:YAG laser with a Raman fiber). At least one data point must be within 100 nm of λ_0 .

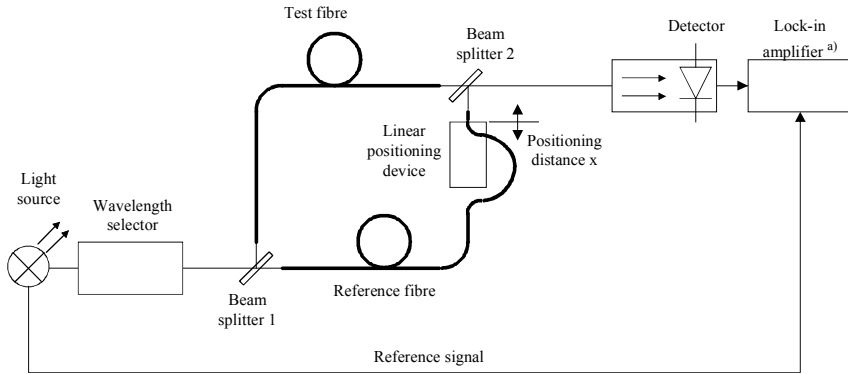
10.9 First alternative test method: The interferometric technique

The first alternative method is characterized by the ITU standard as follows:

- The interferometric test method allows the chromatic dispersion to be measured, using a short piece of fiber (several meters).
- According to the interferometric measuring principle, the wavelength-dependent time delay between the test sample and the reference path is measured by a Mach-Zehnder interferometer. The reference path can be an air path or a single-mode fiber with known spectral group delay.

10.9.1 Measurement setup

Configuration of a measurement setup recommended for application in the first alternative method, is shown in figure Fig. 10.5.



a) When needed.

T1507740-92

Fig. 10.5 Block diagram of a measurement setup recommended for the first alternative method of chromatic dispersion measurements ("Recommendation ITU-T G.650 (04/1997)," 1997).

The two fibers, the reference one and the one under test, constitute the two arms of a Mach-Zehnder interferometer. The light pulse time delays are measured by means of balancing the interferometer, i.e. equating the optical lengths of both the interferometer arms. In the setup visible in figure Fig. 10.5, the balancing is done with the linear positioning device (see end of the reference fiber).

The light source must be suitable, e.g. a YAG laser with a Raman fiber or a lamp and LED optical sources, etc.

10.9.2 Determination of spectral group delay

In the case of using a reference fiber in one of the interferometer arms (as of figure Fig. 10.5), the pulse time delay in the function of light wavelength must be known for the reference fiber. Otherwise, the time delay for pulses propagating over the test fiber, could not be determined. It is explained in more detail in figure Fig. 10.6.

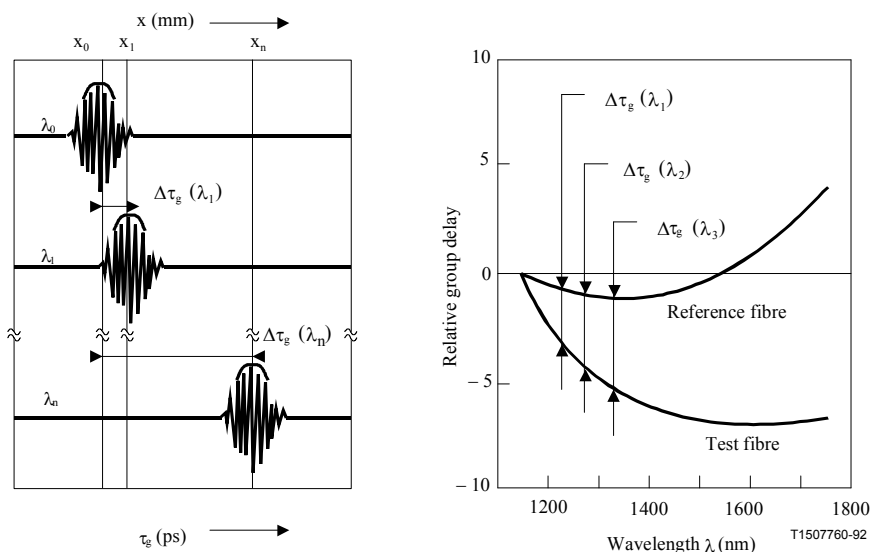


Fig. 10.6 Determining the time delay of pulses propagating in the test fiber, requires the prior knowledge of the pulse time delays occurring in the reference fiber (“Recommendation ITU-T G.650 (04/1997),” 1997).

10.10 Second alternative test method: The pulse delay technique

The ITU standard gives the following characteristics of the second alternative method:

- The fiber chromatic dispersion coefficient is derived from the measurement of the relative group delay experienced by the various wavelengths during propagation through a known length of fiber.
- The group delay is measured in the time domain, by detecting, recording and processing the delay experienced by pulses at various wavelengths.
- The chromatic dispersion may be measured at a fixed wavelength or over a wavelength range.

Measurements employing the second alternative method are performed with the use of the measurement setup shown in the figure Fig. 10.4, i.e. the one used in the reference method.

10.11 Dispersion calculations

As explained in the paragraph 10.7, an analytic expression for $\tau(\lambda)$ needs to be found. More precisely, some general form of the expression is assumed *a priori*, and only the numerical values of the expression coefficients need to be determined. Description of one of the expression types discussed the ITU standard, is cited below.

The measured group delay per unit fiber length versus wavelength shall be fitted by the three-term Sellmeier expression

$$\tau(\lambda) = \tau_0 + \frac{S_0}{8} \left(\lambda - \frac{\lambda_0^2}{\lambda} \right)^2 \quad (10.1)$$

Here τ_0 is the relative delay minimum at the zero-dispersion wavelength λ_0 . The chromatic dispersion coefficient $D(\lambda) = d\tau/d\lambda$ can be determined from the differentiated Sellmeier expression

$$D(\lambda) = \frac{S_0}{4} \left(\lambda - \frac{\lambda_0^2}{\lambda} \right) \quad (10.2)$$

Here S_0 is the zero-dispersion slope, i.e. the value of the dispersion slope $S(\lambda) = dD/d\lambda$ at λ_0 .

11 Telecommunication fiber optic system

Transmitting signals in the optical domain has, in fact, a long history. Simple mirror-based systems would inform about enemy threat for centuries. Light would enable a quick transmission of messages and, thanks to its directional propagation properties, the message exchange was secret enough. In later years, the application of the total internal reflection phenomenon enabled the optical signals to be transmitted over much longer distances. Today, we know that actually it is not the propagation speed that makes light so useful in information exchange, but rather the very high frequency of the electromagnetic waves of light. This very high frequency directly translates into a broad frequency spectrum available to signals being transmitted (significantly broader than that achievable in e.g. the radio transmission techniques). In this chapter, examples will be given of optical networks, their limitations, and of the concept of the WDM and TDM systems.

11.1 Fiber optic link

In figure Fig. 11.1 below, the simplest optical fiber-based telecommunication system is presented. Electrical signal entering the transmitter is converted into optical signal, which is then coupled into optical fiber. Fiber's optical properties enable the optical signal to travel (be transmitted over) distances dozens of kilometers long without the need for any intermediate signal regeneration. Such long distances are possible even though certain level of an external noise affects the transmission. Finally, the receiver brings the optical signal back to the electrical domain.

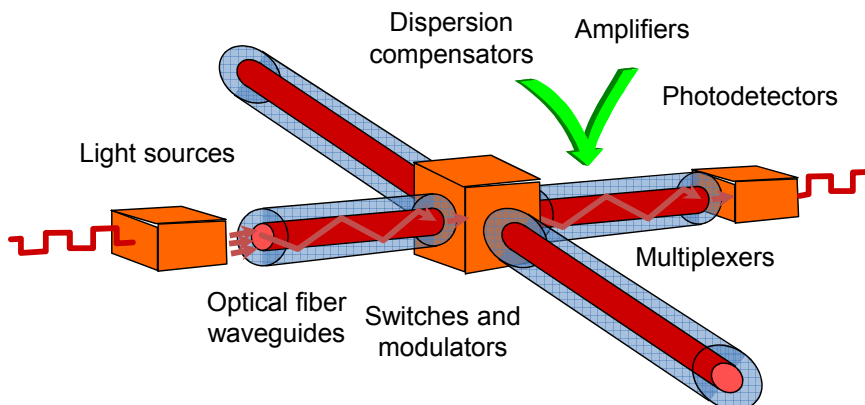


Fig. 11.1 Elements of fiber-optic communication system.

11.2 Attenuation of optical fibers

Attenuation of the telecommunication silica-glass fibers, the telecommunication windows, and the telecommunication system generations were discussed in Chapter 2.

11.3 Reasons to use optical fiber in networks

It is fast, easy and inexpensive to install fiber optic networks

- Capacity -> hundreds of thousands of phone channels,
- Losses -> 0.2dB/km for modern single mode fiber,
- Fiber amplifiers -> possibility to extend the transmission distance in an easy way,

- Lightweight,
- Electromagnetic interference (EMI)

11.4 Fiber optic transmission systems limits

Fiber optic links are either:

- attenuation limited – at long transmission distances, even when fiber core attenuation is low, noise level and signal level become comparable, which may prevent the correct detection of the transmitted signal,
- dispersion limited – fiber material's refractive index varies with light wavelength; thus, as each transmitted data pulse has a finite spectral width (i.e. it contains lightwaves of multiple optical frequencies, not of only one frequency), individual data pulses undergo a temporal broadening (their time of duration becomes longer) after traveling a given stretch of fiber.

Sources/amplifiers are limited by the following factors:

- laser chirp
- electrical bandwidth
- amplifiers noise (ASE)

Detectors are limited by:

- electrical bandwidth

11.5 Fibers communication systems

The four most popular telecommunication systems realizing a point-to-point transmission:

- single-channel system, Fig. 11.1
- amplified single-channel system
- WDM systems Fig. 11.2
- TDM systems Fig. 11.4

11.6 WDM

High transmission capacity of fibers is still far ahead of the data-rate capabilities of today's transmitters and receivers. Moreover, dispersion of fiber can suppress data rate effectively. To avoid these problems and achieve high total transmission speeds, many different wavelengths are simultaneously transmitted over a single fiber. Such a method of increasing system's transmission capacity is known as the wavelength-division multiplexing (WDM) ("Wavelength Division Multiplexing - WDM," 2010). An idea of a telecommunication system utilizing the wavelength-division multiplexing (a WDM system) is depicted in figure Fig. 11.2. There are two standards of the WDM systems: the Coarse WDM (CWDM) and the Dense WDM (DWDM).

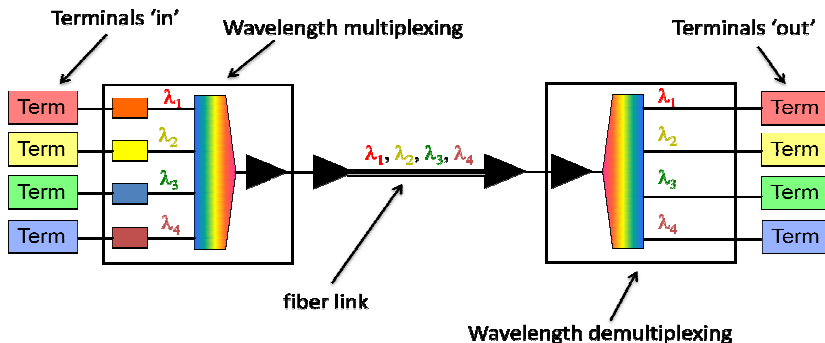


Fig. 11.2 Wavelength-division multiplexing – system.

- Coarse WDM – ITU standard G.694.2 (“Recommendation G.694.2,” 2003) – the spectral distance between adjacent (neighboring) channels is 20 nm, and only 4 or 8 channels are allowed. Working frequencies are in the range of 1310 to 1610 nm. Non-stabilized DFB lasers can be used. Total bit rate transmitted in single fiber is 1 to 3.125 Gbit/s – FTTH.
- Dense WDM – ITU standard G.694.1 (“Recommendation G.694.1,” 2002) – used for very large data-rate transmissions, because large number of channels are allowed: 40 up to 160, and spacing between channels is relatively small: down to 100 GHz. DFB lasers must be temperature-stabilized. Total bit rate transmitted in a single fiber is 10 Gbit/s up to 40 Gbit/s. Used in internet backbone networks.

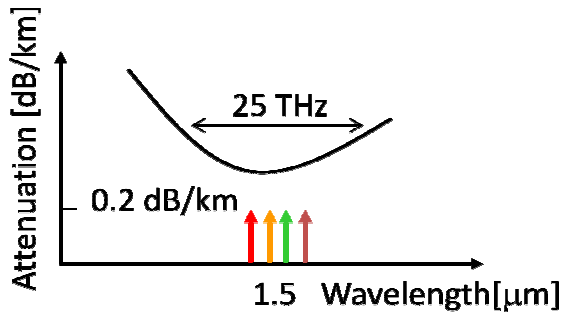


Fig. 11.3 Wavelength-division multiplexing – idea.

Maximal electronics speed remains unchanged (speed of individual channels). Multiplexing and demultiplexing is performed with optical, usually passive, elements. In figure Fig. 11.3 an idea of a WDM system working in the third telecommunication window is presented. Individual channels (colored arrows) have spectral width that is much narrower than spectral width of the entire window. This is the reason why a considerably high numbers of optical signals can be transmitted over a single fiber without the channels being distorted by each other. Thus, the total transmission capacity of the system can be greatly increased, while transmission speed of an individual frequency channel still remains within the capabilities of the available transmitters and receivers.

11.7 TDM

Different channels can be carried in a single fiber by time switching. To increase the bit rate, an extremely narrow time slot is needed Fig. 11.4.

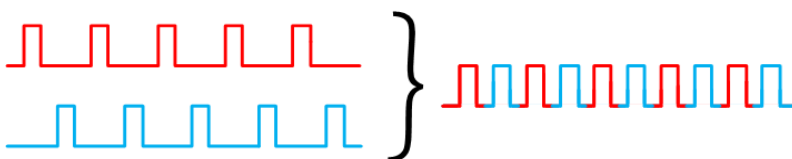


Fig. 11.4 Time division multiplexing of two channels into one train of pulses.

A schematic of time-division multiplexing of two channels into one train of pulses. Each pulse represents the bit value '1', and lack of pulse represents the bit value '0'.

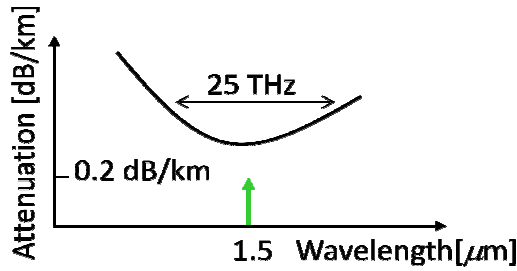


Fig. 11.5 Time division multiplexing on one light wavelength.

Typical contemporary transmission line: TDM on one light wavelength Fig. 11.5. Individual channels' data rates sum up at optical input/output ports as shown in Fig. 11.6. Increasing the speed of (data rates in) individual channels requires optical modules of a very high frequency.

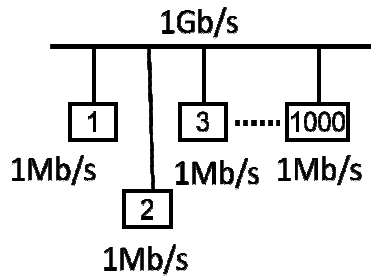


Fig. 11.6 Time division multiplexing – a 1000 of 1 Mb/s channels require a data link of 1 Gb/s total transmission capacity.

11.8 Solitons

Solitons are ultra short optical pulses that propagate through optical fiber but avoid temporal broadening thanks to nonlinear phenomena they induce in fiber material. Usually, short optical pulses propagating in fiber undergo a temporal broadening due to the chromatic dispersion. Such a broadening can severely limit the telecommunication system transmission capabilities.

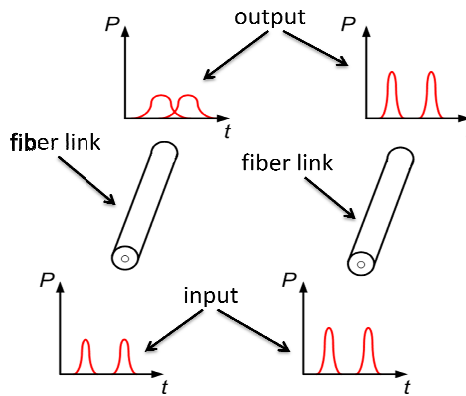


Fig. 11.7 Solitons and normal transmission.

Utilizing the balance between the nonlinear Kerr effect (11.1) and the chromatic dispersion, the soliton can propagate without (temporal) widening. Normal transmission and soliton transmission are visible on the left-hand side and the right-hand side of figure Fig. 11.7, respectively.

Nonlinear refractive index – at points, where local optical power density is high enough (enough to induce any noticeable effects) – the refractive index increases according to the formula

$$n = n_0 + n_2 \langle E^2 \rangle = n_0 + \frac{1}{2} n_2 E^2 \quad (11.1)$$

As has already been mentioned, the refractive index nonlinearity described by (11.1) compensates (prevents) the temporal broadening of the soliton pulse.

12 Measurements of optical fiber

The following chapter is based on the ITU standard: ITU-T G.650 “Definition and Test Methods for the Relevant Parameters of Single-Mode Fibers” - Series G: Transmission Systems and Media, Digital Systems and Networks Transmission Media Characteristics - Optical Fiber by International Telecommunication Union (“Recommendation ITU-T G.650 (04/1997),” 1997).

12.1 Test Methods

Reference Test Method (RTM)

A test method in which a characteristic of a specified class of optical fibers or optical fiber cables is measured strictly according to the definition of this characteristic and which gives results which are accurate, reproducible and reliable to practical use.

Alternative Test Method (ATM)

A test method in which a given characteristic of a specified class of optical fibers or optical fiber cables is measured in a manner consistent with the definition of this characteristic and gives results which are reproducible and reliable to the reference test method and to practical use.

12.2 Parameters of singlemode optical fiber

1. Mode field diameter
2. Cladding diameter, mode field concentricity error and cladding non-circularity
3. Cut-off wavelength
4. Attenuation
5. Chromatic dispersion
6. Proof testing
7. Polarization mode dispersion

12.3 Mode field diameter

The mode field is the single-mode field distribution of the LP₀₁ mode giving rise to a spatial intensity distribution in the fiber. Some examples of shapes of mode field spatial density distributions can be found in figure Fig. 12.6 (in paragraph 12.14).

The Mode Field Diameter (MFD) $2w$ represents a measure of the transverse extent of the electromagnetic field intensity of the mode in a fiber cross-section and it is defined from the far field intensity distribution $F^2(\theta)$, θ being the far-field angle, through the following equation:

$$2w = \frac{\lambda}{\pi} \left[\frac{2 \int_0^{\pi/2} F^2(\theta) \sin \theta \cos \theta d\theta}{\int_0^{\pi/2} F^2(\theta) \sin^3 \theta \cos \theta d\theta} \right]^{1/2} \quad (12.1)$$

12.4 Measurement setup for the MFD

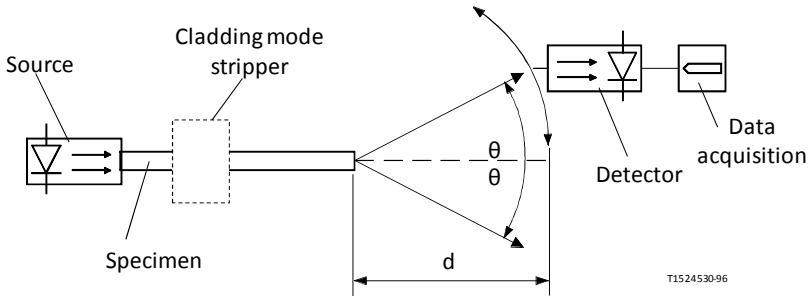


Fig. 12.1 Schematic view of the mode-field diameter measurement setup.

Far field intensity distribution scanning: a scanning photodetector with pinhole aperture or a scanning pig-tailed photodetector. The detector at least 10 mm from the fiber end. The detector-fiber distance greater than $40wb/d$, where $2w$ is the expected mode field diameter of the fiber to be measured and b is the diameter of the active area of the detector.

12.5 Measurement setup for the MFD – details

Light source: Stable in position, intensity and wavelength. The spectral characteristics to preclude multimode operation. The FWHM spectral width no greater than 10 nm.

Modulation: To improve the signal/noise ratio at the receiver.

Cladding mode stripper: To prevent the propagation and detection of cladding modes

Specimen: A short length of the optical fiber. Primary fiber coating removed from the section of the fiber inserted in the mode stripper, if used. The fiber ends clean, smooth and perpendicular to the fiber axes to within 1° .

The minimum dynamic range of the measurement should be 50 dB.

12.6 MFD – measurements procedure

The launch end of the fiber shall be aligned with the launch beam, and the output end of the fiber shall be aligned to the appropriate output device.

The following procedure shall be followed: by scanning the detector in fixed steps no greater than 0.5° , the far-field intensity distribution, $F^2(\theta)$, is measured, and the mode field diameter is calculated from equation

12.7 Presentation of measurements results

Measurements protocol should contain:

- Test set-up arrangement, dynamic range of the measurement system, processing algorithms, and the description of the scanning device used (including the scan angle).
- Launching conditions.
- Wavelength and spectral linewidth FWHM of the source.
- Fiber identification and length.
- Type of cladding mode stripper.
- Type and dimensions of the detector.

- h. Temperature of the sample and environmental conditions (when necessary).
- i. Indication of the accuracy and repeatability.
- j. Mode field diameter.

12.8 MFD measurement – 1st alternative method (1)

The variable aperture technique, determined from the complementary aperture transmission function $a(x)$

$$2w = (\lambda / \pi D) \left[\int_0^{\infty} a(x) \frac{x}{(x^2 + D^2)^2} dx \right]^{-1/2} \quad (12.2)$$

where:

The aperture radius $x = D \cdot \tan \theta$

D the distance between the aperture and the fiber
complementary aperture transmission function $a(x)$:

$$a(x) = 1 - \frac{P(x)}{P_{\max}} \quad (12.3)$$

where P_{\max} is the power transmitted by the largest aperture and x is the aperture radius.

12.9 Variable aperture MFD measurement method

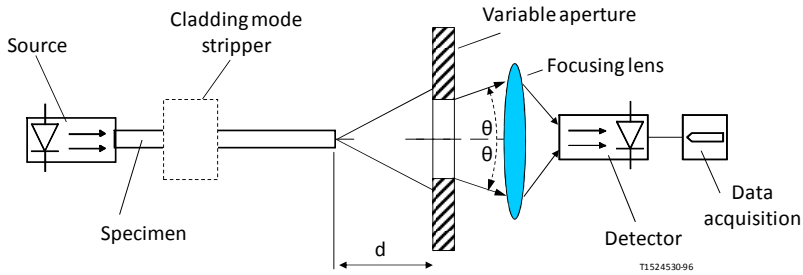


Fig. 12.2 Schematic view of the mode-field diameter measurement setup – the first alternative method.

Aperture apparatus: at least twelve apertures spanning the half-angle range of numerical apertures from 0.02 to 0.25 (0.4 for fibers covered by Recommendation G.653) should be used.

12.10 MFD measurement – 2nd alternative method

The near-field scan. MFD is determined from the near-field intensity distribution $f^2(r)$: (r being the radial coordinate):

$$2w = 2 \left[\frac{\int_0^{\infty} r f^2(r) dr}{\int_0^{\infty} r \left[\frac{df(r)}{dr} \right]^2 dr} \right]^{1/2} \quad (12.4)$$

where: r is the radial coordinate

Far field and near field methods are equivalent through Henkel transform

12.11 2nd alternative measurement setup – near field scan

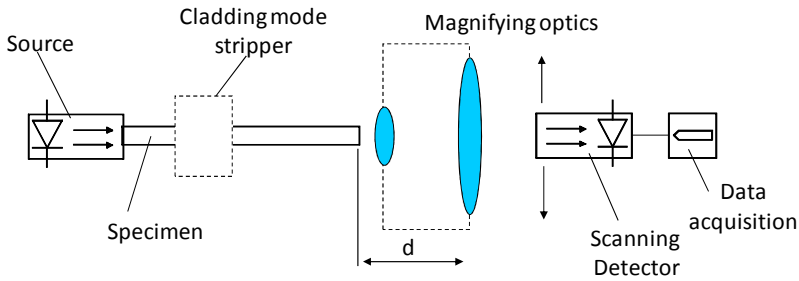


Fig. 12.3 Schematic view of the mode-field diameter measurement setup – the second alternative method.

For calibration, the magnification of the optics should have been measured by scanning the length of a specimen whose dimensions are independently known with sufficient accuracy.

12.12 2nd alternative measurement procedure

The near-field of the fiber is enlarged by the magnifying optics and focused onto the plane of the detector.

The near-field intensity distribution, $I^2(r)$, is scanned and the mode field diameter is calculated from the equation.

Alternatively, the near-field intensity distribution may be transformed into the far-field domain using a Hankel transform and the resulting transformed far-field $F^2(\theta)$ may be used to compute the mode field diameter from the equation for the primary method.

12.13 Test methods for the cladding diameter, mode field concentricity error and cladding non-circularity

Reference test method: The transmitted near-field technique.

Source - see measurements of MFD

The magnifying optics consists of a microscope objective which magnifies the specimen output near-field, focusing it onto the plane of the scanning detector.

Detector

- a. scanning photodetector with pinhole aperture;
- b. scanning mirror with fixed pinhole aperture and photodetector;
- c. scanning vidicon, charge coupled devices or other pattern/intensity recognition devices.

First alternative test method: The refracted near-field technique. Measurement of the refractive index distribution across the entire fiber (core and cladding). The geometrical characteristics of the fiber then obtained from the refractive index distribution.

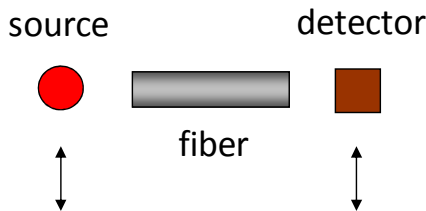


Fig. 12.4 Measurement of the refractive index distribution across the entire fiber

Second alternative test method: The side-view technique. Intensity distributions in the observation plane along the line perpendicular to the fiber axis are recorded. Refractive index profiles and geometrical parameters are then obtained through suitable algorithms.

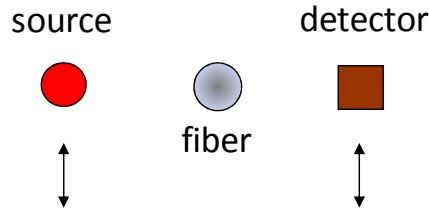


Fig. 12.5 Measurement of the refractive index profiles and geometrical parameters by the side-view technique.

12.14 Cut-off wavelength

Theoretical cut-off wavelength is the shortest wavelength at which a single mode can propagate in a single-mode fiber. This parameter can be computed from the refractive index profile of the fiber. At wavelengths below the theoretical cut-off wavelength, several modes propagate and the fiber is no longer single-mode but multimode.

Cut-off wavelength is defined as the wavelength greater than that at which the ratio between the total power, including launched higher order modes, and the fundamental mode power has decreased to less than 0.1 dB. According to this definition, when all modes are equally excited, the second order (LP_{11}) mode is attenuated by 19.3 dB as compared to the fundamental mode (LP_{01}).

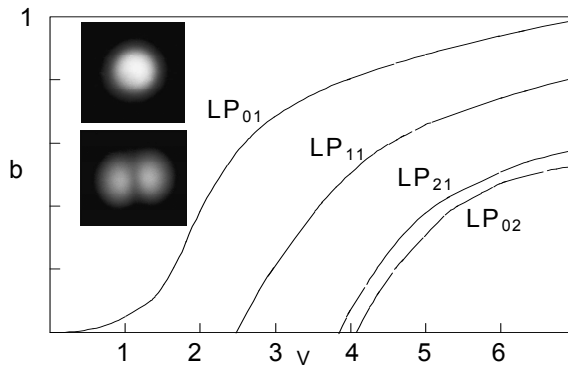


Fig. 12.6 LP modes of an optical fiber.

12.15 Test methods for the cut-off wavelength

Measurement purpose: to assure effective single-mode operation above a specified wavelength.

Reference test method for the cut-off wavelength (λ_c) of the primary coated fiber and reference test method for the cut-off wavelength (λ_{c_j}) of jumper cables: The transmitted power technique.

The transmitted power technique uses the variation with wavelength of the transmitted power of a short length of the fiber under test, under defined conditions, compared to a reference transmitted power. There are two possible ways to obtain this reference power:

- a. the test fiber with a loop of smaller radius; or
- b. a short (1-2 m) length of multimode fiber.

12.16 Test apparatus

Light source: line width not exceeding 10 nm (FWHM), capable of operating over a sufficient wavelength range, shall be used.

Launching conditions: the launching conditions must be used in such a way as to excite substantially uniformly both LP₀₁ and LP₁₁ modes. For example, suitable launching techniques could be:

- a. jointing with a multimode fiber; or
- b. launching with a suitable large spot-large NA optics.

Cladding mode stripper: the cladding mode stripper is a device that encourages the conversion of cladding modes to radiation modes; as a result, cladding modes are stripped from the fiber. Care should be taken to avoid affecting the propagation of the LP₁₁ mode.

12.17 Measurement procedure

The measurement is performed on a 2 m length of fiber, in a form of a loosely constrained loop. The loop shall complete one full turn of a circle of 140 mm radius. The remaining part of the fiber shall be substantially free of external stresses. The output power $P_1(\lambda)$ shall be recorded versus λ in a sufficiently wide range around the expected cut-off wavelength.

Attenuation $\alpha(\lambda)$ is calculated by comparing output power and reference power (next slide)

$$a(\lambda) = 10 \log \frac{P_1(\lambda)}{P_i(\lambda)} \quad (12.5)$$

where: $i = 2$ or 3 for different reference power measurement methods

12.18 Transmission through the reference sample

- a. Using the test sample, and keeping the launch conditions fixed, an output power $P_2(\lambda)$ is measured over the same wavelength range with at least one loop of sufficiently small radius in the test sample to filter the LP₁₁ mode. A typical value for the radius of this loop is 30 mm.
- b. With a short (1-2 m) length of multimode fiber, an output power $P_3(\lambda)$ is measured over the same wavelength range.

12.19 Determination of cut-off wavelength

In the transition region, higher-order mode power is reduced with increasing wavelength. Fiber cut-off wavelength, λ_c , is defined as the wavelength at which the higher-order mode power relative to the fundamental mode power, $\Delta a(\lambda)$, has been reduced to 0.1 dB.

Figure Fig. 12.7 presents an attenuation characteristics of a single-mode optical fiber in the function of light wavelength. A determined value of the cut-off wavelength is marked with a vertical solid line. Similarly, figure Fig. 12.8 shows a determined cut-off wavelength of a multimode fiber.

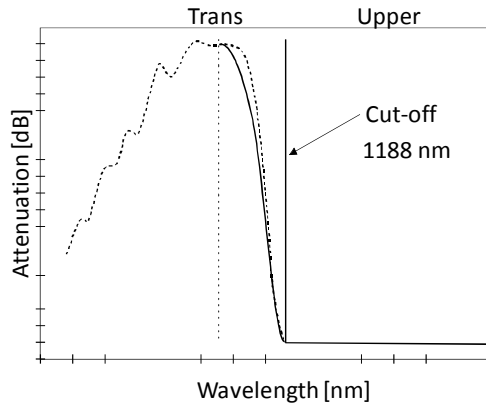


Fig. 12.7 Single-mode reference cut-off plot.

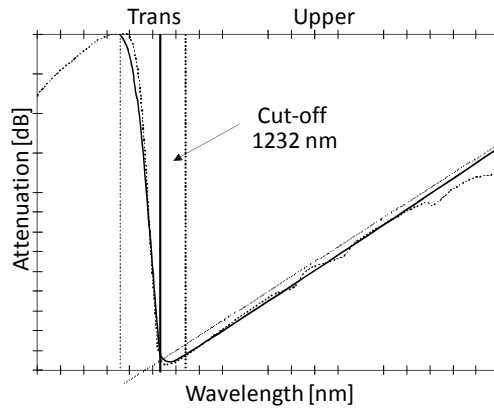


Fig. 12.8 Multimode reference cut-off plot.

12.20 Test methods for the attenuation:

- Reference test method: The cut-back technique
- First alternative test method: The backscattering technique
- Second alternative test method: The insertion loss technique

12.21 The cut-back technique

The cut-back technique is a direct application of the definition in which the power levels P_1 and P_2 are measured at two points of the fiber without change of input conditions. P_2 is the power emerging from the far end of the fiber and P_1 is the power emerging from a point near the input after cutting the fiber.

$$A(\lambda) = 10 \log \frac{P_1(\lambda)}{P_2(\lambda)} \quad (\text{dB}) \quad (12.6)$$

Measurements may be made at one or more spot wavelengths, or alternatively, a spectral response may be required over a range of wavelengths.

12.22 Attenuation: measurement set-up

Diagrams of suitable test equipments, to obtain one loss or the loss spectrum measurements respectively, are shown as examples in Fig. 12.9 and Fig. 12.10.

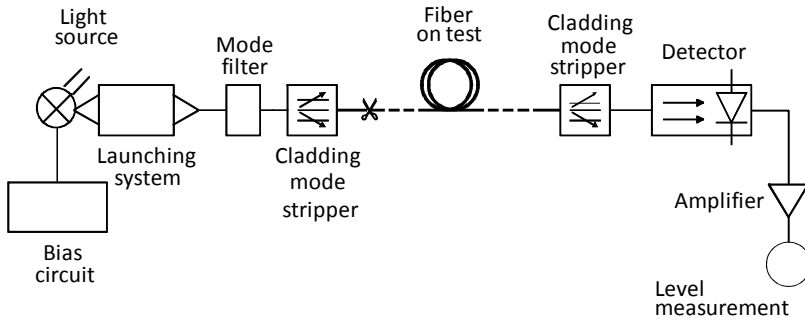


Fig. 12.9 Arrangement of test equipment to make one loss measurement

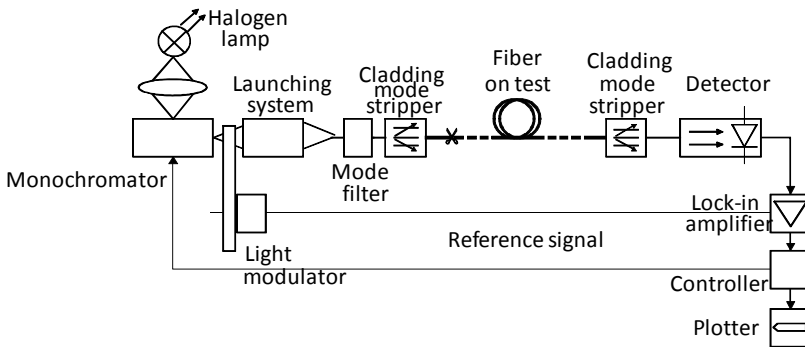


Fig. 12.10 Arrangement of test equipment used to obtain the loss spectrum measurement

12.23 First alternative test method: The backscattering technique

A test method for the attenuation coefficient of single-mode optical fiber based on bidirectional backscattering measurements is described. This technique can also be applied to check the attenuation uniformity, optical continuity, physical discontinuities, splice losses and the length of the fiber. The measurement is performed with Optical Time Domain Reflectometer.

OTDR (Optical Time Domain Reflectometer) is the fundamental device used in building and exploitation of optical fiber networks. It enables measurements of parameters of optical fibers and localization of “events” occurring in the optical tract. Schematic diagram OTDR measurement is presented in the following figure.

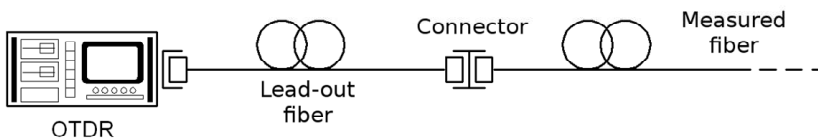


Fig. 12.11 Optical Time Domain Reflectometer (OTDR)

Reflectometry measurement is based on analysis of back-scattered light power as a function of time (or distance from the measurement location). A block diagram of the OTDR is shown below.

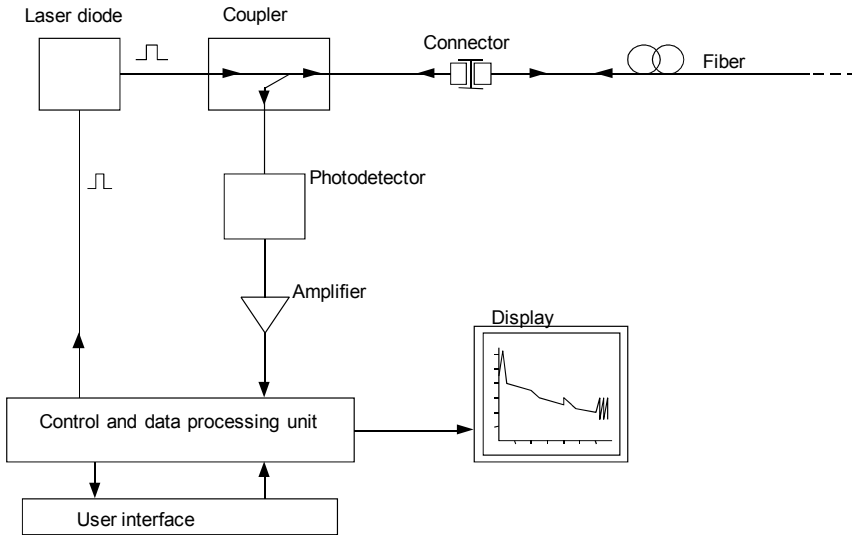


Fig. 12.12 Reflectometer – a block diagram

12.24 Second alternative test method: The insertion loss technique

The insertion loss technique consists of the evaluation of the power loss due to the insertion of the fiber under test between a launching and a receiving system, previously interconnected (reference condition). The powers P_1 and P_2 are thus evaluated in a less straightforward way than in the cut-back method. Therefore, this method is not intended for use on factory lengths of fibers and cables.

The insertion loss technique is less accurate than a cut-back one, but has the advantage of being non-destructive for the fiber under test and for the semi-connectors possibly fixed at both ends. Therefore, it is particularly suitable for field use, and mainly intended for use with connectorized cable lengths.

Two options are considered in the following for this technique. They differ in the nature of the launching and receiving systems.

In Fig. 12.13 the quality of the semi-connectors possibly fixed to the fiber under test (and in general the quality of the used interconnection devices) influences the results, in Fig. 12.14 this influence is nearly excluded.

As a consequence, option from Fig. 12.14 has in general a better accuracy, and it is more suitable when the actual attenuation of the fiber alone is needed. Conversely, when the fiber section under test is fitted with semi-connectors and has to be cascaded with other elements, the results from Fig. 12.13 are more meaningful, as they take into account the deviation of the semi-connectors from the nominal loss.

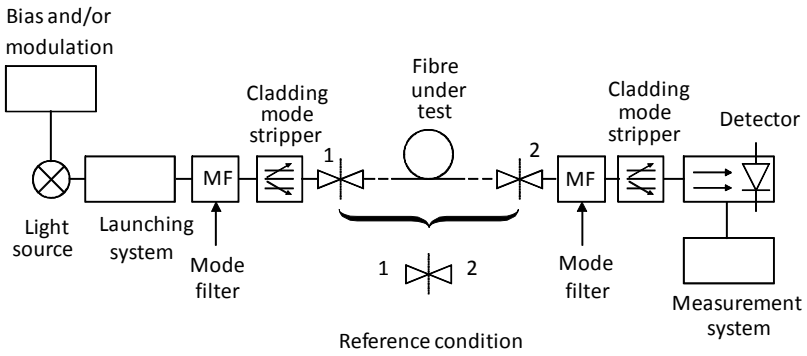


Fig. 12.13 The insertion loss technique - "Laboratory" variant.

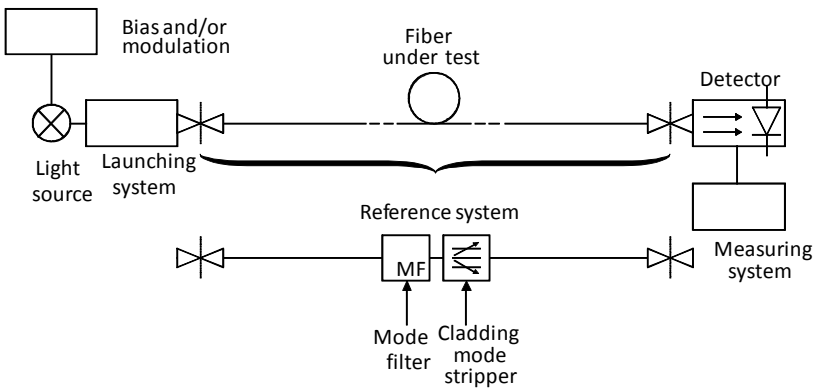


Fig. 12.14 The insertion loss technique – "Field" variant.

12.25 Visual fault locator

The visual fault locator (VFL) is a very versatile tool capable of verifying optical cable integrity and locating optical link faults. Measurement capabilities of a VFL are shown in figure Fig. 12.15.

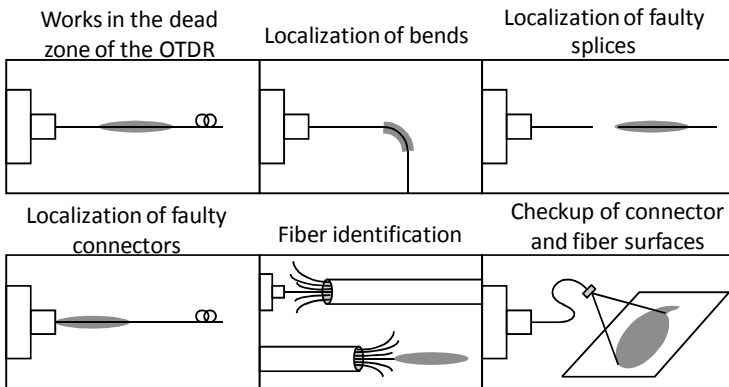


Fig. 12.15 Measurement capabilities visual fault locator (VLT).

12.26 Microscope (x 500)

The microscope enables the observation and assessment of the end-face surfaces of optical fibers that are about to be connected with each other. Microscopes feature an internal light source, which illuminates the investigated fiber end-face surface. The observation field is magnified by a system of lenses and can be acquired by a CCD camera.

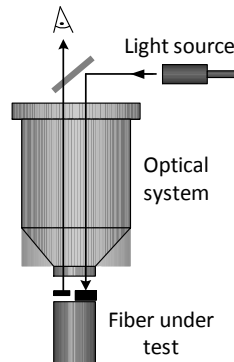


Fig. 12.16 Microscope designed for the observation end-face surfaces of optical fibers.

12.27 Traffic or signal detectors

Principle of operation: light is leaking from a bend or stressed fiber. Two detectors placed on two sides of the bent can detect presence of an optical signal and direction of propagation.

Applications:

- Signal detection,
- Power-signal indicator,
- Identification of modulated signal 2 kHz.

13 Optical Time Domain Reflectometer (OTDR)

13.1 Definition and fundamentals

OTDR (Optical Time Domain Reflectometer) is the fundamental device used in building and exploitation of optical fiber networks. If you have to choose one tool to service your network - the OTDR is the right one. The reason is, that it can measure almost every parameter of optical fiber connection. The OTDR can perform multiple jobs: it can locate events, can evaluate those events or anomalies, is can also measure distance to those events. In addition it can measure insertion loss, attenuation of fiber, return loss.

Optical Time Domain Reflectometer or OTDR works on principle of injecting a pulse of light at one end of the fiber, and measuring the backscattered and reflected light coming back. The measured signal is than plotted as signal power in dB versus distance.

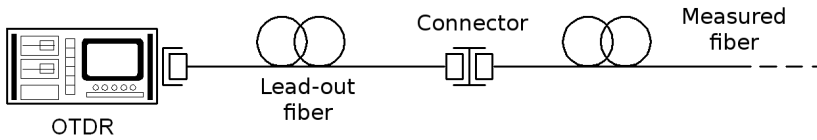


Fig. 13.1 Reflectometry measurement is based on analysis of back-scattered light power as a function of time (or distance from the measurement location).

The first optical reflectometer was build and described in 1976 by Barnoski (Barnoski & Jensen, 1976). Schematic diagram of the first reflectometer is provided on the figureFig. 13.2.

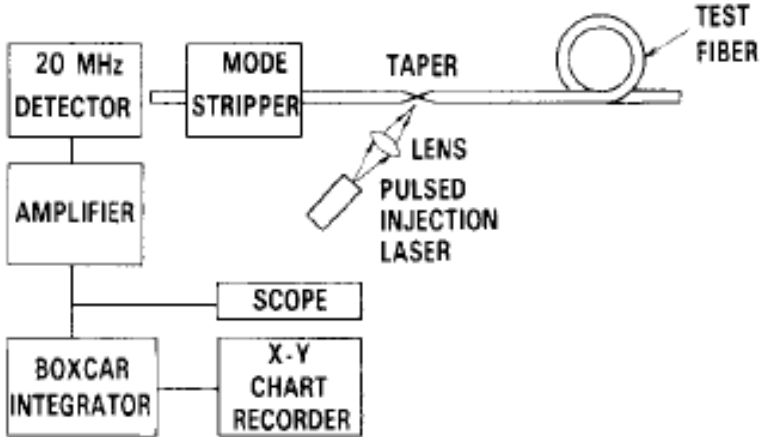


Fig. 13.2 Schematic diagram of the first reflectometer. Light source – pulsed laser diode GaAs. A taper was used to tap a portion of optical power from the fiber (Barnoski & Jensen, 1976).

Optical fiber is made of very pure glass, however there are small impurities that scatter small portion of the guided light. Those impurities may be purposefully put into the fiber core - those are called dopants and they increase refractive index of the cores. There are also impurities or inhomogeneities that are the property of the silica glass structure. Those minor impurities scatter light in all directions, and part of the scattered light is reflected back towards the source, in our case toward the OTDR. This scattering is called Rayleigh scattering. The second phenomena that is used in reflectometric measurements is Fresnel scattering - the scattering that occurs when light encounters boundary of two media with different refractive indices. An example is the end of the fiber, or fiber connector where light travels between glass and air.

A block diagram of the measurement device working on the principle of backreflection is presented on Fig. 13.3

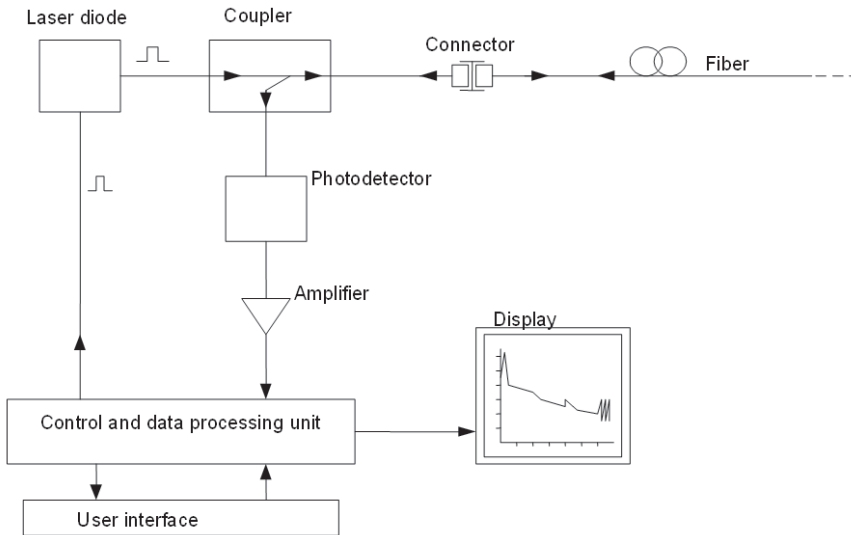


Fig. 13.3 Reflectometer – a block diagram.

What does OTDR measure:

- distance (actually OTDR measures round trip time travel of each pulse, but knowing the speed of light in vacuum, and refractive index of the material one can calculate the distance.)
- The formula to calculate distance from time:
- Fiber distance = (speed of light in vacuum x time) / (2 x refractive index)
- Fiber loss (attenuation), in dB/km
- Event loss (attenuation), in dB
- Reflectance (ration of reflected power to incident power of an event) , in -dB. Reflectance is expressed as negative numbers in dB units. The higher the number, the better, e.g. if we compare two connectors with reflectances of -55 dB and -65 dB - the second one is better.
- Optical Return Loss (ORL), similar as reflectance but ORL may refer to a whole segment of a fiber as well as to a single event. ORL is usually expressed as positive number.

Results measured by the OTDR are displayed as an OTDR trace or reflectogram. Example of the reflectogram is presented on Fig. 13.4.

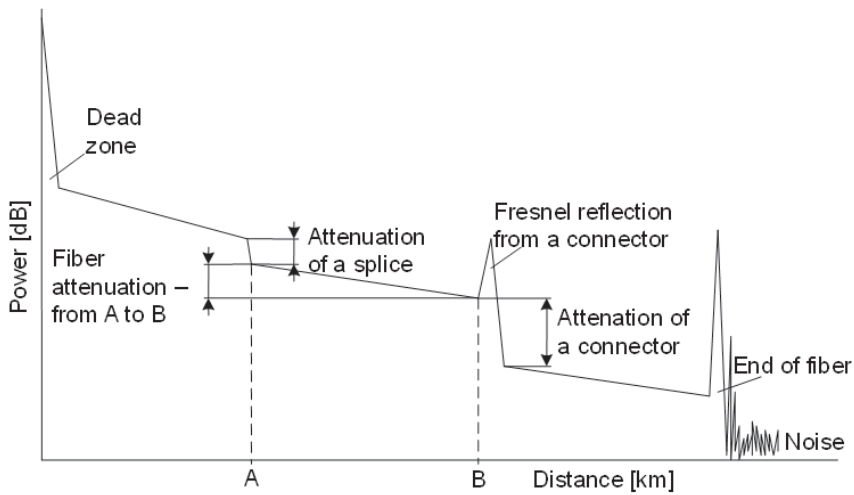


Fig. 13.4 Example of a reflectogram (OTDR trace).

Amount of backscattered power that is available for OTDR analysis is described by the following equation (Personick, 1977):

$$P_s(t) = (P_0 S \alpha_s W v / 2) \exp\{-2\alpha(vt/2)\} \quad (13.1)$$

Where:

- P_b – back-scattered Rayleigh power
- P_0 – peak optical power
- S – Rayleigh scattering recapture rate
- α_s – Rayleigh scattering loss in Nepers per meter
- v – group velocity of light in fiber
- $\alpha(vt/2)$ – total attenuation at distance of $vt/2$ [in Nepers]
- t – time
- W – pulse length [in units of time]

The equation is valid under assumption that $W \ll 2 / \alpha v$

13.2 Parameters and specifications

Fundamental specifications of the reflectometer include:

- Dynamics,
- Measurement range,
- Dead zone length,
- Measurement wavelength.

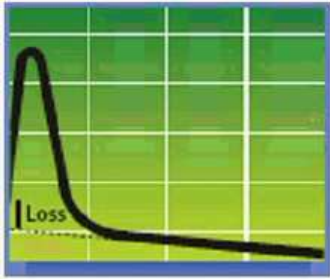
Values measured by the OTDR:

- Distance (distance between events, length of a fiber),
- Attenuation of connectors, macrobends, and splices,
- Attenuation of a fiber per unit length,
- Reflections (reflection coefficient, optical return loss (ORL)).

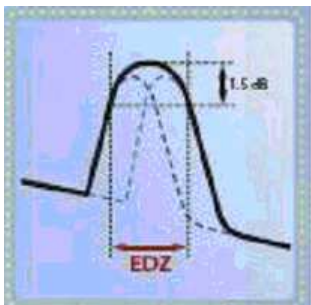
13.2.1 Events and interpretation of traces

The following picture are borrowed from the 2009 JDSU presentation „Performing and analyzing OTDR traces“(Yount, 2009)

- Front-end reflection or dead zone located at the far left end of a trace. One can't measure anything accurately within the dead zone of the front-end reflection.

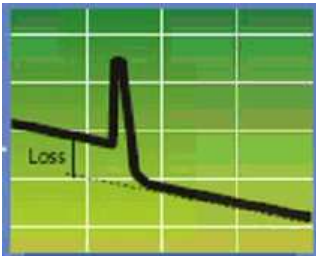


- Dead zone describe the minimum distance between events that this events can be distinguished. Dead zones can be minimized with shorter pulses used for the measurement.

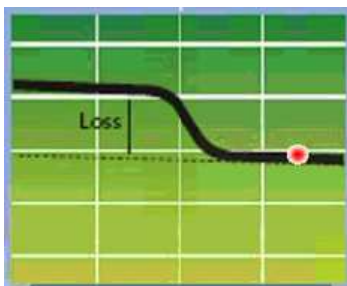


EDZ - Event Dead Zone

- Connector. With OTDR we can measure attenuation and reflectance of a connector.

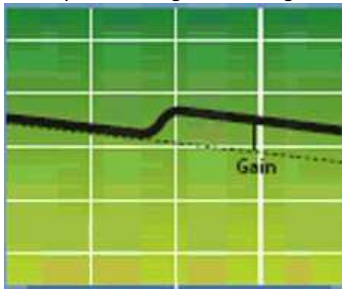


- Fusion splices - permanent connection of two fibers. The splices are prepared with a fusion splicing machine (or a fiber splicer). The main difference between a connector and a splice is that now there is no reflection.



Direction A-B

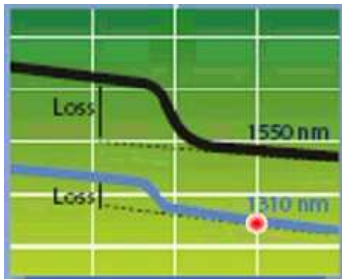
- In some cases, OTDR displays an erroneous image for a splice, called a gainer. The error is caused by different light scattering levels in two joined pieces of fiber.



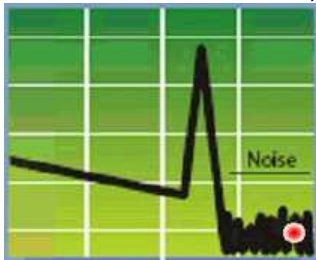
Direction B-A

To eliminate the "gainer" error, one has to measure the fiber in two directions and average the obtained results.

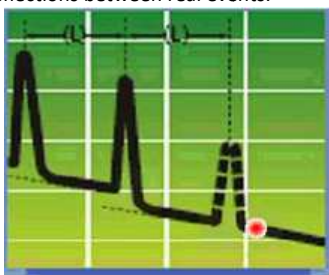
- Macrobend. Macrobends result from physical bending of a fiber. Microbend losses are very sensitive to wavelength - they are much higher for 1550 nm than for 1310 nm. Macrobend events are similar to splice events, but splice losses doesn't depend on wavelength that much. There is no reflectance observable for macrobend losses.



- Fiber end or break is characterized by high reflectance and very noisy signal afterwards.



- Ghosts. Ghosts are "events" that are not there. They are artifacts created by strong reflections between real events.



- For ghost events there is no attenuation, and the distance is exactly equal to distance between other events.

13.3 Other fiber optic measurement devices

13.3.1 Optical power meters

Active element: photodiode

- Silicon for the wavelength of 1100 nm,
- InGaAs or germanium– for 1300 i 1550 nm

Power meter is equipped with

- Constant current amplifier
- Analog-digital converter
- Data processing and display circuits.
- Exchangeable adapters (ST, FC/PC, SC, E2000, and other).

Signal power is displayed in logarithmic scale, as absolute power in dBm, relative in dBr, or on linear scale in units of mW, pW, nW.

Main parameters of optical power meters:

- Dynamic range,
- measuring range,
- measurement wavelengths,
- linearity.

13.3.2 Measurement light sources

- Lasers, dedicated for measurements of singlemode fibers.
- LEDs, for measurements of multimode fibers.

Laser must be stable and reliable. The light source module, should be connectable with different optical connectors.

Main parameters of light measurement sources:

- Output power,
- Emitted light wavelength,
- Spectral width,
- Source stability.

13.3.3 Visual fault locator

Visual fault locators are devices that couple visible light to the optical fiber. Faults and possible problem locations are than visible as areas where light is leaking from the fiber or cable. The following picture illustrates possible applications of the visual fault locator.

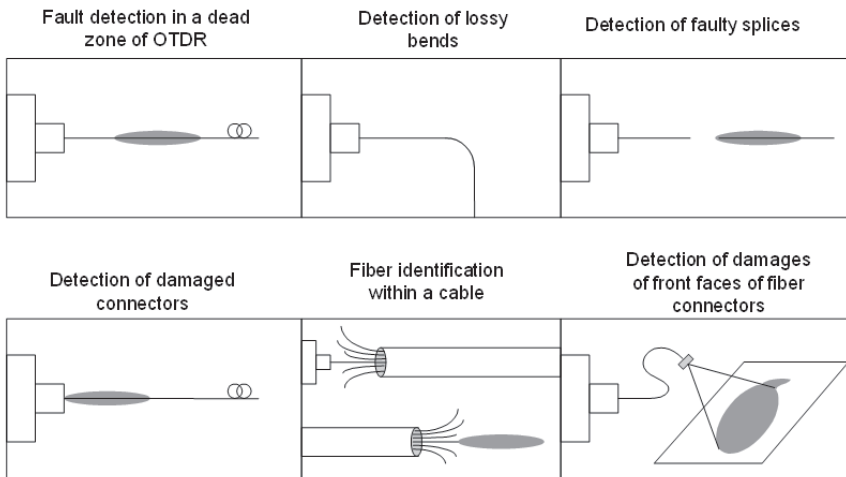


Fig. 13.5 Different applications of a Visual Vault Locator.

13.3.4 Microscope

With a microscope one can visually check and evaluate front faces of optical fibers. The microscope is equipped with an internal light source, which illuminates a face of optical fiber. The picture is amplified by a set of lenses, and can be registered with a CCD camera.

13.3.5 Fiber identifier (Optical traffic detector)

Operation principle of the device is based on detection of light, leaking from a bended fiber. Two photodetectors, located at two ends of the bend register leaking light.

Applications of fiber identifier:

- detection of optical transmission presence and direction,
- Measurement of optical power level in optical fiber,
- Detection of modulate signal (2 kHz).

Maximal diameter of an optical bufer 3 mm.

References

- Agrawal, G. P. (2002). *Fiber-Optic Communication Systems* (3rd ed., p. 580). Wiley-Interscience.
- Barnoski, M. K., & Jensen, S. M. (1976). Fiber waveguides: a novel technique for investigating attenuation characteristics. *Applied Optics*, 15(9), 2112-2115. OSA. doi: 10.1364/AO.15.002112.
- Basics of Fiber Bragg Grating. (2010). . Retrieved February 1, 2011, from <http://www.aos-fiber.com/eng/About.html>.
- Bass, M. (2001a). Optical Fiber Communication Technology and System Overview. *Handbook of optics. Volume IV, Fiber optics and nonlinear optics* (p. 916).
- Bass, M. (2001b). Optical Fibers and Fiber-Optic Communications. *Handbook of optics. Volume IV, Fiber optics and nonlinear optics* (2nd ed., p. 916). McGraw-Hill.
- Chang, W. S. C. (2009). *Fundamentals of Guided-Wave Optoelectronic Devices* (p. 199). Cambridge University Press. Retrieved February 1, 2011, from <http://books.google.com/books?id=EWKlg5D5Mcc&pgis=1>.
- DeCusatis, C. (2008). *Handbook of fiber optic data communication: a practical guide to optical ...* (p. 784). Academic Press. Retrieved February 1, 2011, from <http://books.google.com/books?id=ynvMx7mMgJAC&pgis=1>.
- Fiber Optic Connector Reference. (2010). . Retrieved February 1, 2011, from http://www.ertyu.org/steven_nikkel/fiberconnect.html.
- Fiber Optic Connectors Basics, Styles, Trends. (2010). . Retrieved February 1, 2011, from <http://www.fiberoptics4sale.com/wordpress/fiber-optic-connectors-basics-styles-trends/>.
- Gambling, W. A. (2000). The Rise and Rise of Optical Fibers. *IEEE Journal of Selected Topics in Quantum Electronics*, 6(6), 1084-1093.
- Garmire, E., & Tamir, T. (1975). *Integrated optics. Tamir* (p. 315). Springer. Retrieved February 1, 2011, from <http://books.google.com/books?id=EVsJSQAACAAJ&pgis=1>.
- Giovanni, G. (2010). Introduction: semiconductor lasers. Retrieved from <http://www.fi.isc.cnr.it/users/giovanni.giacomelli/Semic/Samples/samples.html>.
- Harness Optical Polarization with Ease and Elegance. (2008). . Retrieved February 1, 2011, from <http://www.generalphotonics.com/Articles.aspx?a=1004>.
- Hunsperger, R. G. (2009). Integrated Optics. (T. Tamir, Ed.) *Applied Optics*, 7(1c), 399-457. Springer New York. Retrieved from <http://www.springerlink.com/index/10.1007/b98730>.
- Illustrated Fiber-Optics Glossary. (2010). . Retrieved from <http://www.infocellar.com/networks/fiber-optics/glossaries/c.htm>.
- Liu, J.-ming. (2005). *Photonic Devices* (p. 1104). Cambridge University Press.
- Midwinter, J. E. (1983). *Światłowody telekomunikacyjne* (p. 345). Wydawnictwa Naukowo-Techniczne. Retrieved February 1, 2011, from http://books.google.com/books?id=w_qPAQAACAAJ&pgis=1.
- Milligan, B. (2004). Long-range VCSELS take aim at putting zap into structured cabling. Retrieved from <http://www.cablinginstall.com/index/display/article-display/215305/articles/cabling-installation-maintenance/volume-12/issue-11/contents/technology/long-range-vcseles-take-aim-at-putting-zap-into-structured-cabling.html>.
- Mitschke, F. (2010). *Fiber Optics: Physics and Technology* (p. 301). Springer. Retrieved January 31, 2011, from http://books.google.com/books?id=343fg_YU5U4C&pgis=1.
- Nadler, C. K., Wildermuth, E. K., Lanker, M., Hunziker, W., & Melchior, H. (1999). Polarization insensitive, low-loss, low-crosstalk wavelength multiplexer modules. *IEEE Journal of Selected Topics in Quantum Electronics*, 5(5), 1407-1412. doi: 10.1109/2944.806898.
- Paschotta, R. (2008a). Fiber Fabrication. *Encyclopedia of Laser Physics and Technology*. Retrieved from http://www.rp-photonics.com/fiber_fabrication.html.
- Paschotta, R. (2008b). Plastic Optical Fibers. *Encyclopedia of Laser Physics and Technology*. Retrieved from http://www.rp-photonics.com/plastic_optical_fibers.html.
- Personick, S. D. (1977). PHOTON PROBE - AN OPTICAL-FIBER TIME-DOMAIN REFLECTOMETER. *Bell Syst Tech J*, 56(3), 355-366. Retrieved November 2, 2010, from

- <http://www.scopus.com/inward/record.url?eid=2-s2.0-0017472705&partnerID=40&md5=ac5db5d291a652ef1712c6f11afeb0b5>.
- Polarization Controller, Manual. (2010). . Retrieved from <http://www.newport.com/Polarization-Controller-Manual/849509/1033/catalog.aspx>.
- Recommendation G.694.1. (2002). . Retrieved from <http://www.itu.int/rec/T-REC-G.694.1-200206-l/en>.
- Recommendation G.694.2. (2003). . Retrieved from <http://www.itu.int/rec/T-REC-G.694.2-200312-l/en>.
- Recommendation ITU-T G.650 (04/1997). (1997). *Networks*. ITU. Retrieved from <http://www.itu.int/rec/T-REC-G.650-199704-S/en>.
- Sato, T., Mitsuhashi, M., & Kondo, Y. (2009). InAs Quantum-well Distributed Feedback Lasers Emitting at 2.3 μm for Gas Sensing Applications. *NTT Technical Review*, 7(1), 1-7.
- Schubert, E. F. (2003). *Light-emitting diodes* (p. 326). Cambridge University Press.
- Senior, J. M., & Jamro, M. Y. (2009). *Optical fiber communications: principles and practice* (p. 1075). Pearson Education. Retrieved February 1, 2011, from <http://books.google.com/books?id=7HtqsEOMkXUC&pgis=1>.
- Silfvast, W. T. (2004). *Laser fundamentals* (p. 642). Cambridge University Press. Retrieved February 1, 2011, from <http://books.google.com/books?id=x3VB2iwSaxsC&pgis=1>.
- Single Mode Polarization Maintaining Fiber. (2010). . Retrieved from http://www.thorlabs.com/NewGroupPage9.cfm?ObjectGroup_ID=1596.
- Siuzdak, J. (1999). *Wstęp do współczesnej telekomunikacji światłowodowej* (2nd ed., p. 392). Warszawa: Wydawnictwa Łączności i Telekomunikacji.
- Tadeusiak A., Crosignani B., M. G. (1987). *Światłowody w telekomunikacji*. Wydawnictwa Komunikacji i Łączności.
- Wang, X., Nie, Q., Xu, T., & Liu, L. (2006). A review of the fabrication of optic fiber. *Proceedings SPIE Vol. 6034* (p. 60341D).
- Wavelength Division Multiplexing - WDM. (2010). . Retrieved from <http://zone.ni.com/devzone/cda/ph/p/id/303>.
- Yount, T. (2009). Performing and Analyzing OTDR Traces. Retrieved March 17, 2011, from <http://www.jdsu.com/en-us/Test-and-Measurement/Training/Pages/performing-and-analyzing-otdr-traces.aspx>.